The Frozen & Unfrozen Barcelona Basic Model

A verification and validation of a new constitutive model

by

Manuel Aukenthaler

to obtain the degree of Master of Science
at the Delft University of Technology,
to be defended publicly on 15 July –, 2016 at 02:00 PM.

Student number:	4405358	
Project duration:	November 17, 2015 – June 30, 2016	
Thesis committee:	Prof. Dr. M.A. Hicks,	TU Delft, chairman
	Dr. Ir. R.B.J. Brinkgreve,	Plaxis bv & TU Delft, supervisor
	Dr. A. Haxaire,	Plaxis bv, daily supervisor
	Prof. Dr. A. Scarpas,	TU Delft

TU Delft Delft University of Technology

PLAXIS

Preface

Why would one research and write a Master's thesis on frozen ground in a country where ground rarely freezes and snow is something mysterious? I give you, dear reader, the honour of choosing your answer from the following statements, which both answer to the truth.

The representation of real soil behaviour by means of numerical models is fascinating. Therefore, I was sold on the chance to do research on constitutive modelling of frozen soil, where the soil's mechanical behaviour is simultaneously influenced by thermo- and hydrodynamic effects.

I grew up surrounded by majestic mountains in the fantastic Alps, and since I was a child I had to handle with the fact to be surrounded by snow and Dutch tourists every winter.

I have to admit it was probably a combination of both. Seven months ago I started my research on a new constitutive model for unfrozen and frozen soil in the framework of a training project at Plaxis bv. It turned out to be a long battle against literature, bugs and the numerous attempts to improve the robustness of the model. The outcome of this long process is this report. It cannot fully capture the long time spent on discussing with my co-workers and friends, hoping for good results and the sadness and tiredness with each failed calculation phase showing *"NaN"*, *"Soil body seems to collapse"* or the illuminating message *"Unknown error"*. Nevertheless, it has been a period of intense learning for me, not only in the scientific arena, but also on a personal level. The time at Plaxis bv was great and successful and will be sorely missed. While working on my thesis I also published my first papers. Without the help, the useful advice and the motivating words of some important people, this thesis would not have come together. I would like to reflect on the people who have supported and helped me so much throughout this period.

My first thanks goes to *Ronald Brinkgreve*, my supervisor and manager of the research department at Plaxis bv for your valuable guidance. You definitely provided me with inspirations that I needed to choose the right direction and successfully complete my thesis. Still you gave me the freedom to come up with own solutions and to work autonomously. Your door was literally always open, you were willing to listen and able to give an answer to all my questions and problems. For this kind of supervision I would like to thank you.

I want to express my deep thanks to *Adrien Haxaire*, my daily supervisor and "mentor" at Plaxis bv. Your trust, your valuable advice, your daily spiritual and technical support during the whole period of my research made the completion of my thesis possible.

Next, my sincere thanks go to *Seyed Ali Ghoreishian Amiri* from the Norwegian University of Science and Technology in Trondheim. Your inimitable commitment to improving the constitutive model and in answering my, to a greater or lesser extent, scientific questions assisted me greatly. Without your intensive work, this thesis would not have come to be.

Finally, I would like to thank my family and all my friends. Your motivating and heartening words gave me the energy and the will to happily resolve this major step in my life.

Manuel Aukenthaler
Delft, June 2016

Abstract

The replication of the behaviour of frozen soils has been studied for decades. Many attempts have been undertaken to either develop new constitutive models or to improve already existing models to simulate the behaviour of frozen materials. To handle the challenges of ground freezing, cold regions engineering and periglacial processes, it is vital to understand the mechanical behaviour of frozen soil. Knowing that field studies, large scale laboratory tests and centrifuge modelling offer good insights, they are however expensive and time consuming activities to undertake. A numerical modelling approach is therefore necessary. The Norwegian University of Science and Technology (NTNU), in collaboration with Plaxis bv, developed a new numerical model to tackle the afore-mentioned problems. The aim of this new approach is to provide a reliable design tool to assess the impact of climate change and changes in temperature in general on a variety of engineering problems.

The constitutive model requires several parameters of which quite a few are not very common to geotechnical engineers. Furthermore, to analyse frozen soil and the behaviour when phase transition occurs, specific properties have to be taken into account which are not determined in standard site investigation and soil lab testing campaigns. This brings the need for a simplified method to determine such properties based on data that is commonly available, such as the particle size distribution. The idea is, as an initial estimate, to correlate this data to the soil freezing characteristic curve and the hydraulic properties of partially frozen soils. Therefore, a practical approach to obtain crucial properties of frozen soil such as the soil freezing characteristic curve (SFCC), the freezing/melting point of a soil-water system and its hydraulic conductivity by means of limited input data is developed. Different models and empirical equations are combined to provide a closed formulation which can be used in computer simulations to account for moisture migration in partially frozen soils. Input data such as grain size distribution and dry bulk density suffices to obtain the aforementioned properties. Further consideration of the pressure dependence of the freezing/melting temperature of water/ice even allows accounting for the phase change point depression and thus the phenomenon of pressure melting. The model is appropriate not just to represent qualitatively the SFCC of different soil types, but also to provide conformity between the model prediction and measured data of many soil types having a log-normal grain size distribution. This user-friendly approach is tested in the geotechnical finite element code PLAXIS 2D. Although some correlations and default values can be provided, laboratory testing is inevitable in order to provide the complete set of necessary soil parameters. To calibrate some of the most difficult ones, namely the Barcelona Basic Model (BBM) parameters, the idea is to use oedometer test results. The temperature-controlled oedometer test requires equipment which is less sophisticated than a temperature-controlled isotropic compression test. A shorter testing period makes it possible to save time and money. An optimisation approach for identification of material parameters in elasto-plastic models for unsaturated soils, like the BBM, using the results from suction-controlled oedometer tests is developed by Zhang et al. (2016). The same approach, reformulated for the constitutive model for frozen and unfrozen soil, is explained in this thesis. This optimisation approach allows to simultaneously determine parameters governing isotropic virgin behaviour as well as unloading and reloading behaviour.

A number of simplified real life applications are presented in this thesis. They demonstrate the correctness of the model's theoretical implementation and its correct representation of the behaviour of frozen soil found in nature. Temperature gradients under uniaxial compression are applied on a frozen sample, and show that the hardening modulus and the uniaxial compression strength increase as the average temperature and the thermal gradient decrease. Another boundary value problem investigates the pressure melting phenomenon and shows that high confining pressures cause the melting of ice crystals due to the reduction of the phase transition temperature. Two freeze-thaw cycles of a clay sample are simulated and provide information on the ability of the model to simulate the ice segregation phenomenon (frost heave) as well as the thaw settlement behaviour. Furthermore, three more practical applications are presented. First, a pipeline is installed in an unfrozen trench and subsequently cooled down by the streaming of a chilled fluid. The onset of frost heave may potentially cause many engineering problems, like cracking of pavements and the fracturing of the pipeline. It is therefore of particular concern in highway and pipeline engineering. The second application comprises a foundation on frozen soil subjected to a warming period. Settlements due to the thawing of ice enclosed in the frozen soil layers accumulate and should be considered when designing embankments

and building foundations on permafrost. Finally, an application of artificial ground freezing is considered. A tunnel is constructed with the use of freeze pipes in order to stabilise the soil during excavation. The soil is frozen by means of the installed freeze pipes. Watertightness and an increase in strength of the soil are achieved. Once the soil has frozen sufficiently, tunnel construction can take place.

To sum up, many essential features of the mechanical behaviour of frozen and unfrozen soil can be captured with this new constitutive model. The dependence of stiffness and shear strength on temperature are among of these. Furthermore, two main features, namely frost heave and thaw settlements, can be simulated. These phenomena play a key role in designing in, on and with frozen / unfrozen soil and may cause significant engineering problems. Three conference papers for two different conferences have been submitted and reflect my research results. However, all that glitters is not gold. The investigated constitutive model cannot fully capture all the effects influencing the behaviour of frozen soil. The non-incorporation of cyclic and time-dependent behaviour represents one of a few shortcomings.

Contents

List of Figures

List of Tables

Symbols

Lower case symbols

a_j	Coefficients for the melting-pressure equation	–
b	Empirical parameter based on the grain size distribution	–
$\boldsymbol{b}$	Body forces	N
b_j	Exponents for the melting-pressure equation	–
c_s	Specific heat capacity	J/(kgK)
d	Plate thickness	m
d_{cl}	Particle size limit of clay	mm
d_g	Geometric mean of the soil particle diameter	mm
d_{sa}	Particle size limit of sand	mm
d_{si}	Particle size limit of silt	mm
e	Void ratio	–
e_0	Initial void ratio	–
e_{min}	Minimum void ratio	–
e_{max}	Maximum void ratio	–
f_1	Mass flux of water	kg/(m^{2}s)
k	Hydraulic conductivity	m/s
k_{sat}	Saturated hydraulic conductivity	m/s
k_t	Rate of change in apparent cohesion with suction	–
m	Yield parameter	–
m_{cl}	Clay mass fractions	%
m_{sa}	Sand mass fractions	%
m_{si}	Silt mass fractions	%
n	Porosity	–
p^*	Effective mean stress	N/m^2
p_{at}	Atmospheric pressure	N/m^2
p_c^*	Reference stress	N/m^2
p_{ice}	Ice pressure	N/m^2
p_{melt}	Melting pressure	N/m^2
p_t	Vapour-liquid-solid triple point pressure	N/m^2
p_w	Pore water pressure	N/m^2
p_y^*	Pseudo pre-consolidation stress for a frozen condition	N/m^2
$(p_{y0}^*)_{in}$	Initial pre-consolidation stress for unfrozen condition	N/m^2
p_{y0}^*	Pre-consolidation stress for unfrozen condition	N/m^2
q^*	Deviatoric stress	N/m^2
r	Coefficient related to the maximum soil stiffness	–
s_c	Cryogenic suction	N/m^2
s_c^*	Mapped cryogenic suction	N/m^2
$s_{c,seg}$	Segregation threshold	N/m^2
$(s_{c,seg})_{in}$	Initial segregation threshold	N/m^2
t	Time	s
$\boldsymbol{v}_{ice}$	Ice velocity relative to the soil skeleton	m/s
$\boldsymbol{v}_w$	Water velocity relative to the soil skeleton	m/s
w	Water content	m^3/m^3
w_j	Weighting	–
w_u	Unfrozen water content	m^3/m^3
w_{plate}	Specific weight of plate (shell) element	N/(m m)
w_p	Plastic limit	–
z	Elevation	m

Upper case symbols

C_1	Constant related to the initial specific volume of the soil	–
C_c	Compression index	–
E_f	Frozen soil Young's modulus	N/m^2
$E_{f,ref}$	Frozen soil Young's modulus at a reference temperature	N/m^2
$E_{f,inc}$	Rate of change in Young's modulus with temperature	$N/(m^2K)$
EA	Axial stiffness	N/m
EI	Flexural rigidity	Nm^2/m
F_1	Yield criterion due to variation of solid phase	–
F_2	Yield criterion due to variation of suction	–
G_s	Grain specific gravity	–
G	Soil shear modulus of the mixture	N/m^2
G_0	Soil shear modulus in unfrozen state	N/m^2
K	Soil bulk modulus	N/m^2
L	Latent heat of fusion for water	J/kg
M	Slope of the critical state line	–
M_p	Maximum bending moment	Nm/m
$N(0)$	Initial specific volume	–
N_p	Maximum axial force	N/m
$\boldsymbol{Q}$	Heat flux per unit volume	$W/m/m^3$
Q_1	Plastic potential function	–
S_{ice}	Ice saturation	%
S_{uw}	Unfrozen water saturation	%
SSA	Specific surface area	m^2/g
T	Current temperature	K
T_{1st}	First ice lens initiation temperature	K
T_{avg}	Average temperature	K
T_f	Freezing/melting temperature	K
$T_{f,bulk}$	Freezing/melting temperature of bulk water	K
T_{max}	Temperature at which ice lens formation stops	K
T_{new}	Second (new) ice lens initiation temperature	K
T_{ref}	Reference temperature	K
T_{sn}	Temperature of spontaneous nucleation	K
dV	Change in volume	m^3

Greek symbols

α	Thermal expansion coefficient	$1/K$
β	Rate of change in soil stiffness with suction	$(N/m^2)^{-1}$
$d\epsilon$	Increment of strain	–
$d\epsilon^m$	Increment of strain due to solid phase stress variation	–
$d\epsilon^{me}$	Increment of elastic strain due to solid phase stress variation	–
$d\epsilon^{mp}$	Increment of plastic strain due to solid phase stress variation	–
$d\epsilon^p$	Increment of plastic strain	–
$d\epsilon^s$	Increment of strain due to suction variation	–
$d\epsilon^{se}$	Increment of elastic strain due to suction variation	–
$d\epsilon^{sp}$	Increment of plastic strain due to suction variation	–
$d\epsilon^e_q$	Increment of elastic shear strain	–
$d\epsilon^e_v$	Increment of elastic volumetric strain	–
γ	Plastic potential parameter	–
γ_w	Unit weight of water	N/m^3
κ	Elastic compressibility coefficient of the soil mixture	–
κ_s	Elastic compressibility coefficient for suction variation	–
κ_0	Unfrozen Soil elastic compressibility coefficient	–
λ	Elasto-plastic compressibility coefficient for a frozen state	–
λ_0	Elasto-plastic compressibility coefficient for unfrozen state	–
$d\lambda_1$	Plastic multiplier regarding the loading-collapse yield surface	–
$d\lambda_2$	Plastic multiplier regarding the grain segregation yield surface	–
λ_s	Elasto-plastic compressibility coefficient for suction variation	–
λ_{s1}	Thermal conductivity	$W/(mK)$
ν	Specific volume	–
ν^*	Mapped specific volume	–
ν^e	Volume change in the elastic region	–
ν_{ice}	Poisson's ratio of ice	–
ν_{plate}	Poisson's ratio of the plate (shell) element	–
ν_f	Frozen soil Poisson's ratio	–
ϕ	Residual or critical angle of friction	°
$\mathbf{\Phi}$	Heat content of soil per unit volume	J/m^3
ψ	Slope of the water potential	–
ρ_b	Dry bulk density of the unfrozen soil	kg/m^3
ρ_s	Density of the solid material	kg/m^3
ρ_{ice}	Density of ice	kg/m^3
ρ_w	Density of water	kg/m^3
$\boldsymbol{\sigma}$	Net stress	N/m^2
$\boldsymbol{\sigma^*}$	Solid phase stress	N/m^2
σ_g	Geometric standard deviation	–
θ_{ice}	Volumetric ice content	–
θ_{sat}	Volumetric water content of a saturated soil	–
θ_{uw}	Volumetric unfrozen water content	–
θ_w	Volumetric water content	–

1 Introduction

1.1. Background and motivation

Frozen ground engineering has developed rapidly in the past several decades. Due to the increase in engineering activities involving frozen soil, the necessity of research regarding frozen ground engineering has advanced. Hence, the transition from frozen to unfrozen soil and vice versa has become an important research topic. Cold regions engineering, periglacial processes and construction ground freezing are the fields which benefit from this intense research. By reason of the variation of seasonal temperature, global warming and human interference, the thermal regime of the surrounding soil changes and the landscape is reshaped (Glendinning, 2007; Zhang, 2014). All these factors force the geotechnical engineer to deal with their related challenges. Whether freezing in soils is induced by natural weather conditions or by human activities, its impact is profound. Engineers are faced to handle higher risks of slope failure and landslides, lower stability of road embankments and foundations, the cracking of pavements and the degradation of permafrost. Additionally, an increase of the usage of artificial ground freezing is surely expected.

Understanding the mechanical behaviour of frozen soil is vital and plays a key role in mastering the named challenges. Knowing that field studies, large scale laboratory tests and centrifuge modelling offer a good understanding, they are however expensive and time consuming activities to undertake. The necessity of a numerical modelling approach is obvious and evident. The use of a numerical model saves a huge amount of time, can be used as a design tool and may assess the impact of climate change on a variety of engineering and geological problems. Knowing how soil behaves upon freezing and thawing is essential for a geotechnical engineers. Together with the usage of an appropriate constitutive model the potential of changing the operation practices and design philosophies is provided. New methods can be developed to predict and minimise risks and damages.

1.1.1. Engineering considerations

Frost action

Frost action in soils involves the processes of freezing and thawing. Andersland and Ladanyi (2004) describe the term frost action as the detrimental process of frost heaving resulting from the formation of ice lenses at the freezing plane in soil during the freezing period followed by thaw weakening or decrease in bearing strength when seasonally frozen soil thaws. In order to allow frost action to occur, some requirements have to be fulfilled: the presence of a frost-susceptible soil, a supply of water, and soil temperatures low enough to cause some of the soil water to freeze (Hohmann, 1997; Zhang, 2014).

Frost action is responsible of many damaging effects (Alfaro et al., 2009; Wu et al., 2010; Fortier et al., 2011; de Grandpré et al., 2012; Zhang, 2014; Li et al., 2016). Cracked and broken pipelines, malfunctioning utilities, cracked pavements (Figure 1.1a), tilted structures (Figure 1.1b) and differential heave of foundations are only some examples of damage caused by frost action. Long-term records indicate an ongoing warming of the climate, which has resulted in thawing of portions of the permafrost area. Lemke et al. (2007) has reported that temperature at the top of the permafrost layer has increased by up to 3 °C since the 1980s in the Arctic. The permafrost base has been thawing at a rate ranging up to 0.04 meter per year in Alaska since 1992 and 0.02 m/yr on the Tibetan Plateau since the 1960s. Permafrost degradation is leading to changes in land surface characteristics and drainage systems. The increase in permafrost temperature leads to thickening of

the active layer, which is the upper crust layer where active freezing and thawing takes place. The thickening of this layer leads to extensive settlement of the ground surface. The seasonal temperature variation is in charge of the annual freezing of the active layer and for the heave that occurs with the downward movement of the freezing front. The transition of water to ice entails an increase in volume by about nine percent. However, the actual frost heave action is not caused by the volumetric expansion but due to the formation of ice lenses (Taber, 1916, 1929, 1930; Andersland and Ladanyi, 2004; Rempel et al., 2004; Michalowski and Zhu, 2006; Rempel, 2007; Azmatch et al., 2012a; Peppin and Style, 2012). Due to the available free pore water and the seasonal temperature variation, frost heave can cause damage to any engineering structure. The heterogeneous nature of most soils results in a very non-uniform heave. This differential heave may for instance seriously affect the riding quality and the use of traffic surfaces. Whole structures may distort.

(a) Pavement cracking due to freeze-thaw cycles[1]

(b) Tilted building due to thawing of underlaying permafrost (from National Snow and Ice Data Center)

Figure 1.1: Damaging effects caused by frost action

Frost heave

Frost heave is a major cause of damage to transportation infrastructure such as pipelines, railways and roads in regions of seasonal frost. In the United States, over two billion dollars is spent annually repairing frost-heave damage to roads alone (DiMillio, 1999). The costs worldwide are tremendous.

The term frost heave refers to the upward displacement of the ground surface due to ice segregation and ice lens formation. The cracking of the soil in the frozen fringe and the flow of unfrozen water towards the freezing front initiate the formation of ice lenses. Taber (1916), Taber (1929) and Taber (1930) has probably been the first one to study the frost heave phenomenon and has come up with very important insights. Taber demonstrated that frost heave is caused by the migration of water from lower, unfrozen regions of a soil column towards the freezing front. There, it deposits as bands of pure ice in the soil – ice lenses – which force the soil apart as they grow, heaving the surface upwards (see Figure 1.2). This process can cause almost unlimited heave of the soil surface, provided there is a sufficient supply of water and slow enough freezing. The phenomenon of frost heave has been studied over almost a century, but there are still many unanswered questions about the underlying mechanisms. Scientists are still actively working to understand the observations of Taber. Rempel (2007) explains, for instance, that the most significant frost damage occurs when segregated ice grows and pushes apart mineral grains to produce macroscopic deformation of the porous medium. The ice growth is supplied through premelted liquid films (Figure 1.3) that disjoin the ice from the mineral grains. It is the intermolecular interactions across these thin films that are the driving force for frost damage. The process of frost heave is illustrated in Figure 1.2 and 1.3.

[1] http://www.pavementinteractive.org/article/frost-action/

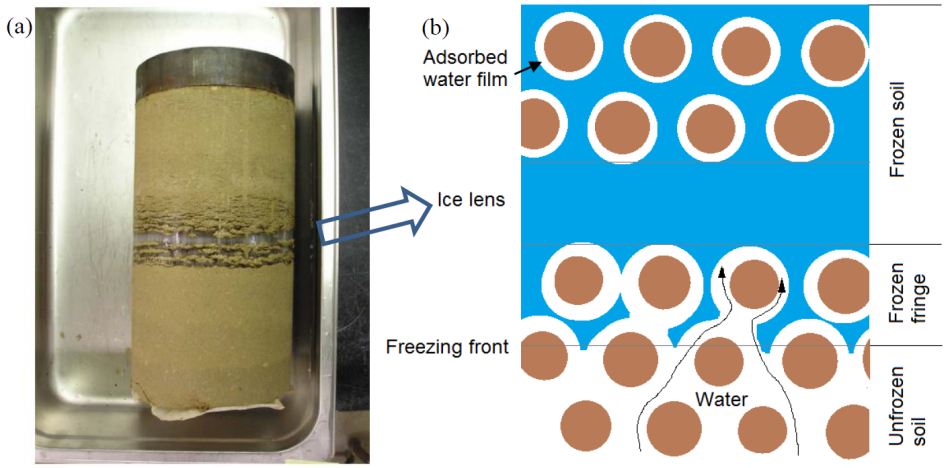

Figure 1.2: Illustration of freezing soil (from Zhang (2014)), (a) Frost heave specimen (Lay, 2005), (b) Illustration of freezing soil

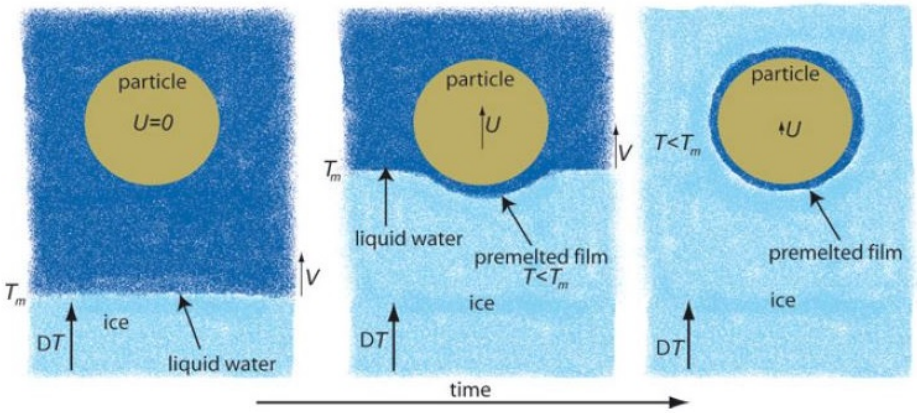

Figure 1.3: Schematic diagrams of the stages of interaction between a freezing front and a foreign solid particle in a temperature gradient ΣT (Rempel, 2010)

Thaw consolidation and thaw settlement

During freezing, ice accumulates and frost heave may occur. When temperatures increase or frozen soil is subjected to a very high pressure, thawing of the frozen soil takes place. The ice lenses formed in the freezing process gradually melt. Due to the disappearance of ice, the soil skeleton must adapt itself to a new equilibrium void ratio (Andersland and Ladanyi, 2004). The excess water melted from ice lenses may exceed the absorption capacity of the soil skeleton. While water tries to find its way through the soil skeleton, either due to its self-weight and/or external forces, thaw consolidation is happening. The rate of the thaw consolidation depends on both the melting rate of the ice and the hydraulic properties of the soil (Zhang, 2014). Volume change will then result from the phase change, the flow of excess water out of the soil and due to applied loads.

The sum of all these settlements can be called thaw settlements. After consolidation is completed the thaw settlements could be larger or smaller than the displacements caused by frost heave (Konrad, 1989). It depends primarily on the history of loading prior to freezing and the number of freeze-thaw cycles the soil has been subjected to. Thawing of a frozen normally consolidated soil in its first freeze-thaw cycle could cause a settlement larger than the heave induced during the freezing phase. However, some heave could remain in an over-consolidated soil subjected to its first freeze-thaw cycle. Artificial ground freezing applied in soft soil construction (e.g. tunnelling or excavations), and pipelines transporting chilled media through unfrozen soil, are examples where soil may be subjected to its first freeze-thaw cycle (Konrad, 1989; Zhang, 2014). Figure 1.1b shows typical thaw settlements caused by a non insulated heated house built on permafrost.

Artificial ground freezing

Controlled artificial ground freezing of soil has been used for over a century as a supporting construction method in geotechnical engineering. Frozen ground may be used to provide ground support, groundwater control, or structural underpinning during construction. The use of artificial ground freezing is shown in Figure 1.4. By installing freezing pipes and circulating liquid (mostly nitrogen) with temperature below the freezing point of water through them, pore water is converted into ice. The ice becomes a bonding agent. It fuses together adjacent particles of soil or blocks of rock and increases the strength and the impermeability of the freezing soils. Temporary stabilisation of the soil and hydraulic seal is provided. Ground freezing may be used in any soil or rock formation, regardless of structure, grain size or permeability (Andersland and Ladanyi, 2004). However, artificial ground freezing is connected with a certain risk of damage of the surface infrastructure. Also controlled freezing can cause the formation of ice lenses and hence frost heave. The significant changes in soil structure and density upon thawing can lead to adverse settlements. The occurrence of differential heave and settlements may cause cracks in existing buildings and roads. Furthermore, groundwater flow plays a vital role. Groundwater or seepage flow is responsible for the time of establishment of a complete frozen body, since it provides a continuous source of heat. In case of large seepage flows, a state of thermal equilibrium can be reached, in which freezing stops and the closure of the desired frost wall cannot be developed (Zhou, 2014). Therefore, artificial ground freezing also requires the knowledge of how the soil strength, the soil stiffness and the permeability change with respect to temperature.

(a) View of frozen ground in a tunnel in Sweden

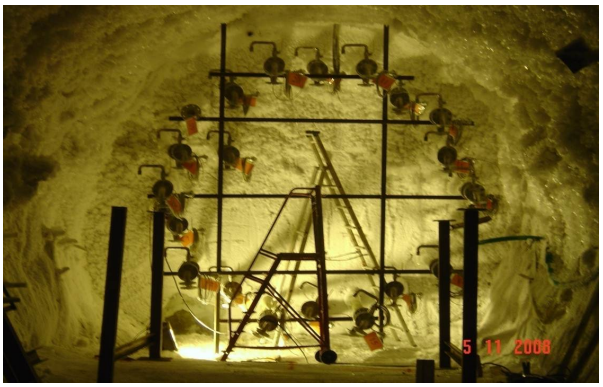

(b) Brine Circulating Pipes at the Face

Figure 1.4: Artificial ground freezing in tunnelling (Madan, 2012)

Beneficial properties of frozen ground

Frozen ground provides some very beneficial properties useful to engineering projects. High strength in compression, excellent bearing capacity and the impervious nature of frozen ground relative to water seepage are properties used by engineers in the design of ground support systems, foundations, earth dams, and other frozen earth structures (Andersland and Ladanyi, 2004).

High strength The strength of frozen ground involves a combination of pore ice strength, soil strength consisting of frictional resistance and interference between soil particles, a dilatancy component, and interaction between the ice matrix and the soil skeleton (Ting et al., 1983; Andersland and Ladanyi, 2004). Also factors such as temperature, confining pressure, strain rate, ice content and deformation history are of importance considering the strength of a frozen soil.

Ice content. The mechanical behaviour depends, to a great degree, on that part of the pore ice, and consequently, so does the strength of frozen soils as well. Sayles and Carbee (1981) have shown that the strength of initial fracture increases non-linearly with the volume of ice per unit volume of the soil mass (see Figure 1.5a). Since the ice matrix is the strongest bonding material in the tested soil, its fracture can be taken as the initiation of failure. However, they distinct between the ice matrix failure, which occur at small strains, and the shear failure of the entire mixture, which takes place at much larger strains. Their tests show that at silt concentrations of less than about 50 %, the ice dominates the strength, while at larger particle concentrations, the stress-strain curves manifest an increasingly strain-hardening character, resulting from a gradual mobilization of friction and interlocking at large strains (Andersland and Ladanyi, 2004). This behaviour is

shown in Figure 1.5b and was also found from Baker (1979). He showed that the strength of a frozen sand increases until the soil is fully saturated with ice, and then decreases until the soil particles no longer influence it (see Figure 1.5c)

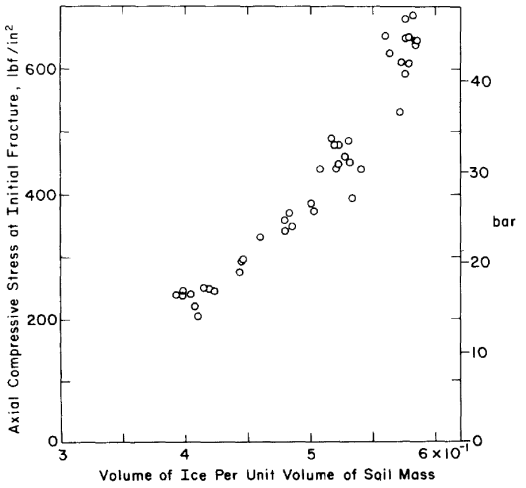

(a) Relation between axial compressive stress at initial fracture and volume of ice per unit volume of soil mass (Sayles and Carbee, 1981)

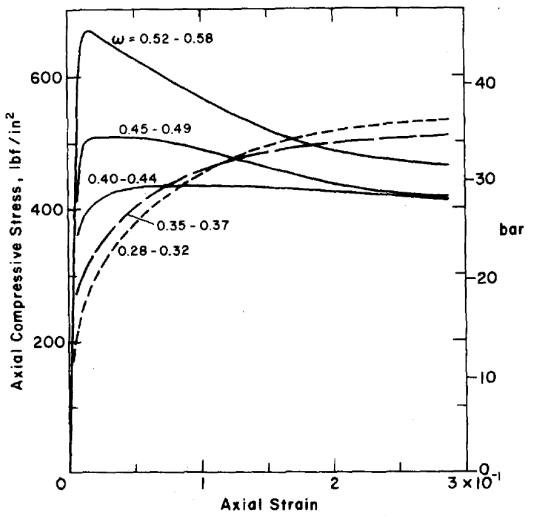

(b) Average stress-strain curves for five different total water content ranges at a temperature of −1.67 °C (Sayles and Carbee, 1981)

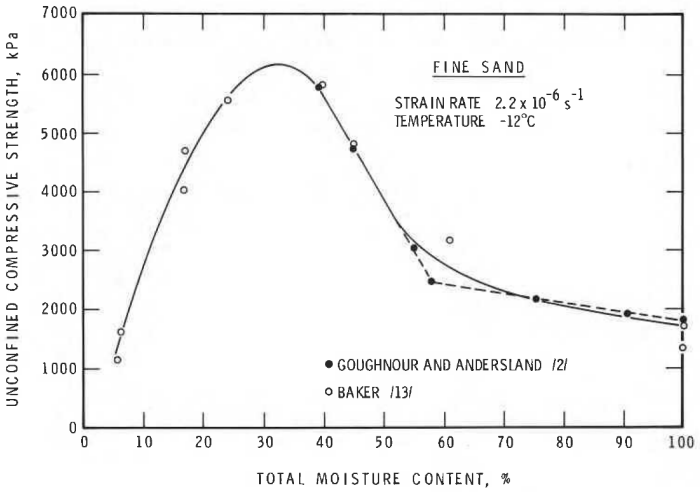

(c) Effect on total moisture content on unconfined compressive strength (Baker, 1979)

Figure 1.5: Influence of the ice content on the strength of frozen soil

Confining pressure. The behaviour of frozen soils under the variation of confining pressure have been reported by many researchers (Alkire, 1973; Parameswaran and Jones, 1981; Ma et al., 1999; Yang et al., 2010; Lai et al., 2010). When the grain concentration is high enough, the strength of frozen soil is a function of the strength of both the ice cement and the soil skeleton. Chamberlain et al. (1972) found that these two sources of strength do not necessarily act simultaneously. This is because the ice matrix, under normal pressure and temperature conditions, is much more rigid than the soil skeleton and reaches its peak strength at much lower strains (Andersland and Ladanyi, 2004). Ladanyi (1981) presented the behaviour observed in compression tests at a constant strain rate and temperature, but at different confining pressures, schematically by the Mohr plot given in Figure 1.6. The plot is composed of three failure lines and four regions, namely:

- **A**: At low confining pressure the ice cement dominates. The stress-strain behaviour is brittle in tension

and strain softening in compression. The first peak strength occurs at strains of about 1 %.

- **B**: In region B, strain hardening takes place and due to friction and dilatancy of the sand-ice mix a second peak dominates at strains about 10 times larger.

- **C**: At high confining pressures the dilatancy might get suppressed, and with increasing confining pressures it even can change sign. The ice takes a large portion of the normal stress and starts melting partially.

- **D**: At confining pressures high enough to crush the grains, the pore ice that is already under compression thaws, and shear failure occurs as in an unfrozen sand under undrained conditions.

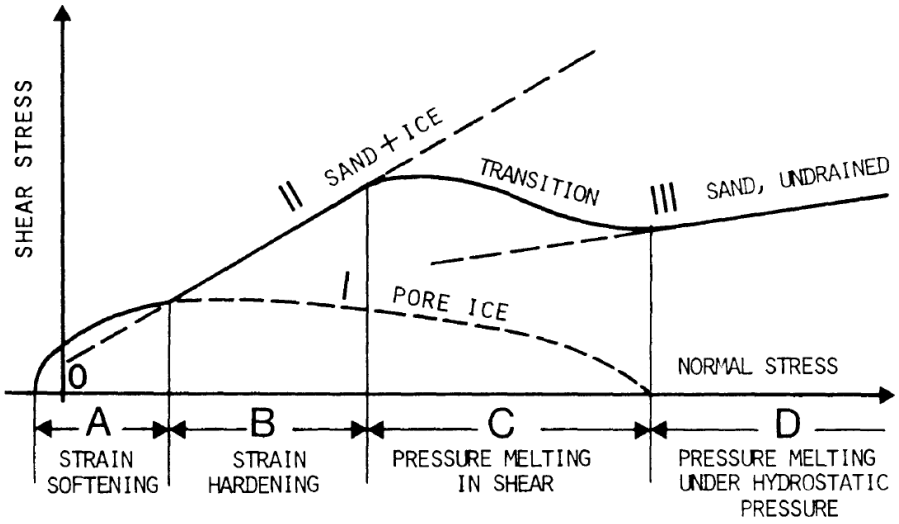

Figure 1.6: Schematic representation of the entire failure envelope for frozen Ottawa sand Chamberlain et al. (1972)

Temperature. The temperature is probably the most important factor affecting the behaviour of frozen soil. Many test results confirm this statement (Haynes, 1978; Baker, 1979; Parameswaran and Jones, 1981; Lai et al., 2010). It directly influences the strength of intergranular ice, the bonding strength of the interface between soil particles and ice, and the amount of unfrozen water in a frozen soil. In general, a decrease in temperature results in an increase in strength of a frozen soil, but at the same time it increases its brittleness, which is manifested by a larger drop of strength after the peak and an increase in the ratio of compressive strength to tensile strength (Andersland and Ladanyi, 2004). Results of compressive strength vs. temperature for Fairbanks silt were conducted by Haynes (1978) and provided in Figure 1.7a.

Strain rate. Ice and consequently frozen soil are highly rate dependent. A decrease in the peak values, as well as in the residual values, can be observed for decreasing strain rates (Haynes, 1978; Andersland and Ladanyi, 2004; Arenson and Springman, 2005). Figure 1.7b shows that for a given temperature the compressive strength increases with increasing strain rate. Additionally, Arenson and Springman (2005) note that as axial strain rates decrease, the peak value approaches the value of the residual shear strength. Their explanation is that the material starts to creep at the lower strain rates and therefore stresses redistribute and relaxation occurs. The tendency for dilation is suppressed, so no additional shear resistance of the frozen soil is activated as the sample undergoes increasing strain.

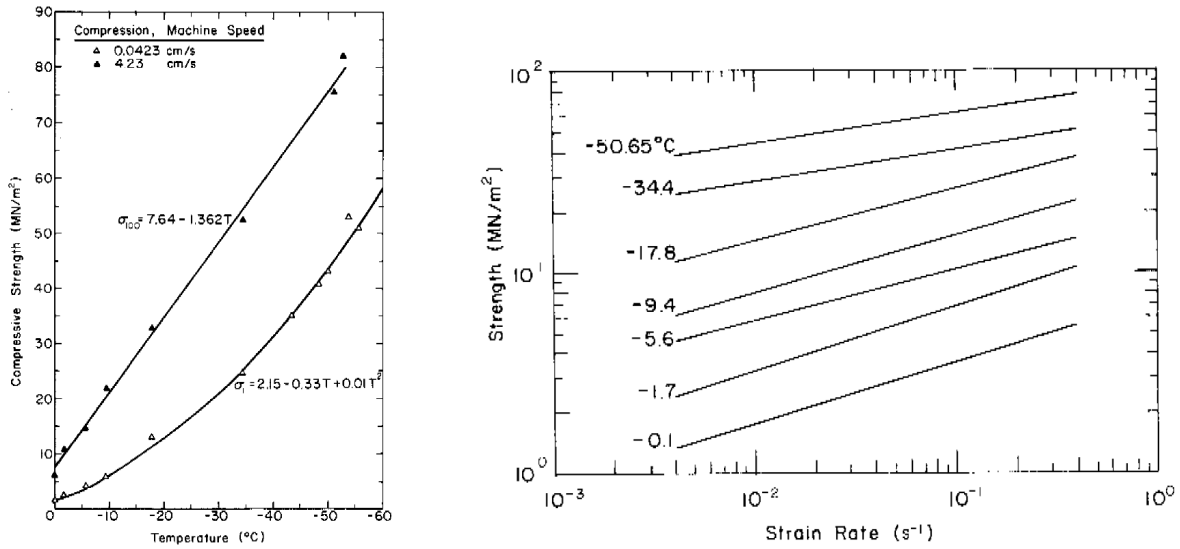

(a) Compressive strength vs temperature for Fairbanks silt (Haynes, 1978)

(b) Compressive strength as a function of strain rate (Haynes, 1978)

Figure 1.7: Influence of temperature and strain rate on the strength of frozen soil

Low permeability Saturated frozen soils show very low permeabilities (Burt and Williams, 1976; Horiguchi and Miller, 1983; Oliphant et al., 1983; Benson and Othman, 1993; Andersland et al., 1996; Tarnawski and Wagner, 1996; McCauley et al., 2002; Watanabe and Wake, 2009). Soils with permeabilities approaching zero can be seen as hydraulic barriers and provide many advantages. Benson and Othman (1993) depict that frozen soil is widely used as waste-containment structures. Examples of their application include landfill liners and covers, caps at hazardous waste sites, and liners for surface impoundments and sewage lagoons. Andersland and Ladanyi (2004) explain that for large excavations, there is no need for a dewatering system anymore when the frozen earth support system extends down into an impermeable soil layer. In addition, for groundwater remediation projects, a subsurface frozen soil wall can provide a temporary impermeable barrier around and under the contaminated site. The potential for frozen soil to serve as a secondary containment lining for fuel storage facilities in Alaska has been evaluated by McCauley et al. (2002). Furthermore, in poorly drained areas where excavation below the water table is required, it can be advantageous to do the work in winter when the ground is frozen. Higher frozen soil strengths permit access by heavy equipment to sites which would normally be soft and marshy during the summer. The imperviousness of frozen soil can be seen as a great benefit. The need of pumping is removed, and costs are saved.

1.1.2. People and frozen ground

Many people worldwide live in places with seasonally frozen ground or on permafrost. The changes in climate and the increases in engineering activities in cold regions lead to the fact that frozen ground affects people's lives more and more. On the one hand, when frozen soil starts thawing, it settles and can damage buildings and transportation infrastructure. On the other hand, when all the water near the surface freezes, it may cause frost heave and can make finding drinking water for towns difficult. Buildings, roads, bridges, railways, water supplies, oil and natural gas wells are all affected by frozen ground and people have to live and deal with all the related problems and consequences.

Buildings built on seasonally frozen ground or permafrost are mostly heated from the inside and give off heat. The heat can thaw the frozen ground underneath the building. Once the frozen soil starts thawing, it sinks due to volume change from ice to water, consolidation and the surcharge of the building, damaging the building it supports (see Figure 1.1b). To prevent this unfavourable happenings to occur, careful design, the choice of an adequate foundation type, insulation method and maintenance of the foundation is required.

Bridges, railways, roads built on embankments and any other type of transportation infrastructure often cross frozen ground and permafrost. If the ground thaws or freezes often differential heave or settlements occur and cause damage. Constant repairs and maintenance is needed to keep them safe.

The drilling of deep wells for oil and gas as well as the transportation to where it is used can cause the thawing of permafrost. If this happens, the wells can collapse and the pipelines can sink and break. Engi-

neers have come up with solutions to mitigate and avoid this detrimental situations. National Snow and Ice Data Center describe that firstly drilling companies put their equipment on special concrete pads built to prevent the ground underneath from thawing. Secondly, cement well liners prevent wells from collapsing. Companies also use special drilling liquids that do not freeze as quickly as water does to lubricate the drill bits. Furthermore, engineers built pipelines above the ground in many places.

Water supply may be difficult in regions with large, continuous stretches with permafrost. Most of the ground water is frozen. If there is any water that is liquid, the ice in the soil pushes its minerals out. The minerals get concentrated and the water in the soil undrinkable (National Snow and Ice Data Center). Villages and towns are forced to build water pipes from the water supply (lakes and rivers) to the buildings.

1.1.3. Modelling frozen soil

The behaviour of frozen soils has been studied for decades. The representation of freezing and thawing of pore fluid within soils involves complex thermal, hydraulic and mechanical processes and is essential in several areas of geomechanics. Depending on their particular application purpose, models have been developed and implemented with different degrees of sophistication (Nishimura et al., 2009).

Thermo-Hydro-Mechanically coupled finite element models

The Thermo-Hydro-Mechanically (THM) coupled numerical modelling deals with multi-physical processes where temperature, hydraulic pressure and mechanical deformation are simultaneously considered. THM modelling is widely used in solving porous medium problems in which temperature changes and mass movement are combined (Zhang, 2014). Bekele (2014) provides an overview of the studies in the fully coupled THM modelling of frozen soils over time, which is visualised in Figure 1.8.

Constitutive models of frozen soil

Existing constitutive models have become increasingly complex. The representation of specific aspects of soil response has demanded this increase in complexity to account for effects of temperature, strain magnitude and rate, relative density and opposing effects of dilatancy and crushing (Springman and Arenson, 2008). Historically, we can distinguish constitutive models of frozen soil into two categories: On the one hand we have total stress-based mechanical treatments and on the other hand we have effective stress-based mechanical treatments. But also hypoplastic constitutive models for frozen soil are getting more interesting (Xu, 2014).

Total stress-based models have been widely used in literature to describe the mechanical behaviour of soils and are adopted for most geotechnical analyses of frozen soils (Arenson and Springman, 2005; Lai et al., 2008, 2009, 2010; Zhu et al., 2010; Xu, 2014). These models, however, only tend to accentuate the influence of confining pressure on the elastoplastic behaviour, placing less emphasis on the influence of important factors like temperature and ice content (Ghoreishian Amiri et al., 2016). This means they are not able to simulate deformations under the variation of ice content and/or temperature during a freezing or thawing period.

Simultaneously to the development of total stress based constitutive models, the effective stress principle by means of total stress minus pore pressure is employed by some researchers for simulating the behaviour of frozen ground (Thomas et al., 2009; Nishimura et al., 2009; Zhou, 2014; Zhang, 2014; Ghoreishian Amiri et al., 2016). The definition, the representation and the incorporation of the pore water pressure is, however, not consistent. Due to the phase change of water to ice and vice versa, difficulties in representing changes in pore water pressure have been encountered and different approaches have been introduced. Thomas et al. (2009) assume, for instance, that in the partially frozen soil the pore ice does not form a continuous phase and is unable to exert a mechanical pressure. However, when the soil is fully frozen the pore ice is continuous, and the pore water pressure effectively represents the mechanical ice pressure. Zhang (2014) employed the effective stress principle, where the total stress is made up of the effective stress and the water pressure. Nishimura et al. (2009), Zhou (2014), and Ghoreishian Amiri et al. (2016) differentiate the ice pressure and the water pressure in the equilibrium equation and the Clapeyron equation is used to define the relationship between the two.

Nishimura et al. (2009) are the first to propose a two stress state variables model for simulating the behaviour of frozen soil. The close analogy between the physics of frozen-saturated and unfrozen-unsaturated soils has lead to adopting an alternative two-stress state variable constitutive relationship than for instance in Alonso et al. (1990). The net stress defined as the excess of total stress over ice pressure or water pressure and the cryogenic suction are the two stress state variables in addition to the deviatoric stress. Using the modified Cam-Clay model for the reference unfrozen condition the model is able to capture many essential features

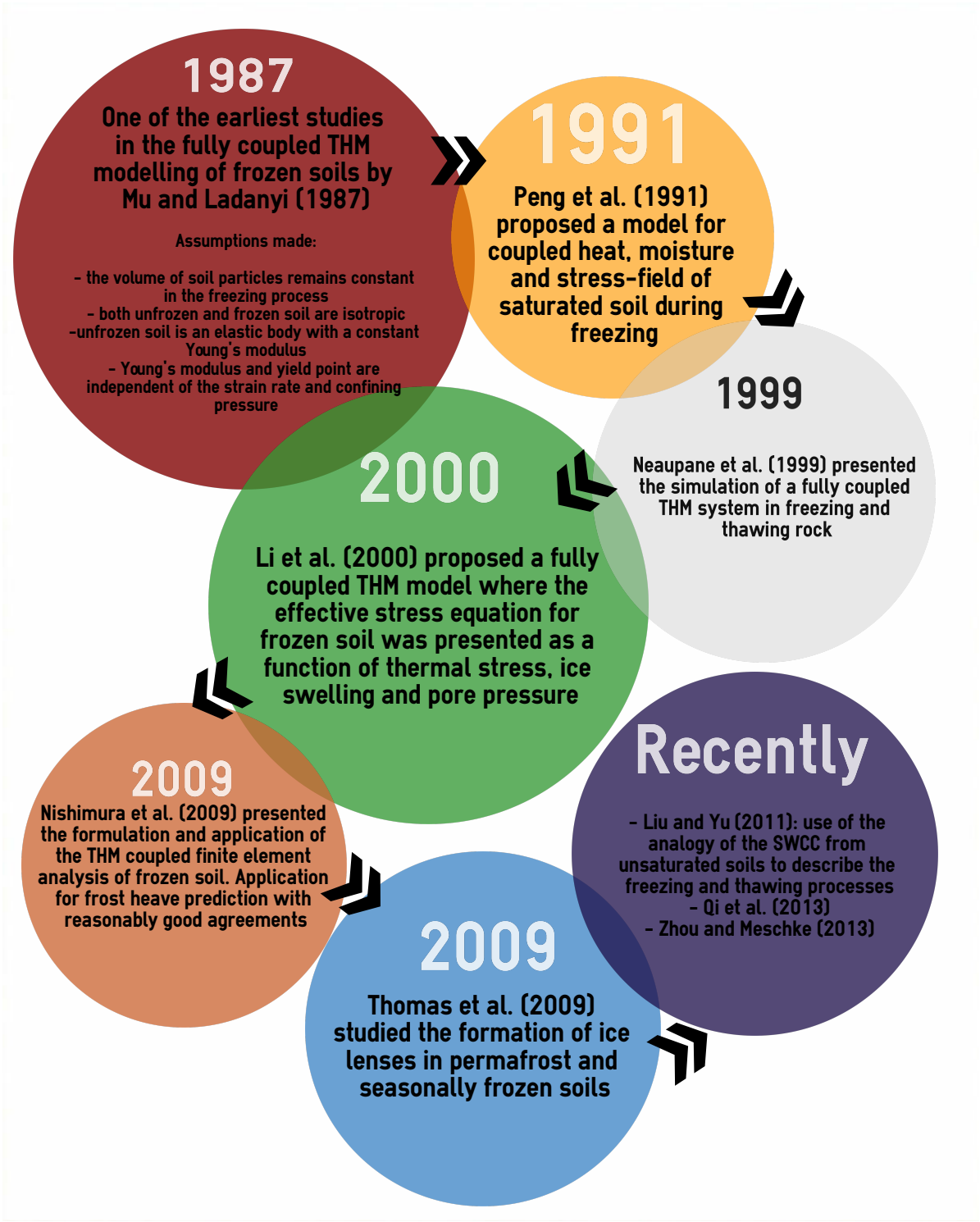

Figure 1.8: Historical developments and studies on THM modelling (adapted from Bekele (2014))

of the complex mechanical behaviour of freezing soils including the dependence of shear strength on temperature and porosity. Ghoreishian Amiri et al. (2016) note that using the model of Nishimura, the increase of ice pressure, during a freezing period, results in zero or negative values of net mean stress, and is followed by a tensile failure and soil particles segregation. This results in an increase in void ratio and a softer behaviour of the soil. Samples which have experienced a tensile failure due to the segregation phenomenon by decreasing temperature under isotropic stress condition will always show dilative behaviour upon shearing. Furthermore, in unfrozen state, the model reduces to an effective stress-based critical state model. The water pressure replaces the ice pressure in the definition of the net stress. The simulation of thawing consolidation is therefore also possible. Nishimura et al. (2009) apply a segregation potential theory to account for the frost heave phenomenon.

Zhou (2014) proposed another approach in the framework of two-stress state variables. He considers the temperature during freezing as the second independent variable, instead of cryogenic suction. For the prediction of the temperature- and porosity-dependent strength criterion of freezing soils a multi-scale strength homogenization procedure is proposed. It allows to determine the macroscopic cohesion and frictional coefficient based on the current state of the microstructure of freezing soils. Ghoreishian Amiri et al. (2016) state that considering the identity of stress measurement and yield mechanism for ice segregation phenomenon between this model and that introduced by Nishimura et al. (2009), the previously mentioned problem for shearing a sample after freezing under isotropic stress condition is still remained.

Zhang and Michalowski (2015) employ the effective stress and the pore ice ratio as the independent variables for their constitutive model. The frost heave phenomenon, in this model, is simulated using a porosity growth function.

The constiutive model developed by Ghoreishian Amiri et al. (2016) is the my main research object. In the following chapters it is presented in detail.

1.2. Research objectives

The main research objective is to verify the implementation of the new numerical model developed by the Norwegian University of Science and Technology (*NTNU*) in collaboration with *Plaxis bv* to tackle the problems of interest mentioned in Section 1.1. Furthermore, testing the model in practical applications by validating whether it represents real data sufficiently and may be used for design and forecast approaches in frost/thaw prone regions is another important research question. The frost heaving and thaw weakening behaviour of soils is examined, which both may cause considerable damage to engineering structures. To undertake the research and to give an answer on the aforementioned research objectives, the adjacent questions are tried to be investigated.

- What are the main features of the new constitutive model for frozen and unfrozen soil developed by *NTNU* and *Plaxis bv* and how does it differ from other constitutive models for frozen soil?
- Is the numerical model implemented according to its theoretical formulation and is the simulated mechanical behaviour in accordance with the observed behaviour in nature?
- Is it possible to model frost heave appropriately?
- How accurate can settlements due to thawing processes be modelled?
- Is the model appropriate to forecast the long term behaviour of an engineering structure?
- What are the shortcomings and limitations of the constitutive model?

1.3. Research activities

In order to achieve my research objectives posed in the previous section, I follow the procedure described below:

- Getting familiar with the PLAXIS thermal module.
- Literature review regarding the behaviour of frozen and unfrozen soil and the transition from frozen to unfrozen and vice versa.
- Learning the backgrounds of thermal analysis and Thermo-Hydro-Mechanical (THM) coupling.

- Learning backgrounds of the frozen/unfrozen soil model.
- Understanding the meaning of the model parameters.
- Testing the model in a single stress point environment.
- Verifying the model against known solutions in single element tests.
- Validating the model in practical FEM applications.

1.4. Contribution to knowledge

The aim of my research is to:

- Validate the new constitutive model considering practical applications (design, forecasts and risks assessments) and how it should be used.
- Give suggestions on how model parameters can be obtained and/or correlated.
- Provide default values for the new constitutive model for various types of soils.
- Present clear limitations and possible improvements of the frozen/unfrozen soil model.

1.5. Thesis structure

The Master's thesis consists of the following chapters:

1. Chapter 1: Introduction

   The Introduction includes background information, a short literature overview, the problem description, the research questions and the research activities.

2. Chapter 2: Description of the constitutive model and its implementation

   Chapter 2 gives a detailed description of the new constitutive model and its implementation in an thermo-hydro-mechanical finite element environment.

3. Chapter 3: Validation of the empirical approach to obtain the soil freezing characteristic curve and hydraulic soil properties

   Chapter 3 explains the possibility to obtain crucial properties of frozen soil, like the soil freezing characteristic curve and the hydraulic conductivity, by means of limited input data.

4. Chapter 4: Parameter determination

   This chapter proposes soil tests, correlations, default values and a calibration method to obtain the necessary input parameters for using the constitutive model.

5. Chapter 5: Verification and validation of the model in a single stress point environment

   This chapter provides single stress point environment test results compared to known solutions in single element tests and provides a comparison to real test data.

6. Chapter 6: Verification of the model in a fully coupled THM finite element environment

   Chapter 6 includes the testing of the model in a THM finite element environment and the verification of boundary value problems, including freezing and thawing of soils.

7. Chapter 7: Discussion and Conclusion

   The final chapter discusses and summarises the contribution of this study. Furthermore it provides suggestions for further research.

2

A new constitutive model

2.1. The new constitutive model and its implementation

2.1.1. Theory

The soil is assumed to be a fully saturated, isotropic and elastic natural particulate composite. It can be unfrozen, partially frozen or fully frozen. Unfrozen soil is composed of solid grains and pore water, whereas partially frozen soil consists of solid grains, pore ice and pore water. When the temperature is low enough, the soil might experience a fully frozen state, where the composite consists of soil grains and pore ice. Each component of the composite is assumed to be incompressible. To account for the local thermal equilibrium, the temperature of soil grains, pore water and ice is the same at each point in the soil (Thomas et al., 2009).

The freezing and melting process

The freezing process in soil is different from the freezing process of pure free water (Low et al., 1968; Andersland and Ladanyi, 2004; Kozlowski, 2004; Lal and Shukla, 2004; Kozlowski, 2009). Freezing or melting of pure normal water occurs at 0 °C, whereas in the soil - water system, it occurs below 0 °C. According to Low et al. (1968), the main macroscopic parameter to cause this freezing point depression is the water content w. For cohesionless soils with small specific surface areas (SSA) this temperature depression is negligible, but for fine-grained soils such as silts and clays with the capability to hold a high unfrozen water content (and thus a high SSA), it can be up to 5 °C (Andersland and Ladanyi, 2004). Next to the importance of the water content w, high pressures and the presence of solutes may lower the freezing/melting point.

Furthermore we have to consider that the initial freezing process does not start at the freezing point. To initiate the ice crystal nucleation and crystal growth some supercooling below the freezing point is needed. This phenomenon even holds for pure water. Figure 2.1 shows the freezing process over time of pure water and a clay-water system, respectively. Emphasizing on the soil-water system, the freezing process in soil can be explained as follows:

1. Generally speaking, water begins freezing when the soil temperature is below the pore water freezing point, T_f. This phase change of pore water occurs in the so-called frozen fringe.

2. Firstly, soil temperatures have to drop below the pore water freezing temperature until enough energy exists to instigate pore water nucleation. This occurs at the temperature of spontaneous nucleation T_{sn}.

3. The formation of ice releases latent heat and the pore water temperature then increases to its initial freezing temperature, T_f.

4. The release of latent heat slows down the cooling until all latent heat of fusion is released.

5. Soil temperatures then decrease if ambient temperatures are below the pore-water freezing point.

6. All free water and most of the bound water is frozen at about −70°C (Andersland and Ladanyi, 2004).

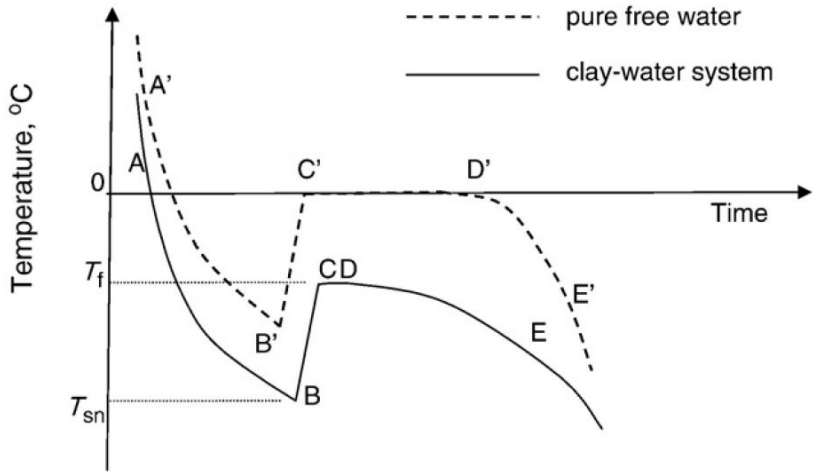

Figure 2.1: Cooling curves for pure free water and the soil-water system (T_f - freezing point for clay-water system, T_{sn} - temperature of spontaneous nucleation for the clay-water system) (Kozlowski, 2009)

Despite the fact that supercooling is needed to initiate ice crystal forming, the incorporation of the temperature of spontaneous nucleation is not considered in the implementation of the constitutive model described in the subsequent chapters. By assuming that the freezing/thawing process of water/ice is to follow the same path, the generally hysteric nature of soil freezing characteristic is not considered in this study.

Many researchers have been engaged in determining the freezing/melting point of a soil-water system (Low et al., 1968; Kozlowski, 2004; Xia et al., 2011; Kozlowski, 2016). However, their approaches are not straightforward. To account for the depression of the freezing/melting point a new empirical approach is proposed in this study.

2.1.2. Governing equations

The needed and used equilibrium equations for the thermo-hydro-mechanical (THM) modelling are presented and described, keeping in mind that emphasis is put on the actual constitutive model. However, the determination of unfrozen water content, cryogenic suction and the formulation of moisture transfer is elaborately described.

Thermodynamic equilibrium

The thermodynamic equilibrium of freezing soil is captured by considering the equilibrium between liquid water and ice phases. This equilibrium is described by the Clausius-Clapeyron equation (Henry, 2000) and can be expressed as follows (Thomas et al., 2009):

$$\frac{p_{ice}}{\rho_{ice}} - \frac{p_w}{\rho_w} = -L \ln \frac{T}{T_f} \tag{2.1}$$

where p_w and p_{ice} indicate the pore water and ice pressure, respectively; ρ_w and ρ_{ice} the density of pore water and ice, respectively, and L is the latent heat of fusion. T represents the current temperature and T_f is the melting/freezing temperature of ice/water for a given soil and pressure. The process of water migration to the freezing zone due to a pressure gradient and temperature gradient is named cryogenic suction, s_c. The freezing zone, also called frozen fringe, can be seen in Figure 2.2. The capillary action due to ice/water interface tension is derived as follows (Thomas et al., 2009)

$$s_c = p_{ice} - p_w \tag{2.2}$$

$$= \rho_{ice}\left(\frac{p_w}{\rho_w} - L \ln \frac{T}{T_f}\right) - p_w \tag{2.3}$$

$$\approx -\rho_{ice} L \ln \frac{T}{T_f} \tag{2.4}$$

According to thermodynamic sign convention pressure is positive. Considering temperatures higher than T_f, the soil is fully saturated with pore water and equations 2.2 to 2.4 are not valid. The cryogenic suction, s_c, is then set to zero.

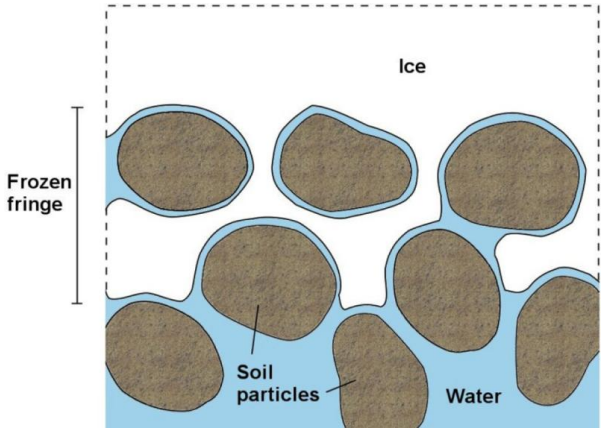

Figure 2.2: Schematic diagram of a freezing soil with a frozen fringe (Peppin and Style, 2012)

The phenomenon of pressure melting can already be described using the Clausius-Clapeyron equation, however the freezing/melting temperature by itself is pressure dependent as well. Probably the most well known and often quoted relation for the pressure dependence of the melting temperature is the empirical equation proposed by Simon and Glatzel (1929). This formulation cannot be used for falling melting curves or curves with maxima (Kechin, 1995). Thus, the application of this formulation to represent the pressure dependence of water freezing and/or ice melting is not appropriate. We therefore propose to use the melting-pressure equation for Ice Ih according to Wagner et al. (2011):

$$\frac{p_{melt}}{p_t} = 1 + \sum_{j=1}^{3} a_j \left(1 - \left(\frac{T}{T_t}\right)^{b_j}\right) \tag{2.5}$$

where $T_t = 273.16$ K refers to the vapour-liquid-solid triple point temperature and $p_t = 611.657$ Pa to the triple point pressure respectively. By substituting

$$p_{melt} = p_{ice} = s_c + p_w \tag{2.6}$$

a pressure-dependent formulation for the freezing/melting temperature, $T_f(p)$ can be obtained

$$\frac{s_c + p_w}{611.657\ \text{Pa}} = 1 + \sum_{j=1}^{3} a_j \left(1 - \left(\frac{T_f}{273.16\ \text{K}}\right)^{b_j}\right). \tag{2.7}$$

The coefficients a_j and exponents b_j are given in Table 2.1.

Table 2.1: Coefficients a_j and exponents b_j of the melting-pressure equation Wagner et al. (2011)

j	a_j [−]	b_j [−]
1	0.119539337×10^7	0.300000×10^1
2	0.808183159×10^5	0.257500×10^2
3	0.333826860×10^4	0.103750×10^3

Pressure melting results in a decrease in cryogenic suction and an increase in water pressure by reducing the thawing temperature of ice. This coupled formulation enables to compute the cryogenic suction s_c and the freezing/melting temperature T_f by providing the actual temperature and the pore water pressure.

Freezing characteristic function

The cooling curve for a soil-water system (Figure 2.1) shows that ice is forming at a freezing temperature T_f. However, not all free pore water freezes at the same temperature in a soil-water system. According to Rempel

et al. (2004), Wettlaufer and Worster (2006) and Zhou (2014), two main mechanisms allow water to remain in its unfrozen state at temperatures below the bulk freezing point. These two mechanisms are namely the curvature-induced premelting and the interfacial premelting mechanism (Figure 2.3). The former is a result of the existence of surface tension of the water meniscus formed between soil particles and is very similar to the capillary suction by bonding grains together. On the contrary, the latter is a result of repulsion forces between ice and solid grains. These forces act as disjoining pressure tending to widen the gap by sucking in more water.

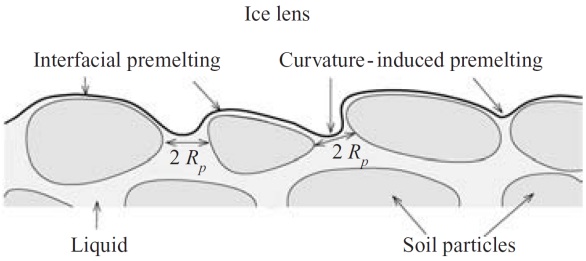

Figure 2.3: Curvature induced premelting and interfacial premelting during intrusion of ice into a wedge-shape wet preferential solid (Wettlaufer and Worster, 2006)

The two mechanisms (see Figure 2.3) could be combined in a single thermodynamic treatment to derive the generalized Clapeyron relationship (see Rempel et al. (2004); Wettlaufer and Worster (2006)). Furthermore Hansen-Goos and Wettlaufer (2010) developed a theoretical description of the premelting of ice contained in a porous matrix, made of a material with a melting temperature substantially larger than ice itself to predict the amount of liquid water in the matrix at temperatures below its freezing point. It combines the interfacial premelting of ice in contact with the matrix, grain boundary melting in the ice, curvature induced premelting and impurities. None of the aforementioned formulations of premelting dynamics are directly applied in this study. However, the aforementioned mechanisms can be captured by considering the cryogenic suction linked to two suction-dependent yield criteria (see Subsection 2.1.3).

The amount of unfrozen water remaining in frozen soil with respect to the freezing temperature can be seen as a soil property and the soil freezing characteristic curve (SFCC) is used to describe this relationship. Due to the analogy of the freezing characteristics and water retention characteristics in unsaturated soils (e.g. Black and Tice (1989); Spaans and Baker (1996); Coussy (2005); Ma et al. (2015)), models like the van Genuchten model (van Genuchten, 1980) and Fredlund and Xing (1994) have been employed to represent the freezing characteristic function (e.g. in Nishimura et al. (2009); Azmatch et al. (2012b)). However, some attempts have also been conducted to find an empirical equation to compute the unfrozen water content w_u (e.g.Tice et al. (1976)). In this study we choose to relate the volumetric unfrozen water content θ_{uw} to the temperature using an empirical formulation based on test results of Anderson and Tice (1972) where the specific surface area (SSA), the bulk density of the unfrozen soil (ρ_b) and the temperature (T) are the only input parameters.

$$\theta_{uw} = \frac{\rho_w}{\rho_b} \exp(0.2618 + 0.5519 \ln(SSA) - 1.4495 (SSA)^{-0.2640} \ln(T_f - T)) \; with \; T \leq T_f \tag{2.8}$$

The specific surface area of a soil is defined as the sum of the surface area of soil particles per unit mass and is expressed in m^2/g. Many physical and chemical soil processes are closely related to the SSA. Sepaskhah et al. (2010) uses a non-linear regression analysis to relate the geometric mean of the soil particle diameter d_g to the measured SSA. This empirical power pedo-transfer function allows the calculation of the specific surface area by just providing the grain size distribution:

$$SSA = 3.89 \cdot d_g^{-0.905} \; [m^2/g] \tag{2.9}$$

with the geometric mean of the soil particle diameter (Shirazi and Boersma, 1984) in millimetres

$$d_g = \exp(m_{cl} \ln d_{cl} + m_{si} \ln d_{si} + m_{sa} \ln d_{sa}) \; [mm] \tag{2.10}$$

where m_{cl}, m_{si}, m_{sa} are clay, silt, and sand mass fractions (%), respectively, and d_{cl}, d_{si}, d_{sa} are the particle size limits separating clay, silt and sand, respectively (d_{cl} = 0.001mm, d_{si} = 0.026mm, d_{sa} = 1.025mm). The

geometric mean and particle size limits are obtained from a texture diagram (Shirazi and Boersma, 1984) which is based on the U.S.D.A. classification scheme, where equivalent diameters are presented in Figure 2.4.

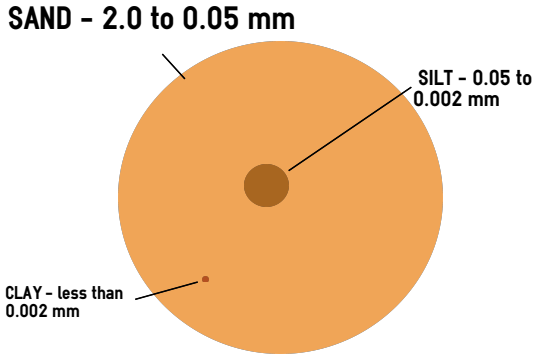

Figure 2.4: U.S.D.A. classification scheme

One main assumption of this new texture diagram is to have a lognormal particle-size distribution within each size fraction. This allows to represent any combination of sand, silt and clay by a geometric (or log) mean particle diameter (d_g, see Equation 2.10) and a geometric standard deviation (σ_g, see Equation 2.19).

By using d_g and σ_g not just the qualitative use but also a quantitative use of textural data is now possible to make judgements of other physical soil properties, like the SSA. Petersen et al. (1996) shows that the magnitude of the specific surface area of a soil depends largely on the amount of clay and type of clay minerals in the soil. However, the fact that the specific surface area differs largely between types of clay minerals can't be taken into account using this textural information approach. Nevertheless, the proposed equation for SSA has also been examined in Fooladmand (2011) and was found to provide a good approximation of the specific surface area of soils. Several reasons have lead to use this empirical approach rather than choosing one of the aforementioned models:

1. Considering engineering practice, it is more likely that the engineer knows the mineralogy of the soil rather than the soil water retention curve (SWRC) and/or the SFCC
2. Despite the fact that the models of van Genuchten (1980) and Fredlund and Xing (1994) are commonly used closed formulations regarding the determination of hydraulic properties of unsaturated soils, the fitting parameters are sensitive and their determination is not a daily geotechnical engineering activity.
3. Limited input data and low effort provide rapid and convenient results when comparing to real test data.
4. By using Campbell's model (Campbell, 1985) which was also proposed in the paper of Tarnawski and Wagner (1996), soil water characteristics like the hydraulic conductivity of partially frozen soils can be calculated. Hence, a closed formulation regarding moisture transfer can be achieved.

Moisture transfer

The law of mass conservation of the moisture for freezing soils can be expressed as (Thomas et al., 2009)

$$\frac{\partial(\rho_w \theta_w dV)}{\partial t} + \frac{\partial(\rho_{ice} \theta_{ice} dV)}{\partial t} + \rho_w \nabla \boldsymbol{v}_w dV + \rho_{ice} \nabla \boldsymbol{v}_{ice} dV = \mathbf{0} \tag{2.11}$$

where the subscripts w and ice refer to pore water and ice respectively; ρ is the density; θ is the volumetric water/ice content; $\boldsymbol{v}$ is the velocity relative to the solid skeleton; dV refers to the volume element of the soil and t is the time. The velocity of pore ice relative to the solid soil skeleton can be ignored, so $\boldsymbol{v}_{ice} = 0$. Moreover, the term dV appears in all the terms and can be cancelled. The equation reduces to

$$\frac{\partial(\rho_w \theta_w)}{\partial t} + \frac{\partial(\rho_{ice} \theta_{ice})}{\partial t} + \rho_w \nabla \boldsymbol{v}_w = \mathbf{0} \tag{2.12}$$

Using the thermodynamics of irreversible processes, Ratkje et al. (1982) propose the transport equation of water given as:

$$\boldsymbol{f_1} = \rho_w \boldsymbol{v}_w = -k(\nabla P + \frac{\rho_{ice} L}{T_f} \nabla T) \tag{2.13}$$

where f_1 is the mass flux in kg/(m^{2}s). Thomas et al. (2009) propose to adapt Darcy's law to describe the pore water flow in terms of piezometric head (Bear and Verruijt, 1987) and to assume the pressure and temperature to be independent driving forces like proposed in Equation 2.13 (Ratkje et al., 1982; Nakano, 1990).

$$\boldsymbol{v}_w = -\frac{k}{\gamma_w} [\nabla (p_w - \gamma_w z) + \frac{\rho_{ice} L}{T_f} \nabla T] \tag{2.14}$$

where γ_w is the unit weight of water; p_w the pore water pressure; z is the depth and k is the hydraulic conductivity. Azmatch et al. (2012b) assert that the most used approach to determine the hydraulic conductivity of partially frozen soils is probably the use of the soil-water-retention curve in combination with different hydraulic conductivity estimation methods (e.g. van Genuchten (1980); Fredlund et al. (1994)). However, this method postulates that the SWRC is known. Relating the SWRC to the SFCC and determining the parameters needed to fit the curve even complicate the determination of the hydraulic conductivity of a partially frozen soil and is not daily engineering practice. The costs for direct measurements, the lack of data, as well as time pressure, require a quick and reliable estimation of hydraulic properties for frozen soil. Tarnawski and Wagner (1996) suggests to calculate the hydraulic conductivity for partially frozen soils by using the hydraulic conductivity function of the same unsaturated soil but unfrozen. This is based on the assumption that partly frozen pores have a similar effect on water flow as air filled pores, i.e., hindering moisture flow and that moisture flow takes place only through the smaller pores filled with water. Taking these assumptions into account, Campbell's model (1985) is used to calculate the hydraulic conductivity for partially frozen soils as:

$$k = k_{sat} (\frac{\theta_{uw}}{\theta_{sat}})^{2b+3} = k_{sat} (S_{uw})^{2b+3} = k_{sat} k_r \text{ [m/s]} \tag{2.15}$$

where θ_{sat} is the volumetric water content of a saturated soil and therefore assumed to be equal to the porosity n. θ_{uw} is the current volumetric unfrozen water content, which can be obtained from the empirical Equation 2.8. The ratio θ_{uw} over θ_{sat} is the so-called unfrozen water saturation S_{uw}, whereas the relative permeability k_r is defined as:

$$k_r = (S_{uw})^{2b+3} \tag{2.16}$$

b is an empirical parameter based on the grain size distribution (Campbell, 1985). k_{sat} is the hydraulic conductivity of saturated soil. Campbell (1985) mentions that the saturated hydraulic conductivity depends on the size and distribution of pores, therefore a number of equations have been derived for predicting this hydraulic property from soil texture. The same book describes an equation for k_{sat} which is obtained from soil texture (considering clay and silt mass fractions), dry bulk density and which weighs clay more heavily than silt. Tarnawski and Wagner (1996) modified this equation slightly and propose the following empirical equation to provide a default value for k_{sat}:

$$k_{sat} = 4 \times 10^{-5} (\frac{0.5}{1-\theta_{sat}})^{1.3b} \cdot \exp(-6.88 m_{cl} - 3.63 m_{si} - 0.025) \text{ [m/s]} \tag{2.17}$$

where m_{cl}, m_{si}, m_{sa} are clay, silt, and sand mass fractions (%), respectively. The empirical parameter b (Campbell, 1985) can be calculated as follows:

$$b = d_g^{-0.5} + 0.2\sigma_g \text{ [}-\text{]} \tag{2.18}$$

where d_g is the geometric mean particle diameter in mm (see Equation 2.10) and σ_g is the geometric standard deviation (Shirazi and Boersma, 1984):

$$\sigma_g = \exp[\sum_{n=1}^{3} m_i (\ln d_i)^2 - (\sum_{n=1}^{3} m_i \ln d_i)^2]^{0.5} \; [-] \tag{2.19}$$

where m_i and d_i are again the particle mass fractions and particle size limits respectively. The parameter b represents the slope of the water potential (ψ) versus the volumetric water content (θ_w) on a log-log scale plot. However, one has to keep in mind that Equation 2.17 is an estimation and will never correctly predict the saturated hydraulic conductivity of a soil which contains large, interconnected cracks or root channels (Campbell, 1985).

Heat transfer

The law of energy conservation of heat for freezing soils can be expressed as (Thomas et al., 2009)

$$\frac{\partial(\boldsymbol{\Phi} dV)}{\partial t} + \nabla \boldsymbol{Q} dV = 0 \tag{2.20}$$

where $\boldsymbol{\Phi}$ and $\boldsymbol{Q}$ refer to the heat content of soil and heat flux per unit volume respectively.

Mechanical equilibrium

Mechanical equilibrium says that the sum of a change in total stresses and body forces is equal to zero and can be written as:

$$\nabla \cdot \boldsymbol{\sigma} + \boldsymbol{b} = 0 \tag{2.21}$$

where $\boldsymbol{\sigma}$ are total stresses and $\boldsymbol{b}$ are body forces.

2.1.3. The mechanical model

The adjacent description of the mechanical model is mainly based on Ghoreishian Amiri et al. (2016). In their paper an initial version of the constitutive model is described. Revisions regarding the yield surface formulation and the plastic potential formulation are incorporated in my thesis. The proposed model is a critical-state elasto-plastic mechanical soil model formulated within the framework of two-stress state variables. The stress state variables are the cryogenic suction and the solid phase stress. The latter is considered as the combined stress of soil grains and ice and is defined as

$$\boldsymbol{\sigma^*} = \boldsymbol{\sigma} - S_{uw} p_w \boldsymbol{I} \tag{2.22}$$

where $\boldsymbol{\sigma^*}$ is the solid phase stress, $\boldsymbol{\sigma}$ is the net stress, S_{uw} is the unfrozen water saturation, p_w is the pore water pressure and $\boldsymbol{I}$ denotes the unit tensor. According to this formulation the saturated frozen soil can be viewed as a porous material composed of soil grains and ice in which the pores are filled with water. Ice is part of the solid phase stress because it is able to bear shear stresses. This kind of effective stress based formulation is a Bishop single effective stress, which involves the unfrozen water saturation S_{uw} as the effective stress parameter or Bishop's parameter. The solid phase stress is able to reflect the effect of unfrozen water on the mechanical behaviour. The cryogenic suction, used as the second state variable, allows to build a complete hydro-mechanical framework. By considering the cryogenic suction, it is possible to take the effects of ice content and temperature variation into account. Any strain increment can therefore be additively decomposed into:

$$d\epsilon = d\epsilon^{me} + d\epsilon^{se} + d\epsilon^{mp} + d\epsilon^{sp} \tag{2.23}$$

where $d\epsilon^{me}$ and $d\epsilon^{mp}$ are the elastic and plastic parts of strain due to the solid phase stress variation; $d\epsilon^{se}$ and $d\epsilon^{sp}$ the elastic and plastic parts of strain due to cryogenic suction variation, respectively.

Elastic response

The elastic part of the strain due to the solid phase stress variation can be calculated based on the equivalent elastic parameters of the mixture:

$$K = (1 - S_{ice}) \frac{(1+e) p^*_{y0}}{\kappa_0} + \frac{S_{ice} E_f}{3(1-2\nu_f)} \tag{2.24}$$

$$G = (1 - S_{ice}) G_0 + \frac{S_{ice} E_f}{2(1+\nu_f)} \tag{2.25}$$

where G and K are the equivalent stress-dependent shear modulus and bulk modulus of the mixture, respectively. κ_0 and G_0 stand for the constant elastic compressibility coefficient and the shear modulus of the soil in an unfrozen state, respectively. p^*_{y0} is the pre-consolidation stress for unfrozen condition, E_f and ν_f denote the Young's modulus and Poisson's ratio of the soil in the fully frozen state, respectively. Finally, S_{ice} is the ice saturation, which in a fully saturated soil can be determined as follows:

$$S_{ice} = (1 - S_{uw}) \tag{2.26}$$

where S_{uw} is the unfrozen water saturation. Considering the temperature-dependent behaviour of ice:

$$E_f = E_{f,ref} - E_{f,inc}(T - T_{ref}) \tag{2.27}$$

where $E_{f,ref}$ is the value of E_f at a reference temperature T_{ref} and $E_{f,inc}$ is considered as the rate of change in E_f with temperature. Having defined the elastic part of the strain due to the solid phase stress variation, the elastic part of the strain due to suction variation can be computed as follows

$$d\epsilon^{se} = \frac{\kappa_s}{1+e} \times \frac{ds_c}{(s_c + p_{at})} \tag{2.28}$$

where κ_s is the compressibility coefficient due to suction variation within the elastic region, $(1+e)$ is the specific volume with e the void ratio and p_{at} is the atmospheric pressure. The atmospheric pressure is added to s_c to avoid infinite values when s_c approaches zero.

The volumetric and shear elastic components of strain are then given by

$$d\epsilon^e_v = \frac{1}{K} dp^* + \frac{\kappa_s}{1+e} \frac{ds_c}{(s_c + p_{at})} \tag{2.29}$$

$$d\epsilon^e_q = \frac{1}{3G} dq^* \tag{2.30}$$

where K and G can be obtained using Equation 2.24 and 2.25 respectively. dp^* is the change in solid phase mean stress and dq^* is the change in solid phase deviatoric stress respectively.

Yield surfaces

In an unfrozen state the model becomes a conventional critical state model. In other words when the value of cryogenic suction equals zero, the model reduces to a common unfrozen soil model. The simple modified Cam-clay model is adopted for the unfrozen state. Considering the frozen state, two suction-dependent yield functions are applied to account for the premelting effects described in Section 2.1.1. To take the curvature-induced premelting effect into account which acts by bonding the grains together, a yield criterion expanding the yield surface with increasing suction is considered. Based on the Barcelona Basic Model (BBM) (Alonso et al., 1990) the so-called loading collapse (LC) yield surface due to variation of solid phase stress is expressed as

$$F_1 = (p^* + k_t s_c)[(p^* + k_t * s_c){S_{uw}}^m - (p_y^* + k_t s_c)] + \frac{(q^*)^2}{M^2} = 0 \tag{2.31}$$

where

$$p_y^* = p_c^* (\frac{p_{y0}^*}{p_c^*})^{\frac{\lambda_0 - \kappa}{\lambda - \kappa}} \tag{2.32}$$

$$\lambda = \lambda_0[(1-r)exp(-\beta s_c) + r] \tag{2.33}$$

and p^* is the solid phase mean stress, q^* is the solid phase deviatoric stress, M denotes the slope of the critical state line (CSL), k_t is the parameter for describing the increase in apparent cohesion with cryogenic suction, p_c^* indicates the reference stress, and κ denotes the compressibility coefficient of the system within the elastic region. κ now reflects the compressibility coefficient of the soil composite as a whole (Equation 2.34). Thus, κ is to some extent pressure and temperature dependent as well. Furthermore, λ_0 is the elasto-plastic compressibility coefficient for unfrozen state along virgin loading, r is a constant related to the maximum stiffness of the soil (for infinite cryogenic suction) and β is a parameter controlling the rate of change in soil stiffness with cryogenic suction.

$$\kappa = \frac{1+e}{K} p_{y0}^* \tag{2.34}$$

With decreasing temperature, the amount of water remaining unfrozen decreases. At a fully frozen state, when there is very little unfrozen water content, the soil should behave like pure ice or ice rubble. The behaviour of pure ice is comparable with the one of metal, whereas the one of ice rubble is similar to the one of sand. Considering the isotropic behaviour of sand, it is observed that it will crack or crush but there is no yield without shearing. The most common model used for simulating sand or ice rubble is Mohr-Coulomb. To account for this behaviour the Cam-Clay type yield surface has to migrate to a Mohr-Coulomb like yield surface at a low unfrozen water saturation. This issue is covered by considering and incorporating the dependence of the unfrozen water saturation S_{uw}. The exponent m dictates how much this behaviour wants to be taken into account. The magnitude of m has to be chosen in the range between 0 and 1.

This formulation, therefore, is able to change from a Cam-Clay type (which is able to yield with isotropic compression) for high unfrozen water saturation to a Mohr-Coulomb type (where there is no yield for isotropic compression) for very low unfrozen water saturation. However, also at a very low unfrozen saturation the yield surface still has a cap (see 2.5). The cap disappears when S_{uw} equals zero.

The curvature-induced premelting effect, discussed in Section 2.1.1, acts by bonding the grains together. The resulting compressive deformation is considered as the elastic part of the deformation due to suction variation. When the premelting dynamic behaviour is dominated by the interfacial premelting mechanism, an increase in cryogenic suction leads to grain segregation and ice lens formation, and results in soil expansion. This deformation is considered as the part of the deformation due to suction variation which induces irrecoverable strains, the so called plastic part. Therefore, a simple second suction-dependent yield criterion is adopted to capture this phenomenon. The Grain Segregation (GS) yield criterion can be written as follows:

$$F_2 = s_c - s_{c,seg} \tag{2.35}$$

where $s_{c,seg}$ is the threshold value of suction for ice segregation phenomenon and bounds the transition from the elastic state to the virgin range when cryogenic suction is increased. Figure 2.6 illustrates the three-dimensional view of the yield surfaces in the $p^* - q^* - s_c$ space.

Hardening rules

Irreversible deformations control the position of the LC and GS yield surfaces. However, both yield curves in the $p^* - s_c$ stress space are not considered to move independently but the following definite coupling between them is proposed.

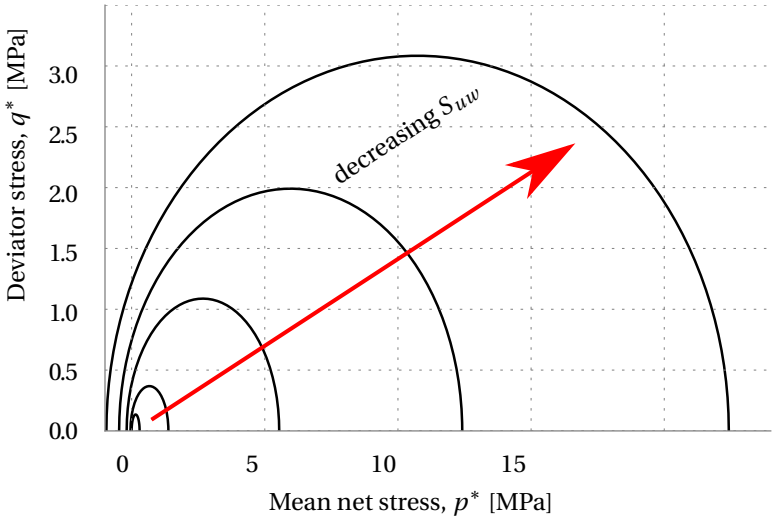

Figure 2.5: Yield surface evolution at constant $m = 1$ and decreasing unfrozen water saturation

According to Ghoreishian Amiri et al. (2016), considering a plastic compression due to variation of solid phase stress results on the one hand in a stiffer behaviour and causes the LC yield surface to move outward and on the other hand, this plastic compression results in a decrease in the dimension of voids. A lower segregation threshold value is, therefore, expected. Figure 2.7a indicates this coupling hardening rule, which causes the LC yield surface to expand and the GS yield surface to shift downward.

Additionally, a plastic dilation due to the occurrence of ice segregation causes the GS yield surface to move upward, and reversely results in a softer behaviour of the soil, provoking an inward movement of the LC yield surface. This coupling rule is shown in Figure 2.7b. To couple both yield curves, it is chosen that their position is controlled by the total plastic volumetric deformation.

$$d\epsilon_v^p = d\epsilon_v^{mp} + d\epsilon_v^{sp} \tag{2.36}$$

As a starting point the increase of p^* in the elastic region induces a compressive volumetric deformation. Adopting a linear dependence between the specific volume $v = 1 + e$ and $\ln p^*$, both in the elasto-plastic and elastic range, one may write for the elastic region

$$d\epsilon_v^{me} = \frac{\kappa}{1+e}\frac{dp^*}{p^*} \tag{2.37}$$

Once the net mean stress p^* reaches the yield value p_y^* the total volumetric deformation may be computed as follows

$$d\epsilon_v^{m} = \frac{\lambda}{1+e}\frac{dp_y^*}{p_y^*} \tag{2.38}$$

and, therefore, the plastic component of volumetric strain due to an increase in p_y^* will be given by

$$d\epsilon_v^{mp} = \frac{\lambda-\kappa}{1+e}\frac{dp_y^*}{p_y^*} \tag{2.39}$$

Taking into account equation 2.32 for the LC yield locus,

$$\frac{p_y^*}{p_c^*} = \left(\frac{p_{y0}^*}{p_c^*}\right)^{\frac{\lambda_0-\kappa}{\lambda-\kappa}} \tag{2.40}$$

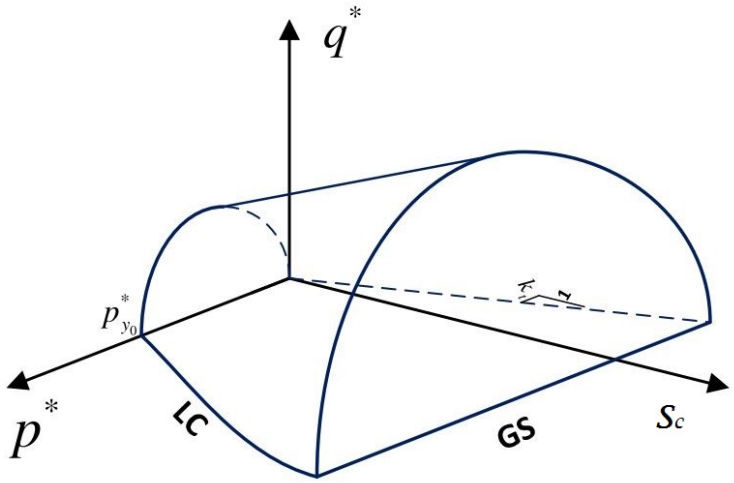

Figure 2.6: Exemplary three-dimensional view of the yield surfaces in $p^* - q^* - s_c$ space (based on Ghoreishian Amiri et al. (2016))

it is simple to show that the plastic volumetric strain (equation 2.39) is also given by

$$d\epsilon_v^{mp} = \frac{\lambda_0 - \kappa}{1+e} \frac{dp^*_{y0}}{p^*_{y0}} \tag{2.41}$$

Combining Eq. 2.40 and 2.41 results in

$$\frac{dp^*_{y0}}{p^*_{y0}} = \frac{1+e}{\lambda_0 - \kappa} d\epsilon_v^{mp} \tag{2.42}$$

Assuming the similar effect from the plastic deformation due to suction variation (equation 2.36), the hardening rule for the LC yield surface can be expressed as

$$\frac{dp^*_{y0}}{p^*_{y0}} = \frac{1+e}{\lambda_0 - \kappa} (d\epsilon_v^{mp} + d\epsilon_v^{sp}) \tag{2.43}$$

Similarly, adopting the same assumptions for the behaviour in the $v : \ln(s_c + p_{at})$ plane, and considering the contractive and dilative behaviour of the soil with respect to the curvature-induced and interfacial premelting mechanisms, an increase in cryogenic suction within the elastic region results in

$$d\epsilon_v^{se} = \frac{\kappa_s}{1+e} \frac{ds_c}{s_c + p_{at}} \tag{2.44}$$

and, if the yield locus $s_c = s_{c,seg}$ is reached, the following total and plastic deformations will be induced

$$d\epsilon_v^{s} = -\frac{\lambda_s}{1+e} \frac{ds_{c,seg}}{s_{c,seg} + p_{at}} \tag{2.45}$$

$$d\epsilon_v^{sp} = -\frac{\lambda_s + \kappa_s}{1+e} \frac{ds_{c,seg}}{s_{c,seg} + p_{at}} \tag{2.46}$$

Rearranging Eq. 2.46, results in

$$\frac{ds_{c,seg}}{s_{c,seg} + p_{at}} = -\frac{1+e}{\lambda_s + \kappa_s} d\epsilon_v^{sp} \tag{2.47}$$

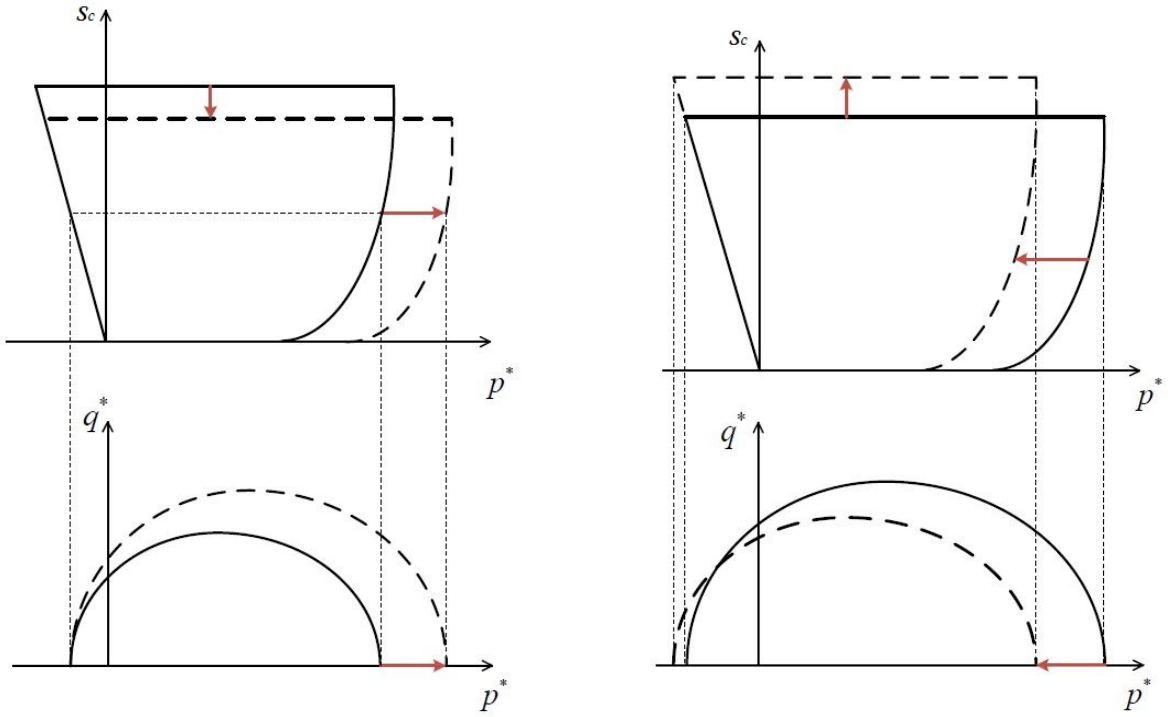

(a) Plastic compression due to variation of solid phase stress

(b) Plastic dilation due to occurrence of ice segregation

Figure 2.7: Coupling of the GS- and the LC-yield curves (Ghoreishian Amiri et al., 2016)

Assuming the similar effect from the plastic deformation due to solid phase stress variation (Eq. 2.36), the hardening rule for the GS yield surface can be expressed as

$$\frac{ds_{c,seg}}{s_{c,seg}+p_{at}} = -\frac{1+e}{\lambda_s+\kappa_s}(d\epsilon_v^{sp}+d\epsilon_v^{mp}) \tag{2.48}$$

However, the interfacial premelting mechanism acts by sucking in more water. The availability of water is therefore essential to have a higher influence of this mechanism on the accumulation of plastic strains. The lower the unfrozen water saturation of the freezing fringe, the lower the permeability for water to be sucked in. This results in a smaller amount of possible strains due to increase of cryogenic suction. The plastic resistance of the soil increases with decreasing water saturation. In very low water saturation, by decreasing temperature, cryogenic suction will increase, while due to very limited relative permeability, very little water can come in; there is thus no possibility for the volume to increase. The GS curve should be able to move upward without any change in the volume. This is also consistent with the reality: if there is no water to come in, increasing cryogenic suction will not result in frost heave. Adopting this modifications, the hardening rule of the GS yield surface is proposed as follows:

$$\frac{ds_{c,seg}}{s_{c,seg}+p_{at}} = -\frac{1+e}{S_{uw}(\lambda_s+\kappa_s)}d\epsilon_v^{sp} - \frac{1+e}{\lambda_s+\kappa_s}(1-\frac{s_c}{s_{c,seg}})d\epsilon_v^{mp} \tag{2.49}$$

Flow rules

Regarding the direction of plastic strain increments, associated with the LC yield surface a non-associated flow rule in the planes $s_c = constant$ is used. For the GS yield surface an associated flow rule is employed instead

$$d\boldsymbol{\epsilon}^{mp} = d\lambda_1 \frac{\partial Q_1}{\partial \boldsymbol{\sigma}^*} \tag{2.50}$$

$$d\boldsymbol{\epsilon}^{sp} = -d\lambda_2 \frac{\partial F_2}{\partial s_c}\boldsymbol{I} \tag{2.51}$$

where $d\lambda_1$ and $d\lambda_2$ are the plastic multiplier regarding LC and GS yield surfaces and can be obtained through plastic consistency conditions. Q_1 is the plastic potential function defined as

$$Q_1 = {S_{uw}}^{\gamma}[p^* - (\frac{p_y^* - k_t s_c}{2})]^2 + \frac{(q^*)^2}{M^2} \tag{2.52}$$

where S_{uw} is the unfrozen water saturation and γ is the plastic potential parameter. This plastic potential parameter is added to have more control on the volumetric behaviour. Considering the volumetric behaviour for a frozen soil having a high unfrozen water saturation, there is significant amount of water in the pores; this water is able to move and provides the possibility of plastic volume changes. However, when the unfrozen water saturation is very low, there is no water to move, and the frozen soil will behave like a non-porous material. By increasing ice content, the plastic potential surface will change from an ellipse to a straight line, since the tendency of volume change is decreasing by increasing ice saturation. In the unfrozen state, the plastic potential function is identical to the yield surface. This so-called associated plasticity is also used in the modified Cam clay model (MCC).

2.1.4. Model parameters

The current model requires seventeen parameters in total (see Table 2.2). Eleven parameters describe the behaviour under the variation of solid phase stress, these are namely κ_0, G_0, $E_{f,ref}$, $E_{f,inc}$, ν_f, p_{y0}^*, p_c^*, λ_0, M, m, and γ. Three parameters describe the behaviour regarding to suction-induced strains: $s_{c,seg}$, λ_s and κ_s. Finally, β, r and k_t account for coupling effects between variation of solid phase stress and cryogenic suction. The determination of the parameters is explained in Chapter 4.

Table 2.2: Model parameters of the constitutive model

Parameter	Description	Unit
G_0	Unfrozen soil shear modulus	$\mathrm{N/m^2}$
κ_0	Unfrozen soil elastic compressibility coefficient	–
$E_{f,ref}$	Frozen soil Young's modulus at a reference temperature	$\mathrm{N/m^2}$
$E_{f,inc}$	Rate of change in Young's modulus with temperature	$\mathrm{N/m^2/K}$
ν_f	Frozen soil Poisson's ratio	–
m	Yield parameter	–
γ	Plastic potential parameter	–
$(p_{y0}^*)_{in}$	Initial pre-consolidation stress for unfrozen condition	$\mathrm{N/m^2}$
p_c^*	Reference stress	$\mathrm{N/m^2}$
λ_0	Elasto-plastic compressibility coefficient for unfrozen state	–
M	Slope of the critical state line	–
$(s_{c,seg})_{in}$	Segregation threshold	$\mathrm{N/m^2}$
κ_s	Elastic compressibility coefficient for suction variation	–
λ_s	Elasto-plastic compressibility coefficient for suction variation	–
k_t	Rate of change in apparent cohesion with suction	–
r	Coefficient related to the maximum soil stiffness	–
β	Rate of change in soil stiffness with suction	$(\mathrm{N/m^2})^{-1}$

3

Validation of the empirical approach to obtain the soil freezing characteristic curve and hydraulic soil properties

An empirical approach is suggested in Section 2.1.2 to obtain the soil freezing characteristic curve (SFCC) as well as the hydraulic properties of a given soil. The described procedure contains a mathematical model for predicting the unfrozen water content and the hydraulic conductivity of partially frozen soils on the basis of limited input data such as grain size distribution and porosity. However, further consideration of the pressure dependence of the freezing/melting temperature of water/ice even allows to account for the freezing/melting point depression and thus the phenomenon of pressure melting. Knowing that extensive field tests and laboratory tests are time-consuming and expensive, by applying this practical approach it is possible to sidestep unfrozen water content and temperature measurements inside soil samples. Good and rapid estimations of soil properties can be obtained for any freezing soil having a log-normal grain size distribution. The following sections show quantitative and qualitative confirmation of the proposed empirical approaches.

3.1. Soil freezing characteristic curve

The SFCC is the relation between freezing soil temperatures and unfrozen water content. Although the widespread use of the time-domain reflectometry (TDR) has become a well-established method to measure unfrozen water content in partially frozen soils, the determination of the SFCC by means of the particle size distribution (PSD) and void ratio seems more user-friendly and avoids additional input parameters. The verification and validation of this approach using limited input data are conducted in the following sections. Soil type and pressure dependence of the SFCC are investigated by comparing estimated volumetric unfrozen water contents over temperature and measured SFCC. The measured data is obtained from Smith and Tice (1988) and Zhang et al. (1998).

3.1.1. Soil type dependence

Smith and Tice (1988) performed measurements of unfrozen water content on a variety of soils. Their selection cover a representative range in grain size distribution as well as specific surface area (SSA). The soil samples were fully saturated with distilled water. Initially the soil samples were cooled to between -10 °C and -15 °C and progressively warmed to 0 °C. The unfrozen water content at 0 °C equals the porosity of the soil sample. The method of warming the sample might provide slightly different results of the unfrozen water content than when freezing the sample. One of the reasons is that the pore water has to overcome the supercooling effect (Kozlowski, 2009). The test results of Oliphant et al. (1983) on Morin Clay and the ones from Williams (1963) show this effect.

Smith and Tice (1988) don't provide the grain size distribution curve of the different soils, they are therefore estimated by taking the limiting values of the U.S.D.A. soil triangle into account. The assumed particle size mass fractions are given in Table 3.1 and are visualised in Fig. 3.1.

The SFCC obtained by the time domain reflectometry (TDR) method of five different soils and the calculated comparison graphs are presented in Fig. 3.2. The graph clearly shows that the suggested approach,

Table 3.1: Assumed particle size mass fractions for soils tested in Smith and Tice (1988)

Soil	m_{clay}	m_{silt}	m_{sand}
Castor Sandy Loam	0.06	0.22	0.72
Athena Silt Loam	0.15	0.58	0.27
Niagara Silt	0.08	0.87	0.05
Suffielt Silty Clay	0.41	0.41	0.18
Regina Clay	0.52	0.25	0.23

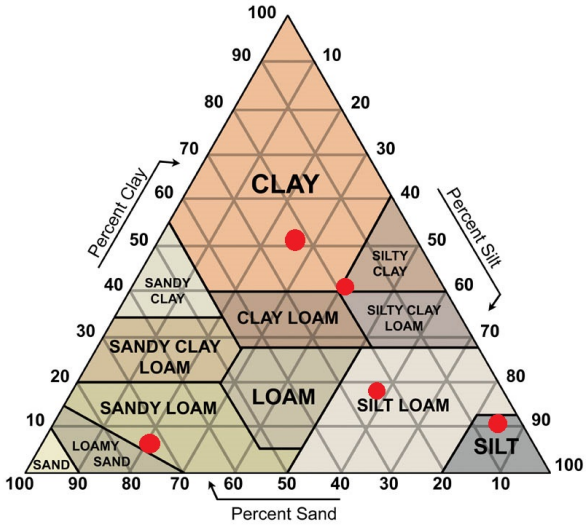

Figure 3.1: USDA soil triangle

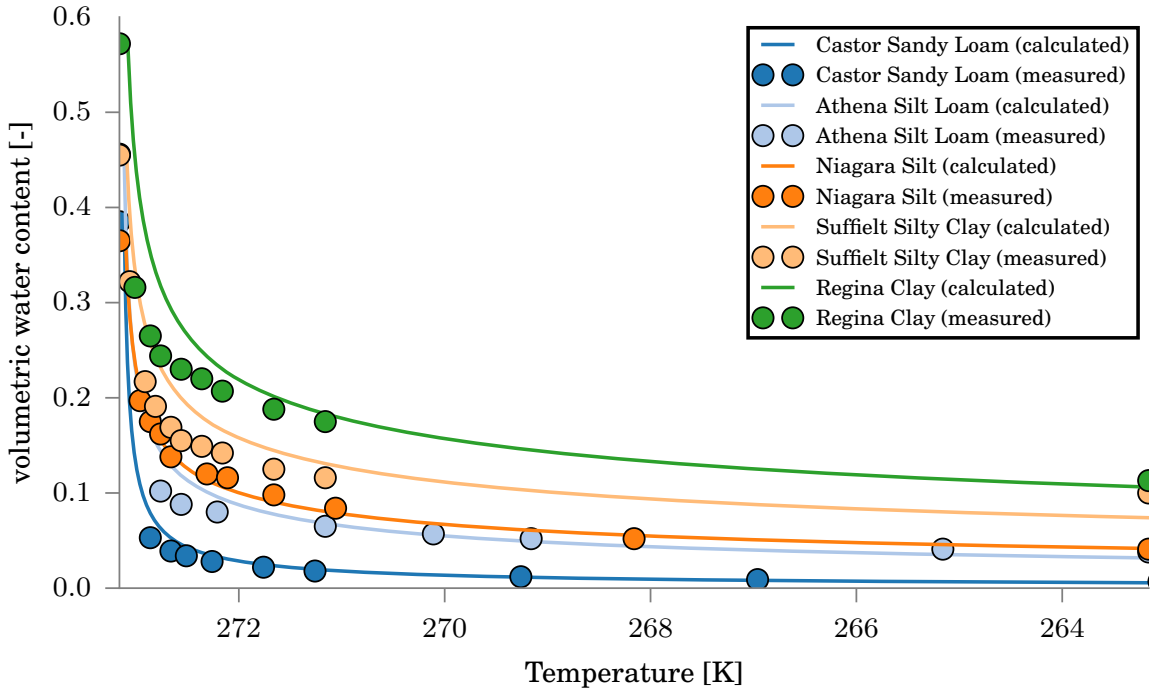

Figure 3.2: Comparison of measured and calculated SFCC for Castor sandy loam, Athena silt loam, Niagara Silt, Suffielt silty clay and Regina clay

using the mineralogy of soils, is appropriate as a first and default approach to obtain the SFCC for most soil types. The higher the amount of fines, the higher the specific surface area. This allows a higher capability to hold a certain amount of unfrozen water and hence causes a freezing point depression (Petersen et al., 1996; Andersland and Ladanyi, 2004; Watanabe and Flury, 2008). The calculated soil freezing characteristic curves not only present the correct qualitative behaviour but also show a good quantitative agreement.

3.1.2. Pressure dependence

The pressure dependence of the freezing point as explained in Section 2.1 also affects the amount of water kept unfrozen at negative temperatures. The relationship between unfrozen water content and pressure is important in studying the physical properties and mechanical behaviours of frozen soils under high pressure (Zhang et al., 1998). To validate this relationship experimental data from Zhang et al. (1998) is chosen. The soil used is a Lanzhou Loess. Its particle size mass fractions are $m_{clay} = 0.12$, $m_{silt} = 0.80$ and $m_{sand} = 0.08$. The applied pressure on the sample in the test tube is 0, 8, 16, 24, 32 and 40 MPa, respectively. The pressure is kept constant at every stage while determining the unfrozen water content of the frozen soil at different negative temperatures. The pore water pressure is set equal to the applied pressure on the sample. The initial void ratio is assumed to be 0.7, which equals a porosity of $n = 0.41$. Figure 3.3 provides the comparison between measured data and calculated SFCC at the six different pressure levels.

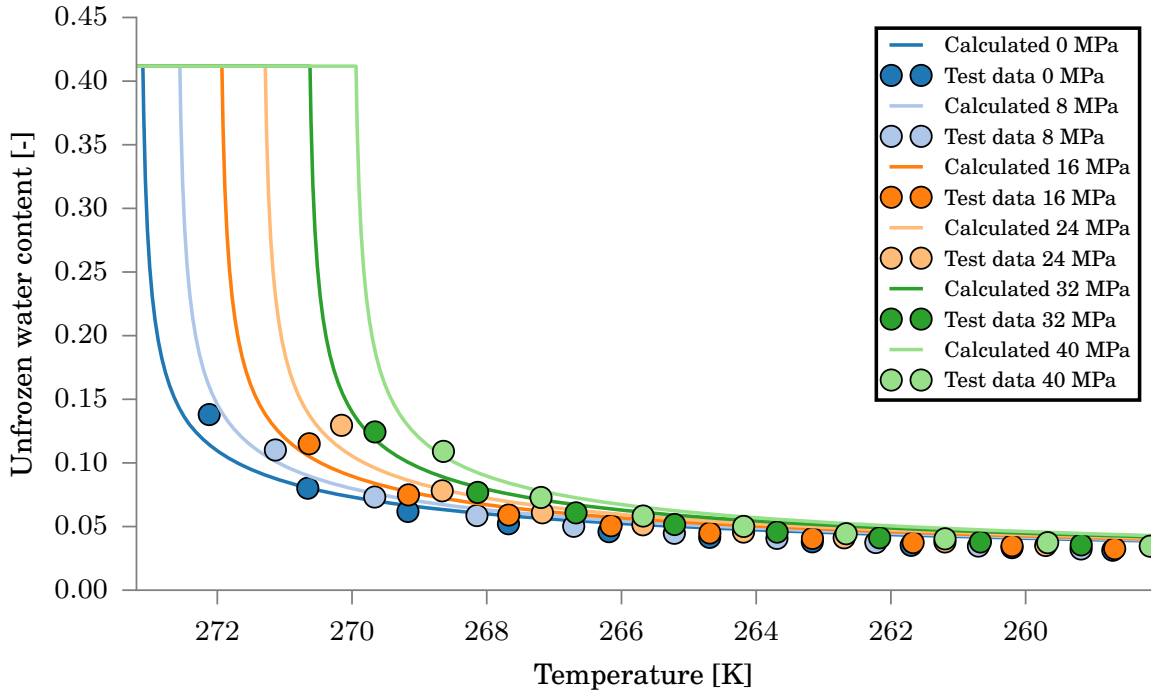

Figure 3.3: Comparison of measured and calculated SFCC of Lanzhou Loess at high pressures

Figure 3.3 reproduces accurately the ability of the empirical formulation to compute the volumetric unfrozen water content after Anderson and Tice (1972) by considering the pressure dependence of the freezing point (Equation 2.7).

3.2. Hydraulic properties

Knowing hydraulic properties is not only important for unfrozen soils but also for partially frozen soils. Flow in the frozen soil is important in detailed analysis of a number of periglacial landforms and processes, such as thermokarst, patterned ground and soil creep (Burt and Williams, 1976). The interest in the hydraulic conductivity has also increased due to the need for improved prediction methods and environmental concerns (Andersland et al., 1996; Andersland and Ladanyi, 2004). Furthermore, water movement in frozen soil may have a significant role in frost heave. It may affect the slope stability as well as highway and pipeline construction.

In Section 2.1.2 the approach to estimate the saturated hydraulic conductivity, k_{sat}, as well as the hydraulic conductivity for partially frozen soil, k, is explained. The following sections try to give a deeper insight whether their use is justified or not.

3.2.1. Saturated hydraulic conductivity

The saturated hydraulic conductivity, k_{sat}, is a hydraulic property of water-saturated unfrozen ground. k_{sat} depends on the size and the distribution of the pores and is generally assumed to remain constant for a given material and location. However, sometimes k_{sat} is not known in engineering practice. In this case the use of Equation 2.17 provides an empirical estimation of the saturated hydraulic conductivity for soil types having a lognormal particle size distribuation (PSD) within each size fraction.

To validate this empirical approach, soil textural classes and related saturated hydraulic conductivity classes provided by U.S.D.A. are chosen to be comparative values. The calculated k_{sat} values are obtained by using the default grain size distribution of the U.S.D.A. soil textural classes and appropriate ranges of their void ratio (Table 3.2). The comparison of calculated and provided ranges for the saturated hydraulic conductivity can be seen in Figure 3.4.

Table 3.2: Particle size mass fractions according to the U.S.D.A. soil textural classes and assumed void ratio ranges

Soil	m_{clay}	m_{silt}	m_{sand}	e_{min}	e_{max}
Sand	0.04	0.04	0.92	0.30	0.75
Loamy Sand	0.06	0.11	0.83	0.30	0.90
Sandy Loam	0.11	0.26	0.63	0.30	1.00
Loam	0.20	0.40	0.40	0.30	1.00
Silt	0.06	0.87	0.07	0.40	1.10
Silty Loam	0.14	0.14	0.21	0.40	1.10
Sandy Clay Loam	0.28	0.12	0.60	0.30	0.90
Clayey Loam	0.34	0.34	0.32	0.50	1.20
Silty Clay Loam	0.34	0.55	0.11	0.40	1.10
Sandy Clay	0.42	0.05	0.53	0.30	1.80
Silty Clay	0.48	0.45	0.07	0.30	1.80
Clay	0.70	0.13	0.17	0.50	1.80

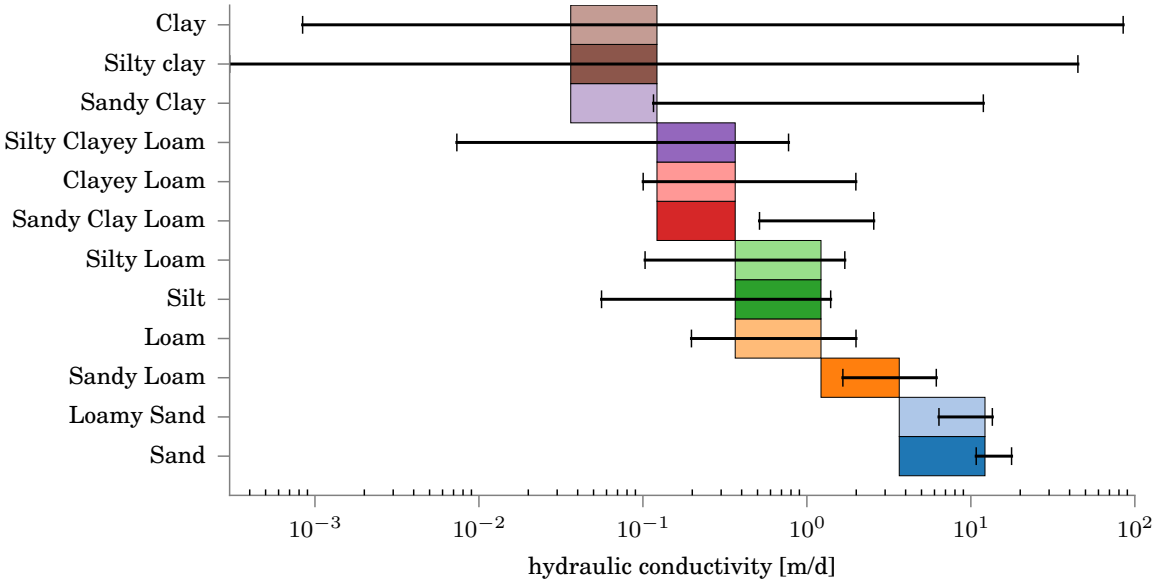

Figure 3.4: Comparison of saturated hydraulic conductivity ranges - U.S.D.A. ranges (coloured bars) vs. calculated k_{sat} ranges based on the PSD and the void ratio (lines)

By comparing the ranges provided by U.S.D.A. (coloured bars in Figure 3.4) with the calculated k_{sat} ranges (lines) it can be seen that the range of the estimated k_{sat} values is highly dependent on the void ratio. The U.S.D.A. rates shown for saturated hydraulic conductivity in relation to texture are only a general guide and differences in bulk density may alter the rate. This dependence on the initial void ratio of the soil is demonstrated in this graph when looking at the calculated ranges where a minimum void ratio (loose state) and a maximum void ratio (dense state) is considered. Two soil types, namely sandy clay and sandy clay loam show significant deviation between the two illustrated ranges. However, all other U.S.D.A. soil types show conformity with the estimated values. One has to keep in mind, that estimating the saturated hydraulic conductivity using this approach is only suggested when there is no other available information on the actual k_{sat}. Still, budding estimations can be expected (see Figure 3.6).

3.2.2. Hydraulic conductivity of frozen soil

Many researchers contributed to the determination and measurements of hydraulic properties of frozen soil: Burt and Williams (1976), Horiguchi and Miller (1983), Oliphant et al. (1983), Benson and Othman (1993), Andersland et al. (1996), Tarnawski and Wagner (1996), McCauley et al. (2002) and Watanabe and Wake (2009). However, due to major challenges in measuring the hydraulic conductivity of partially frozen soils, only a limited number of experimental data is available. One of the first direct measurement of hydraulic conductivity of partially frozen soil was conducted by Burt and Williams (1976). They found that the hydraulic conductivity coefficient depends on soil type and temperature and is related to the unfrozen water content. At temperatures within a few tenths of 0 °C, the coefficient apparently ranges from 10^{-5} to 10^{-9} cm/s, and decreases only slowly below about -0.5 °C. Furthermore, they showed that soils known to be susceptible to frost heave have significant hydraulic conductivities well below 0 °C. Horiguchi and Miller (1983) measured the hydraulic conductivity of frozen soils as a function of temperature in the range of 0 °C to −0.35 °C. Due to the fact that direct measurements are difficult to make, their results may present some inaccuracies. Therefore, indirect measurements and empirical approaches to obtain hydraulic properties of partially frozen soils have become the general approach, which is presented in Azmatch et al. (2012b) and is explained in Section 2.1.2.

The test data of Burt and Williams (1976) and Horiguchi and Miller (1983) serve as a comparison basis. The hydraulic conductivity values can be estimated using Equation 2.15. This equation makes use of the PSD, as well as Equation 2.8 to obtain the volumetric unfrozen water content empirically and Equation 2.17 to predict the saturated hydraulic conductivity. The comparison between estimated and predicted values of hydraulic conductivities is illustrated in Figures 3.5 and 3.6. For the comparison with measured data from Burt and Williams (1976) k_{sat} was estimated using Equation 2.15, whereas for the comparison with measured data from Horiguchi and Miller (1983) a value of 10^{-8} m/s is chosen. The PSD was given for most of the soil types. The initial void ratio, however, had to be estimated. In Table 3.3 the used values are shown.

Table 3.3: Particle size distribution and void ratio for tested soils in Burt and Williams (1976) and Horiguchi and Miller (1983)

Soil	m_{clay}	m_{silt}	m_{sand}	e_0
Chena Silt	0.05	0.88	0.07	0.48
NWA Silt	0.02	0.85	0.13	0.50
Manchester Silt	0.04	0.96	0.00	0.43
Carleton Silt	0.03	0.40	0.57	0.60
Oneyda Clayey Silt	0.28	0.42	0.30	0.60
Leda Clay	0.40	0.45	0.15	0.50
Fine Sand	0.06	0.06	0.88	0.50

A very crucial issue, which both measured data show, is the drop in hydraulic conductivity occurring within a very small temperature range of less than 0.50 °C. This drop can be reproduced by using the proposed approach. The zone of a freezing soil where this temperature range appears is the so-called frozen fringe (see Figure 2.2). Another conclusion is that after this sudden steep decline in hydraulic conductivity a threshold value is reached, meaning that no further relevant decrease in k is expected. The minimum k value is therefore related to the initial saturated hydraulic conductivity, k_{sat}, and chosen to be $k_{sat} \times 10^{-6}$. This limiting value is important regarding the numerical implementation of the moisture transfer equation in order to avoid numerical problems.

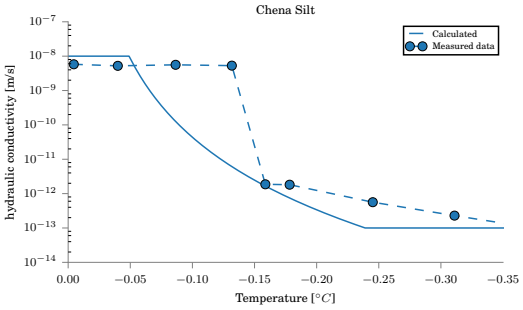

(a) Chena Silt

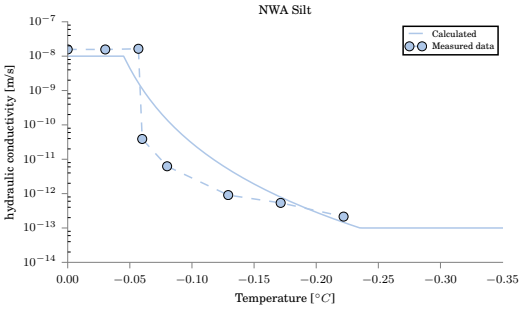

(b) NWA Silt

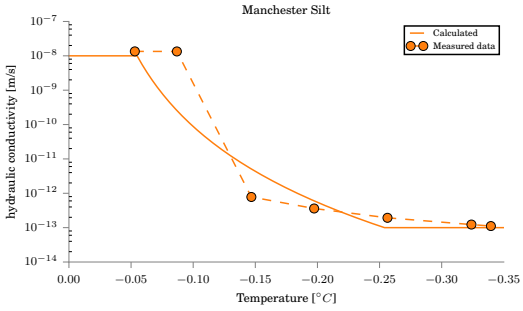

(c) Manchester Silt

Figure 3.5: Comparison of measured and estimated hydraulic conductivities of different frozen soil types (Horiguchi and Miller, 1983)

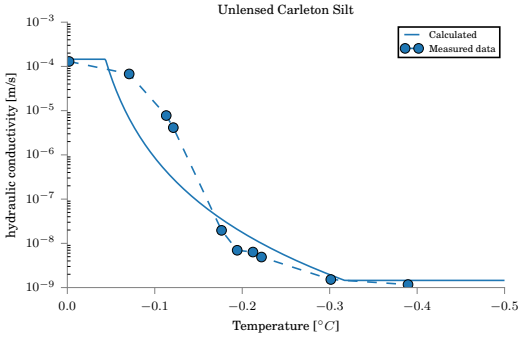

(a) Unlensed Carlton Silt

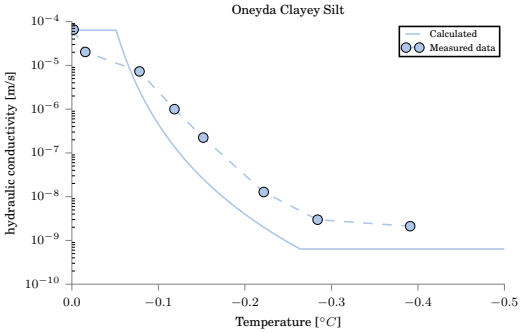

(b) Oneyda Clayey Silt

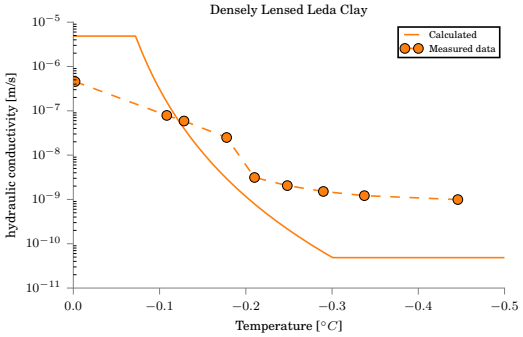

(c) Densely Lensed Leda Clay

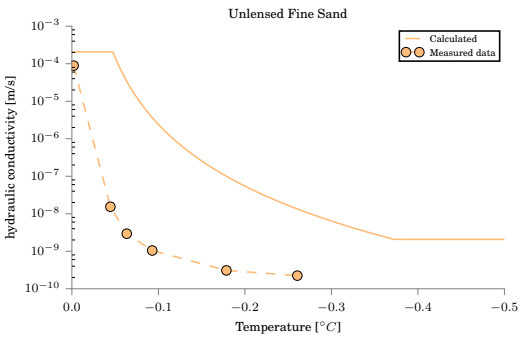

(d) Unlensed Fine Sand

Figure 3.6: Comparison of measured and estimated hydraulic conductivities of different frozen soil types(Burt and Williams, 1976)

4

Parameters and their determination

Every model result is highly dependent on the right choice of input parameters. One has to keep in mind, that the selection of inappropriate parameters can end up with some unexpected results. However, proper determination of soil parameters is related to laboratory testing and therefore time-consuming and expensive. Furthermore, the quality of the sample and of the experiment itself play a vital role in determining soil parameters. Considering the Barcelona Basic Model for unsaturated soil, on which the constitutive model for frozen and unfrozen soil is based upon, it is more employed by researchers than by practitioners. Although it is the best known elasto-plastic model for unsaturated soil, the lack of simple and objective methods for selecting parameter values from laboratory tests doesn't make it attractive for geotechnical engineers. This has been one of the major obstacles to the dissemination of this constitutive model beyond the research context (Wheeler et al., 2002; Gallipoli et al., 2010; D'Onza et al., 2012, 2015). Hence, this chapter tries to provide a guideline describing soil tests, empirical correlations and iterative calibration in order to obtain all the necessary input parameters from soil tests to use the new constitutive model for frozen and unfrozen soil. By elaborating this guideline, emphasis is put on finding a compromise which on the one hand provides accurate and reliable soil parameters and on the other hand minimizes the effort and expenses of performing laboratory soil tests. As an additional point, this compromise entails the reduction of input parameters. Reducing the needed input parameters is vital in an engineering practice sense. It increases the user-friendliness and the applicability regarding real projects.

4.1. Categorisation of model parameters

Before explaining the proposed strategy to obtain all seventeen parameters, let us divide the model parameters, given and described in Table 2.2, into the following three categories:

Table 4.1: Categorization of model parameters

Elastic parameters	Strength parameters	Parameters controlling virgin loading under isotropic stress state and cryogenic suction variation
κ_0	M	β
κ_s	k_t	λ_0
G_0	$(s_{c,seg})_{in}$	r
$E_{f,ref}$	m	${p_c}^*$
$E_{f,inc}$	γ	$(p^*_{y0})_{in}$
ν_f		λ_s

Elastic parameters The elastic parameters are generally of minor importance for unfrozen soil, because elastic strains are significantly smaller than plastic strains. However, when we consider frozen soil, it is more

likely that elastic strains are not negligible, and the determination of elastic parameters gains importance. The elastic response for partially frozen soil highly depends on temperature and on the availability of unfrozen water. Hence, elastic parameters related to this temperature dependence carry weight on the elastic response. These are namely E_{ref}, E_{inc} and ν_f (see Equation 2.24 and 2.25). For this reason the pressure-dependent part of the elastic response, influenced by κ_0 and G_0, play a minor role. Nevertheless they characterize elastic behaviour in an unfrozen state and contribute to the elastic response when phase transition occurs. The elastic compressibility coefficient for cryogenic suction variation, κ_s, is assumed to be a constant parameter. It describes thawing and freezing reversals. Positive values of κ_s cause the volume to increase during thawing, but at the same time volume can also decrease due to consolidation or due to the decrease in size of the yield surface. There is a competition between these different effects, and selecting low values of κ_s will help the other mechanisms to dominate the behaviour.

Strength parameters The five strength parameters M, k_t, $(s_{c,seg})_{in}$, m and γ include and describe some important soil behaviour. M describes the effect of shear stresses, k_t the increase in apparent cohesion (tensile strength), $(s_{c,seg})_{in}$ the effect of grain segregation and the dilative behaviour due to ice accumulation. The meaning of the yield parameter m and the plastic potential parameter γ are explained in Section 2.1.3 and 2.1.3, respectively.

It is assumed that the slope of the critical state line (CSL) for saturated conditions, M, is maintained for non-zero cryogenic suction conditions. Furthermore, the CSL will also represent the increased strength (apparent cohesion) induced by the cryogenic suction. The increase in cohesion is assumed to follow a linear relationship with cryogenic suction, represented by the constant slope k_t. This is a simplification. Real frozen soil behaviour shows that the increase in tensile strength with cryogenic suction is not linear (Akagawa and Nishisato, 2009; Wu et al., 2010; Azmatch et al., 2011; Zhou et al., 2015). The threshold value for grain segregation is $(s_{c,seg})_{in}$: when reaching this value, elastic and plastic strains occur due to an increase in cryogenic suction. Related to this irrecoverable strain and the separation of the soil skeleton is the formation of new ice lenses.

Parameters controlling virgin loading under isotropic stress state and cryogenic suction variation The parameters β, λ_0, r and ${p_c}^*$, together with the initial value of the pre-consolidation stress p^*_{y0} and λ_s, are the most difficult parameters to determine in the general Barcelona Basic Model and therefore in its unfrozen/frozen formulation as well. They simultaneously influence many aspects of soil behaviour under isotropic stress states (Alonso et al., 1990; Wheeler et al., 2002; Gallipoli et al., 2010; D'Onza et al., 2012). Their influence is shown in Appendix A. Gallipoli et al. (2010) propose a straightforward sequential calibration procedure where degrees of freedom in the model are progressively eliminated in a specific order, so that the corresponding parameter values are selected one at a time without having to make assumptions about the values of remaining parameters.

The starting point is the selection of β, which is the single parameter controlling the relative spacing of normal compression lines in the $v^* - \ln p$ plane (see Appendix A). The relative spacing is defined as the vertical distance between a given constant temperature (cryogenic suction) normal compression line and the normal compression line at a reference temperature, T_{ref1}, normalized by the vertical distance between the normal compression lines at two reference temperatures, T_{ref1} T_{ref2}, where all distances are computed at the same reference stress, p_f. The parameters λ_0 and $r\lambda_0$ are calculated in a simplified way by reducing the optimization process to a straightforward linear interpolation of experimental data by transforming the cryogenic suction, s_c, to a *mapped* cryogenic suction, s_c^*. This has considerable mathematical advantages. A similar linearisation by a suitable mapping process is used in the recommended procedure for determining the initial value of the hardening parameter, p^*_{y0}.

This approach requires isotropic testing of soil samples at different constant positive and negative temperatures. Knowing that this type of testing requires sophisticated equipment and is time-consuming, the idea is to use oedometer test results rather than isotropic test results. The temperature-controlled oedometer test requires equipment which is less sophisticated. Furthermore, a shorter testing period makes it possible to save time and money. However, the major disadvantage of the oedometer test is that its lateral stress is controlled by the condition of zero lateral strain and remains unknown during the testing process. Additionally, no well-established, simple, and objective methods were available until the research of Zhang et al. (2016) on using oedometer test results for constitutive modelling purposes. Zhang et al. (2016) derive an explicit formulation of the at-rest coefficient for unsaturated soils and develop an optimisation approach for simple and objective identification of material parameters in elasto-plastic models for unsaturated soils, like BBM, using

the results from suction-controlled oedometer tests. The same approach, reformulated for the constitutive model for frozen and unfrozen soil, is explained in Section 4.4.

4.2. Proposed soil tests

The following laboratory soil tests are proposed in order to obtain all needed material parameters :

Table 4.2: Suggested soil tests

1	*Oedometer tests in an unfrozen and frozen state*
	The $v : \ln\sigma_1^*$ plane provides data to find the initial pre-consolidation stress for unfrozen condition $(p_{y0}^*)_{in}$, furthermore the parameters β, κ_0, r and ${p_c}^*$ can be determined by the calibration method described in Section 4.4. The elasto-plastic compressibility coefficient for unfrozen state under isotropic loading, λ_0, can be obtained by taking the compression index, C_c, of the oedometer test in an unfrozen state into account ($\lambda_0 = \frac{C_c}{\ln 10}$).
2	*Simple shear test in unfrozen state*
	To obtain the shear modulus of the soil in unfrozen state, G_0, and also for the slope of the critical state line (CSL), M.
3	*Unconfined axial compression test at an arbitrary reference temperature at a frozen state*
	To determine the Young's modulus of the frozen soil, $E_{f,ref}$ and Poisson's ratio of the soil in frozen state, ν_f.
4	*Unconfined axial compression test at a different temperature at a frozen state*
	To determine the rate of change of Young's modulus with temperature of the frozen soil, $E_{f,inc}$, and the increase in apparent cohesion, k_t.
5	*Frost heave test (freezing - thawing cycle)*
	To determine the initial segregation threshold value, by finding the temperature at which the frost heave phenomenon starts. Further plotting of the freezing-thawing cycle in the $v : \ln(s_c + p_{at})$-plane is required to determine the values of λ_s and κ_s

4.3. Possible correlations and default values

The following correlations and default values should be seen as first estimations. Laboratory test data, if available, is more reliable and should be preferred and taken as a basis.

4.3.1. Young's modulus and change in Young's modulus with temperature

Based on the results of cyclic compression tests on 200 mm cubes of three different frozen soils, Tsytovich (1975) found that under a pressure of 200 kPa, the variation of Young's modulus E with temperature could be represented by the following equations (Johnston, 1981):

1. For *frozen sand* (grain size between 0.05 and 0.25 mm, and total moisture content of 17 - 19%) at temperatures down to -10°C,

$$E = 500(1 + 4.2|T|) \tag{4.1}$$

2. For *frozen silt* (grain size between 0.005 and 0.05 mm, and total moisture content of 26 - 29%) at temperatures down to -5°C,

$$E = 400(1 + 3.5|T|) \tag{4.2}$$

3. For *frozen clay* (with 50+% passing the 0.005 mm sieve) and a water content of 46 - 56% at temperatures down to -5°C,

$$E = 500(1 + 0.46|T|) \tag{4.3}$$

where E is the Young's Modulus in MPa and $|T|$ is the number of °C below 0°C. Table 4.3 provides possible default values for $E_{f,ref}$ and $E_{f,inc}$ for three different soil types.

Table 4.3: Default values of elastic parameters

	Frozen Sand	*Frozen Silt*	*Frozen Clay*
$E_{f,ref}$	500 MPa	400 MPa	500 MPa
$E_{f,inc}$	2100 MPa/K	1400 MPa/K	230 MPa/K

According to Andersland and Ladanyi (2004) it can be observed that the modulus for ice in similar conditions is smaller than the ones for dense frozen sand and silt but is much larger than the one of clay, due to the large amount of unfrozen water in the latter. As a comparison the Young's modulus of ice at 0°C is 8700 MPa.

4.3.2. Poisson's ratio in a frozen state

The Poisson's ratio for the three frozen soil types in Section 4.3.1 was found to decrease with decreasing temperatures until all the pore water is frozen and the soil becomes rigid. However, this model assumes a constant Poisson's ratio for soil in frozen state. As a comparison the Poisson's ratio of ice is about $\nu_{ice} = 0.31$. We propose to use a value for ν_f close to ν_{ice}.

4.3.3. Slope of the critical state line

In Muir Wood (1991) it is suggested that soils are failing in a purely frictional manner at the critical state. After failure, the deformations are so large that the soil is thoroughly churned up. All bonding forces between particles have broken down. No cohesive strength is available any more. Hence, for triaxial compression the slope of the CSL, M, can be estimated as:

$$M = \frac{6\sin\phi'}{3-\sin\phi'}. \tag{4.4}$$

And for triaxial extension M results in

$$M = \frac{6\sin\phi'}{3+\sin\phi'}. \tag{4.5}$$

ϕ' is called the residual or critical angle of friction. Ortiz et al. (1986) provide some default values for ϕ' shown in Table 4.4.

Table 4.4: Selected strength properties (drained, laboratory-scale) for soils after Ortiz et al. (1986)

	Peak friction angle [°]	Residual friction angle [°]
gravel	34	32
sandy gravel with few fines	35	32
sandy gravel with silty or clayey fines	35	32
mixture of gravel and sand with fines	28	22
uniform sand - fine	32	30
uniform sand - course	34	30
well-graded sand	33	32
low-plasticity silt	28	25
medium- to high-plasticity silt	25	22
low-plasticity clay	24	20
medium-plasticity clay	20	10
high-plasticity clay	17	6
organic silt or clay	20	15

4.3.4. Threshold value for grain segregation

The threshold value is closely linked to the inititation of ice lenses. Once the temperature drops to the point where the cryogenic suction exceeds this threshold value, plastic strains accumulate and the soil expands. In

several papers (Rempel et al., 2004; Rempel, 2007; Wettlaufer and Worster, 2006), the formation of ice lenses and frost heave is described. Rempel (2007) provides a table for lens temperatures calculated for three different types of porous media at the formation of the first lens, subsequent new lenses and lenses at their maximum extent. Table 4.5 provides these values.

Table 4.5: Lens temperatures at the formation of the first lens, subsequent new lenses, and lenses at their maximum extent

Parameter	Idealised Soil	Chena Silt	Invuik Clay
$T_{f,bulk} - T_{1st}$ [K]	0.57	1.27	3.48
$T_{f,bulk} - T_{new}$ [K]	0.68	1.66	5.06
$T_{f,bulk} - T_{max}$ [K]	2.63	4.86	10

To provide values in terms of cryogenic suction, let us transform the given temperatures in Table 4.5 by means of the approximation $s_c \approx |T_{f,bulk} - T| \frac{\text{MPa}}{\text{K}}$. This approximation provides reasonable values. Furthermore let us assume that: the idealised soil can be seen as a sand, Chena silt is representative for any type of silt and Invuik clay for clay. Table 4.6 provides the proposed default values when no frost heave test has been performed.

Table 4.6: Proposed initial threshold values for grain segregation

Parameter	Sand	Silt	Clay
$(s_{c,seg})_{in}$ [MPa]	0.55	1.25	3.50

4.4. Calibration method of parameters controlling virgin loading, unloading and reloading

This section explains how it is possible to use oedometer test results at different constant positive and negative temperatures to obtain some of the model parameters. This approach is developed and described in Zhang et al. (2016) and adopted for the current model. The used input parameters and the derivation of the explicit formulation of the at-rest coefficient K_0 are found in Appendix B.

4.4.1. Modified state surface approach

A modified state surface approach (MSSA) (Zhang and Lytton, 2009b,a, 2012) to model the elasto-plastic behaviour of unsaturated soils is adopted, and facilitates the model parameter calibration for the frozen and unfrozen BBM. Under triaxial stress state (Zhang, 2010), the volume change can be represented by an elastic surface in the elastic region as follows:

$$v^e = C_1 - \kappa \ln p^* - \kappa_s \ln (s_c + p_{at}) \tag{4.6}$$

where C_1 is a constant and related to the initial specific volume of the soil. A plastic hyper-surface in the elasto-plastic region is defined as follows:

$$v = N(0) - \kappa \; ln\frac{p^*}{{p_c}^*} - \kappa_s \ln (\frac{s_c + p_{at}}{p_{at}}) - (\lambda_s - \kappa)[\ln(\frac{(q^*)^2}{M^2(p^* + k_t s_c)} + (p^* + k_t s_c){S_{uw}}^m - k_t s_c) - \ln({p_c}^*)] \tag{4.7}$$

4.4.2. Use of the K_0 explicit formulation to calibrate model parameters

The goal of the calibration is to find a combination of the model parameters $N(0)$, κ_0, β, r, ${p_c}^*$, M, k_t, m and γ that best fits the oedometer test results for the K_0 stress paths defined by Eq. B.36. This is done by minimizing the overall difference between the experimental data at virgin states and the theoretical results (specific volume predicted by Eq. 4.7). The least-squares method, where all of the experimental results have

the same weight ($w_j = 1$), is used. The objective function can be expressed as follows:

$$\begin{aligned} F(X) &= \sum_{j=1}^{n} w_j (v_j - \hat{v}_j)^2 \\ &= \sum_{j=1}^{n} w_j [v_j - [N(0) - \kappa \; ln \frac{p_j^*}{{p_c}^*} - \kappa_s \ln(\frac{s_{c,j} + p_{at}}{p_{at}}) \\ &- (\lambda_s - \kappa)[\ln(\frac{(q_j^*)^2}{M^2(p_j^* + k_t s_{c,j})} + (p_j^* + k_t s_{c,j}){S_{uw,j}}^m - k_t s_{c,j}) - \ln {p_c}^*]]]^2 \end{aligned} \tag{4.8}$$

4.4.3. Optimisation strategy

To minimize the overall difference between the experimental data at virgin states and the theoretical results, the particle swarm optimization (PSO) technique is used. The PSO algorithm is described in Kennedy and Eberhart (1995). It works by having a population, the so-called swarm, of candidate solutions of the optimisation problem (called particles). These particles are moved around in the search space according to several simple laws. The movements of the particles are guided by their own best known position in the search space as well as the entire swarm's best known position. When improved positions are discovered, they will guide the movements of the swarm. The process is repeated and by doing so, it is hoped that a satisfactory solution of the optimisation problem is eventually discovered. The PSO isn't guaranteed to find an optimal solution to the problem, but it often works remarkably well.

4.4.4. Constraints, upper and lower bounds

In order to secure a fast and accurate optimisation, the right choice of upper and lower bounds is important. The general constraints are given in Table 4.7.

Table 4.7: General constraints for the optimisation strategy

Parameter	Constraint
$N(0)$, κ_0, β, r, p_c^*, M, k_t	$x > 0$
m, γ	$0 \leq x \leq 1$

In addition to these constraints, we specify some other dependencies. Due to the lack of data of isotropic or one-dimensional compression tests on frozen soil, the following dependencies are borrowed from the BBM and unsaturated soil behaviour (Alonso et al., 1990; Wheeler et al., 2002; Gallipoli et al., 2010). When the normal compression lines for different values of cryogenic suction diverge with decreasing mean net stress, the coefficient related to the maximum soil stiffness r should be chosen smaller than 1.0. Furthermore, when $r < 1.0$, the reference stress p_c^* has to be chosen very small and smaller than the initial preconsolidation pressure $(p_{y0}^*)_{in}$. If the normal compression lines converge with increasing p^* then a value greater than 1.0 for the model parameter r should be chosen. With r greater than 1.0, a very large value must be selected for the reference stress p_c - much larger than the largest value of p^* envisaged in any modelling exercise. This is to ensure a sensible shape for the LC yield curve as it expands and sensible locations for the normal compression lines for different values of cryogenic suction (Wheeler et al., 2002). $N(0)$ should be chosen close to the initial specific volume $(1 + e)$. It is proposed that the strength parameters M, k_t, m and γ should be fixed, because oedometer testing doesn't say anything about the strength of a soil.

5

Verification and validation of the model in a single stress point environment

The verification of the constitutive model is based on the simulation of standard laboratory tests at constant temperature. More advanced testing, where freezing and thawing is considered, is treated when solving boundary value problems in Chapter 6. The implementation of the new constitutive model for frozen and unfrozen soil is first tested regarding its theoretical formulation in a single stress point environment. Keeping in mind that the constitutive model is formulated in a THM framework, finite-element calculations considering thermodynamic effects are essential to verify the model and are performed in Chapter 6. The implemented *Soil test* facility in PLAXIS is used to simulate standard laboratory tests and to verify the model in a single stress point environment.

In order to execute a meaningful verification of the constitutive model and its implementation, a test plan is set up, which is explained in Section 5.1 and shown in Table 5.1. In Section 5.2 a reference soils is defined, which is used for further calculations unless stated otherwise. The tests undertaken and the results obtained are explained in the subsequent sections. Emphasis is placed on the evolution of stiffness and strength at different confining pressures and temperatures. The results are judged in a qualitative manner and compared to real test data, where possible. Thermodynamic effects cannot be considered in single stress point environment tests. Hence, all tests performed are drained tests to avoid the build-up of excess pore water pressure. However, due to the low permeability of partially frozen soil and its long drainage time, the majority of laboratory tests on frozen soil should be considered as undrained tests (Andersland and Ladanyi, 2004). Focus is put on the mechanical behaviour of frozen ground, therefore the initial segregation threshold value $(s_{c,seg})_{in}$ is set to a very high value as well.

5.1. Procedure

The verification of the constitutive model takes place in the $p^* - q^*$-plane. Loading paths of standard laboratory soil tests are shown in Figure 5.1 and applied to verify the model. The corresponding soil tests are given in Table 5.1.

For all tests the following constant temperatures are chosen: 0.0, -0.5, -2, -5, -10 °C. Pressure is chosen to be a fraction or a multiple of the initial pre-consolidation pressure $(p^*_{y0})_{in}$ of the unfrozen soil specimen. More details are given in the corresponding sections.

Table 5.1: Test matrix for the verification of the constitutive model

Test type	Loading path
Isotropic compression	A
Oedometer	B
Triaxial compression	C, D
Triaxial extension	E, F
Direct simple shear	G

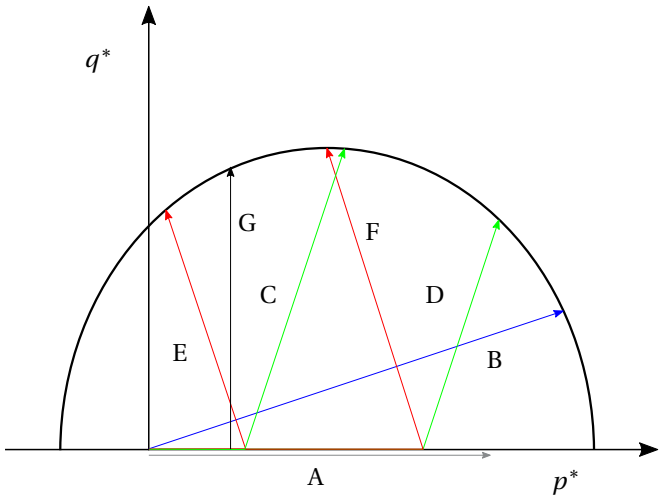

Figure 5.1: Loading paths used to verify the constitutive model

5.2. Reference soil

Before a comparison with some experimental results is made, the capabilities of the model are verified by using a reference soil chosen to be a clay with the following parameters from Wu et al. (2010):

Table 5.2: Mechanical parameters from Wu et al. (2010)

Soil type	Mechanical parameters	-20 °C	-10 °C	-5 °C	-2 °C	0 °C
Clay	Elastic modulus [MPa]	200	100	50	23.4	6
	Poisson's ratio [-]	0.32	0.32	0.32	0.32	0.35
	Cohesion [MPa]	0.6	0.6	0.6	0.57	0.15
	Angle of internal friction [°]	26	26	26	26	24

Based on the given mechanical parameters in Table 5.2 some of the input parameters of the constitutive model can be determined quite accurately, namely $E_{f,ref}$ = 6 MPa, $E_{f,inc}$ = 9.5 MPa/K, ν_f = 0.32. When comparing these values with the ones suggested in 4.3.1 it can be seen that the obtained values from Wu et al. (2010) are very low. Noting this, we should be warned to avoid relying only on the proposed values. Moreover, G_0 can be estimated as follows:

$$G_0 = \frac{E}{2(1+\nu)} = \frac{6\ MPa}{2(1+0.35)} = 2.22\ MPa \tag{5.1}$$

The slope of the critical state line is estimated with a residual friction angle of 20 °. For triaxial compression the slope of the CSL can then be estimated as:

$$M = \frac{\sin\phi'}{3-\sin\phi'} = \frac{\sin 20}{3-\sin 20} = 0.77 \tag{5.2}$$

And for triaxial extension M results in

$$M = \frac{\sin\phi'}{3+\sin\phi'} = \frac{\sin 20}{3+\sin 20} = 0.61 \tag{5.3}$$

The rate of change in apparent cohesion with suction is given as a constant value and assumes a linear increase in tensile strength. This discrepancy has already been discussed in Section 4.1 and can also be observed in Table 5.2. Considering test temperatures down to -10 °C and a cryogenic suction of about 10 MPa at this temperature, it is chosen to set k_t = 0.06. This value provides the correct cohesion at a temperature of -10 °C, but underestimates the tensile strength at higher temperatures. All other parameters are estimated. Because the thermodynamic effects in a single stress point environment cannot be considered, and also because focus is put on the mechanical behaviour of frozen ground, the initial segregation threshold value ($(s_{c,seg})_{in}$) is set to a very high value of 15.0 MPa. Table 5.3 provides the full list of input parameters for the reference soil.

Table 5.3: Model parameters of the reference soil

Parameter	Description	Clay	Unit
G_0	Unfrozen soil shear modulus	2.22×10^6	N/m^2
κ_0	Unfrozen soil elastic compressibility coefficient	0.08	–
$E_{f,ref}$	Frozen soil Young's modulus at a reference temperature	6.00×10^6	N/m^2
$E_{f,inc}$	Rate of change in Young's modulus with temperature	9.50×10^6	$N/m^2/K$
ν_f	Frozen soil Poisson's ratio	0.35	–
m	Yield parameter	1.00	–
γ	Plastic potential parameter	1.00	–
$(p^*_{y0})_{in}$	Initial pre-consolidation stress for unfrozen condition	300×10^3	N/m^2
p^*_c	Reference stress	45.0×10^3	N/m^2
λ_0	Elasto-plastic compressibility coefficient for unfrozen state	0.40	–
M	Slope of the critical state line	0.77	–
$(s_{c,seg})_{in}$	Segregation threshold	15.0×10^6	N/m^2
κ_s	Elastic compressibility coefficient for suction variation	0.005	–
λ_s	Elasto-plastic compressibility coefficient for suction variation	0.80	–
k_t	Rate of change in apparent cohesion with suction	0.06	–
r	Coefficient related to the maximum soil stiffness	0.60	–
β	Rate of change in soil stiffness with suction	0.60×10^{-6}	$(N/m^2)^{-1}$

To fully define this reference soil, the grain size distribution, the void ratio, the soil freezing characteristic curve and the corresponding evolution of the cryogenic suction are presented. The U.S.D.A. data set is used to provide the PSD of a clay, which gives $m_{cl} = 0.70$, $m_{si} = 0.13$ and $m_{sa} = 0.17$. The initial void ratio is chosen to be $e_0 = 0.90$. The SFCC and the corresponding cryogenic suction are shown in Figure 5.2. The initial three-dimensional yield surface is illustrated in Figure 5.3.

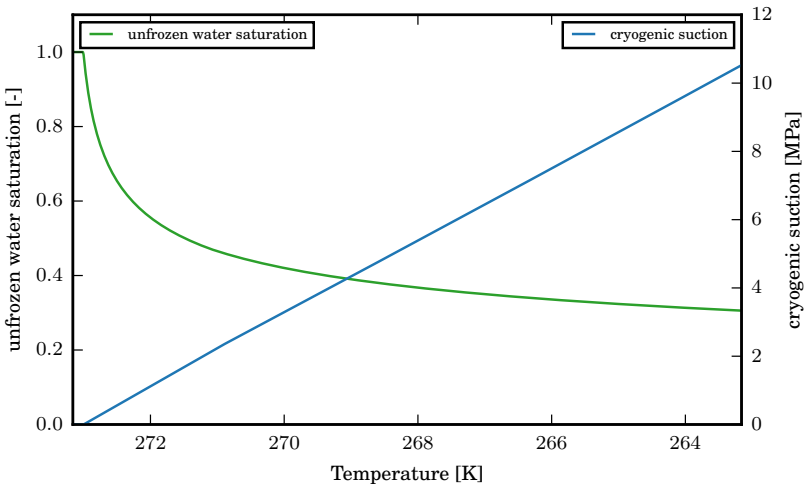

Figure 5.2: SFCC and cryogenic suction development of the reference soil: Clay

5.3. Compression testing

Isotropic and one-dimensional compression tests are performed in a single stress point environment. To avoid excess pore water pressure build-up, we choose a long time period to reach drained behaviour. Thus, thermodynamic effects like pressure melting do not influence the results. Typical phenomena observed in compression testing are settlements and consolidation.

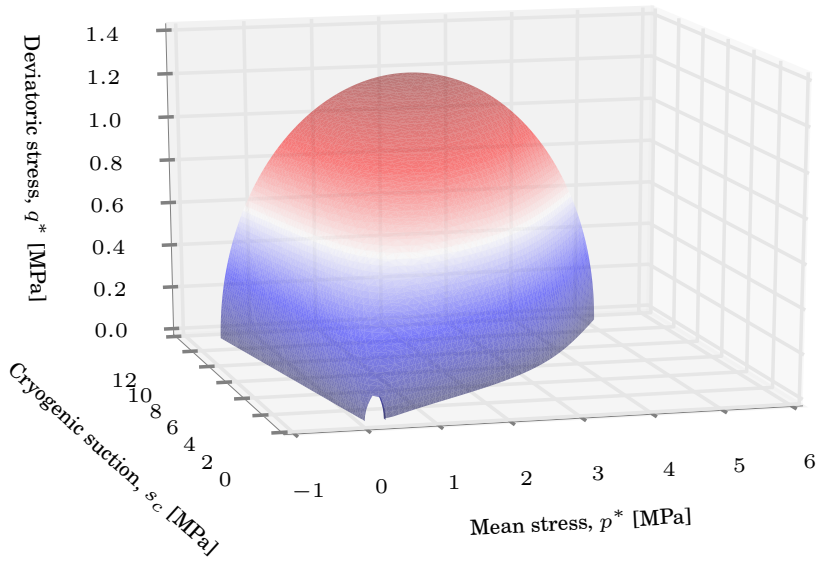

Figure 5.3: Three dimensional yield surface of the reference soil: Clay

5.3.1. Isotropic compression test

Isotropic or hydrostatic stress states are described in the (p^*, s_c) stress space where the loading-collapse yield surface forms the transition of pure elastic and elasto-plastic behaviour. Once the mean solid phase stress hits the LC yield surface, plastic compression occurs and results in stiffer behaviour of the soil in unloading - reloading. The LC yield surface moves outward. The stiffer behaviour can be observed when investigating the bulk modulus K of the soil.

The hydrostatic compression tests at different temperatures below the freezing point are performed using the PLAXIS Soil test facility. The confining pressure in all the tests increases up to 10 MPa. The volumetric strain versus mean solid phase stress plot (see Figure 5.4) records the behaviour of the soil at the stress point due to the increase in confining pressure at different temperatures. Two unloading and reloading loops are conducted at a hydrostatic pressure of 5 and 10 MPa, respectively. The slope of the unloading-reloading lines represents the bulk modulus K defined as the ratio between the hydrostatic pressure and the volumetric strain.

From Figure 5.4 the following observations can be made:

- With decreasing temperature the stiffness of the soil increases.
- With decreasing temperature there is a lower availability of water and hence a lower possibility of plastic volume change. The plastic resistance of the soil increases.
- With increasing confining pressure the stiffness of the soil increases.
- Due to the low values of $E_{f,ref}$ and $E_{f,inc}$ the influence of temperature and ice saturation leads to an initial reduction of stiffness and hardening modulus compared to the ones in an unfrozen state. A decrease in temperature with the choice of higher values of the elastic parameters would lead to an increase in stiffness.

5.3.2. One-dimensional compression test

The oedometer test is a standard laboratory test in soil mechanics and simulates the in-situ at-rest stress state. In general, a one-dimensional compression test is telling something about the stiffness E_{oed}, the stress-

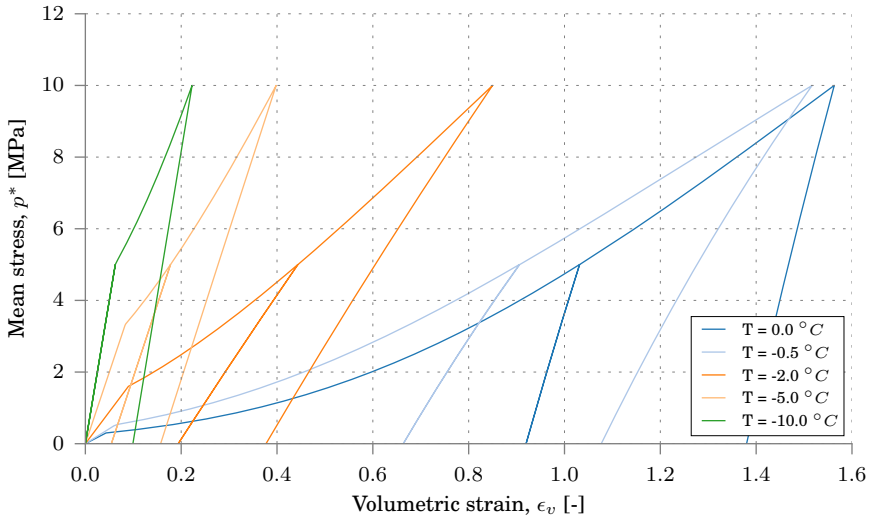

Figure 5.4: Isotropic compression test results at different temperatures for the reference soil: Clay

dependency of stiffness $E_{oed}(\sigma)$, the coefficient of lateral stress K_0, the stress history of the soil p_y^* and the structure and bonding of the soil, respectively.

The one-dimensional compression tests at different temperatures below the freezing point are performed using the PLAXIS Soil test facility. The stress point is compressed in increments up to a designated vertical pressure σ_{yy} of 6 MPa. Unloading and reloading loops are performed at a vertical stress of 3 and 6 MPa, respectively.

The results of the oedometer tests on clay are presented in Figure 5.5. The vertical strain versus vertical stress plot (Fig. 5.5a) records the behaviour of the stress point due to the increase in vertical pressure at different temperatures. The observations are the same as for the isotropic compression tests, hence, we refer to Section 5.3.1. Traditionally, it is assumed that the coefficient of lateral stress K_0, which is the ratio of horizontal over vertical stress, is a constant. Figure 5.5b shows the relation between lateral and vertical effective stress. The following observations can be made:

- In the elastic zone, the coefficient of lateral stress is constant. The current formulation assumes that there is no influence of temperature on K_0 in the elastic region.
- When entering the elasto-plastic zone, we see that the increase in lateral stress is larger than the increase in vertical stress, and then the trends reverse when the applied vertical loads are increasing. This means that K_0 values increase to peak values and then decrease to constants when the applied vertical stresses are large.
- Furthermore, this also results in a decrease in deviatoric stress with an increase in mean net stress (shown in Fig. 5.5c) at the initial stage of plastic loadings, and the trends are opposite as mean net stress increases.
- At low temperatures the decrease to constant K_0 values is much slower than at higher temperatures.

5.4. Shear testing

In order to verify the model in terms of shear resistance, typical shearing modes and corresponding tests are considered. Figure 5.6 represents the three prevailing shearing modes, namely triaxial compression, triaxial extension and simple shear. Each test can tell something about stiffness, stress-dependency of stiffness, strength parameters and dilatancy. To consider the strength anisotropy, however, different shearing tests have to be performed.

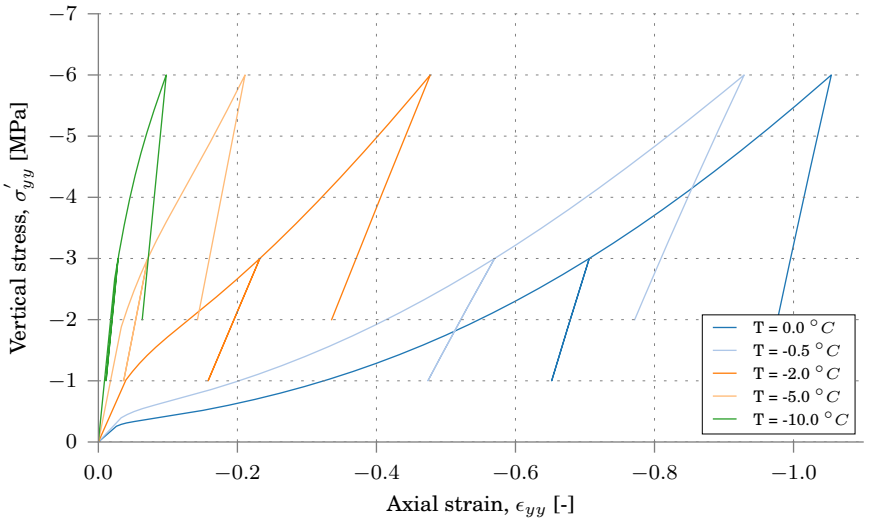

(a) Vertical stress σ_{yy} over axial strain ϵ_{yy}

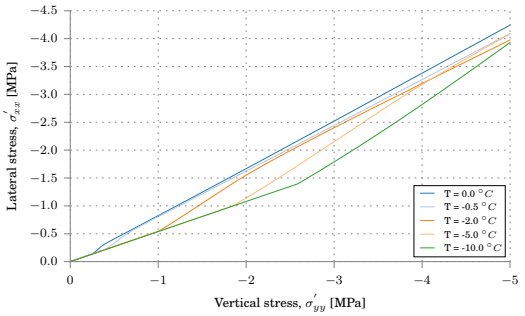

(b) Vertical stress σ_{yy} over lateral stress σ_{xx}

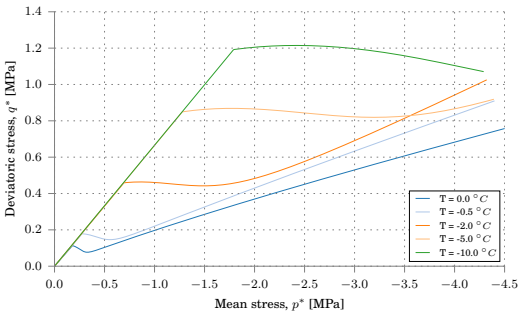

(c) Deviatoric stress q^* over mean net stress p^*

Figure 5.5: Oedometer test results at different temperatures of the reference soil: Clay

5.4.1. Triaxial compression test

Triaxial compression tests may provide strength information at the top of a cut slope. There are three primary triaxial tests conducted in the laboratory, each allowing the soil response for differing engineering applications to be observed. These are:

- Unconsolidated Undrained test (UU)
- Consolidated Undrained test (CU)
- Consolidated Drained test (CD)

In triaxial testing of frozen soils, hydrodynamic consolidation after a hydrostatic stress application will be up to several months. The majority of tests reported in literature should therefore be classified as unconsolidated undrained tests (UU) (Andersland and Ladanyi, 2004).

The reference soil clay is used to perform the single stress point environment test regarding triaxial loading. Due to the fact that clay is able to hold a certain amount of unfrozen water at temperatures below the freezing point, consolidated and drained behaviour is considered in order to obtain negligible pore pressure variation. The soil sample is initially compressed isotropically by simply increasing the cell pressure without applying any deviator stress so that the initial mean stress is equal to the cell pressure at the end of this initial isotropic compression step. A confining pressure equal the initial pre-consolidation pressure is chosen to be the representative cell pressure when triaxial behaviour at different temperatures below the freezing point is investigated. After applying the representative cell pressure the sample is subjected to an incremental vertical loading. The soil is sheared by applying an axial vertical strain ϵ_{yy} = 10% to the test specimen at a constant rate through vertical compression. When investigating the influence of pressure, we keep the temperature

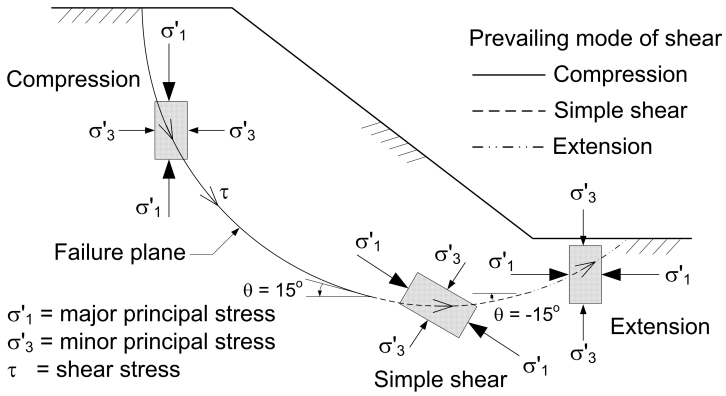

Figure 5.6: Prevailing shearing modes[1]

constant (0 and −5 °C) and vary the confining pressure ($0.33 \times (p_{y0})_{in}$, $0.66 \times (p_{y0})_{in}$ and $1.00 \times (p_{y0})_{in}$). The single stress point environment test results regarding the influence of temperature change and the ones regarding confining pressure variation are both shown in Figure C.1. The graphs represent the evolution of deviatoric stress over axial strain as well as the volumetric behaviour with axial strain. The following objective features can be presented:

- In the elastic zone, the stiffness increases with decreasing temperature.
- With decreasing temperature and/or increasing confining pressure the strength increases.
- Hardening and softening behaviour, as well as the associated compressive and dilative behaviour can be represented.
- The volumetric deformation is significantly affected by the confining pressure. The volume reduces with the increase in axial strain under high confining pressures. At low confining pressures the volume always reduces to a critical value, before volume expansion in the strain softening stage takes place.

5.4.2. Triaxial extension test

Triaxial extension tests (lateral compression) may provide strength information at the slope base of a cut slope. The same testing conditions as in Section 5.4.1 are chosen. However, the slope of the critical state line is reduced to $M = 0.61$ according to Equation 4.5. Furthermore, after applying the representative cell pressure a decrease in vertical loading is assumed. The soil is sheared by applying an axial vertical strain $\epsilon_{yy} = 10\%$ to the test specimen at a constant rate through vertical extension. The single stress point environment test results regarding the influence of temperature change and the ones regarding confining pressure variation are both shown in Figure C.2. The graphs represent the specimen response during shearing stage monitored by plotting the deviator stress against the axial strain as well as the volumetric strain against the axial strain. In general the same observations as given in Section 5.4.1 can be made.

5.4.3. Direct simple shear test

Direct shear tests are of great importance. They give indications on the strength and the dilatancy behaviour of frozen and unfrozen soils. The results provide valuable information on the stability of slopes and of creeping rock glaciers (Yasufuku et al., 2003). When performing a direct simple shear test, the vertical stress is applied during a consolidation phase, followed by a shear phase consisting of the application of a horizontal displacement at constant volume.

After applying a vertical stress of p^*_{y0} the sample is sheared at constant volume up to a strain of 10 %. This procedure is repeated at five different temperatures: 0.0, −0.5, −2.0, −5.0 and −10.0 °C. The results regarding the influence of temperature can be seen in Figure C.3a and the corresponding volumetric behaviour with increasing shear strain in Figure C.3b. In addition to the temperature dependency, the pressure dependency of the clay soil in direct simple shear tests is investigated. We keep the temperature constant (0 and −5 °C) and vary the vertical pressure ($0.33 \times (p_{y0})_{in}$, $0.66 \times (p_{y0})_{in}$ and $1.00 \times (p_{y0})_{in}$). The results representing the

[1] http://www.eng.uwo.ca/civil/faculty/sadrekarimi_a/img/variations_prinipal_stress_directions.jpg

stress-strain behaviour as well as the volumetric behaviour with increasing strain are shown in Figure C.3c, C.3d, C.3e and C.3f, respectively. The following objective features can be presented:

- With lower temperature an increase in shear strength and shear modulus is observed.
- With decreasing temperature and constant vertical pressure the soil behaves more and more in a dilative manner.
- With increasing pressure up to $0.5 \times p_y^*$ and constant temperature the shear strength in the elastic region increases. From the moment on that the vertical pressure exceeds $0.5 \times p_y^*$ the elastic shear strength decreases again. However, the final shear strength might be higher due to the hardening behaviour.
- To end up with dilative behaviour the yield surface has to be hit on its dry side.

5.5. Validation - comparison to real test data

5.5.1. Triaxial compression tests

Triaxial compressive tests of frozen silt from Qinghai–Tibet Railway constructions' site were carried out by Lai et al. (2010). Confining pressures varied from 0.0 to 14.0 MPa at the temperatures of −2, −4 and −6 °C. A shear strain rate of 1.64×10^{-4} s^{-1} has been used. In Table 5.4 the physical parameters of the silt tested are listed. The plasticity index (PI) equals 8. This low PI value indicates a slightly plastic silt. Referring to Table 4.4, we can assume a residual friction angle of $\phi' = 25$ ° and, hence, a slope of the critical state line of $M = 1.0$ in triaxial compression is proposed. In order to obtain a best-fit of the simulated results with the test results, it was necessary to estimate the majority of the input parameters. Their magnitudes are, however, in a reasonable range. The slope of the critical state line had to be changed to $M = 1.2$. Two slightly different parameter sets had to be chosen to represent the temperature and the confining pressure dependency. Table 5.5 summarises the used input parameters. The simulation provides an accurate representation of the temperature dependency. To obtain conformable results regarding the pressure dependency, the critical slope line M had to be changed with pressure.

Table 5.4: Physical properties of silt tested in Lai et al. (2010)

Composite of particle diameters (%)			Liquid limit (%)	Plastic limit (%)
2.0 – 0.05 mm	0.05 – 0.002 mm	< 0.002 mm		
≈ 54	≈ 37	≈ 9	23.2	15.0

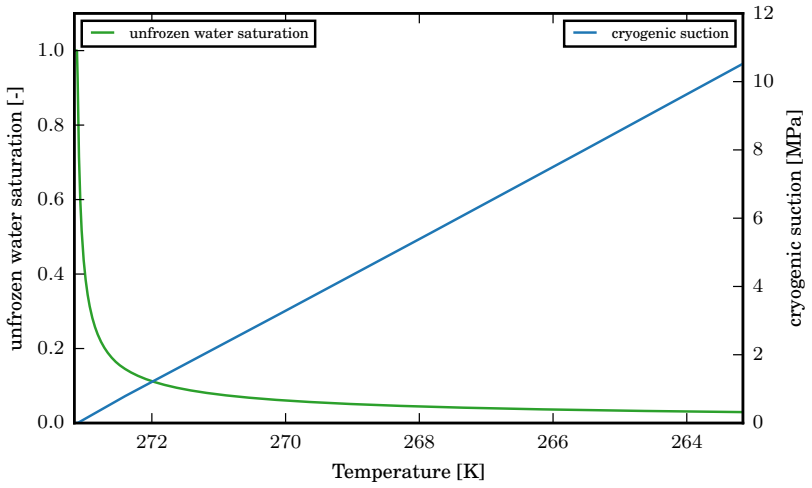

Figure 5.7: SFCC and cryogenic suction development of frozen silt tested by Lai et al. (2010)

The void ratio is estimated to 0.60. The specific gravity was chosen to be 2.60. The resulting soil freezing characteristic curve and the corresponding evolution of the cryogenic suction are presented in Figure 5.7. The

initial three-dimensional yield surface for the parameter set used to simulate the temperature dependency is illustrated in Figure 5.8.

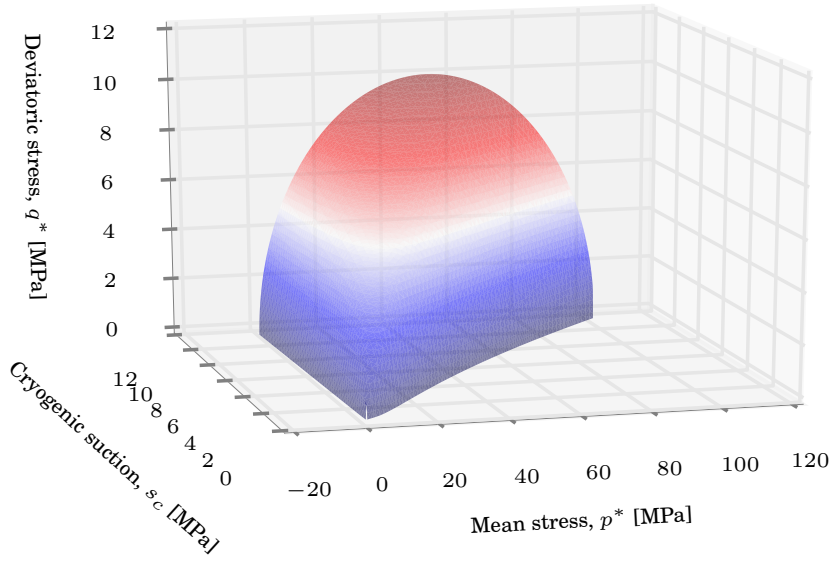

Figure 5.8: Three dimensional yield surface of silt tested by Lai et al. (2010)

Temperature influence
From Figure 5.9 it can be seen that the stress–strain curves of the tested frozen silt and the simulated results are in agreement. Under the same confining pressures at different negative temperatures all curves show the same behaviour. The stress–strain curves under the relative low confining pressure show apparent strain softening behaviour. The strengths and initial slopes of the stress–strain curves are higher at low negative temperatures than those at high negative temperatures under the same confining pressures.

Confining pressure influence
The stress–strain curves of the tested frozen silt and the simulated results under different confining pressures at a temperature of −6 °C are shown in Figure 5.10. It is found that the stress–strain behaviour of the tested frozen silt approximately experiences three stages: (1) the initial linear elastic stage, stress increases linearly with the increase of axial strain; (2) the hardening stage, where the plastic deformation is dominating over the specimen deformation process, and the elastic deformation is relatively subordinate; and (3) the softening stage, where the slopes of the stress–strain curves are negative.

Table 5.5: Model parameters of frozen silt tested by Lai et al. (2010)

Parameter	Description	Clay		Unit
		Temperature	Pressure	
G_0	Unfrozen soil shear modulus	30×10^6	30×10^6	N/m^2
κ_0	Unfrozen soil elastic compressibility coefficient	0.10	0.10	–
$E_{f,ref}$	Frozen soil Young's modulus at a reference temperature	50.00×10^6	50.00×10^6	N/m^2
$E_{f,inc}$	Rate of change in Young's modulus with temperature	100×10^6	100×10^6	$N/m^2/K$
ν_f	Frozen soil Poisson's ratio	0.30	0.30	–
m	Yield parameter	1.00	1.00	–
γ	Plastic potential parameter	1.00	1.00	–
$(p^*_{y0})_{in}$	Initial pre-consolidation stress for unfrozen condition	1.2×10^6	1.2×10^6	N/m^2
p^*_c	Reference stress	200×10^3	200×10^3	N/m^2
λ_0	Elasto-plastic compressibility coefficient for unfrozen state	0.40	0.40	–
M	Slope of the critical state line	1.20	0.6 (0.8, 0.95, 1.00, 1.10)	–
$(s_{c,seg})_{in}$	Segregation threshold	15.0×10^6	15.0×10^6	N/m^2
κ_s	Elastic compressibility coefficient for suction variation	0.005	0.005	–
λ_s	Elasto-plastic compressibility coefficient for suction variation	0.10	0.10	–
k_t	Rate of change in apparent cohesion with suction	0.12	0.12	–
r	Coefficient related to the maximum soil stiffness	0.80	0.60	–
β	Rate of change in soil stiffness with suction	0.10×10^{-6}	0.10×10^{-6}	$(N/m^2)^{-1}$

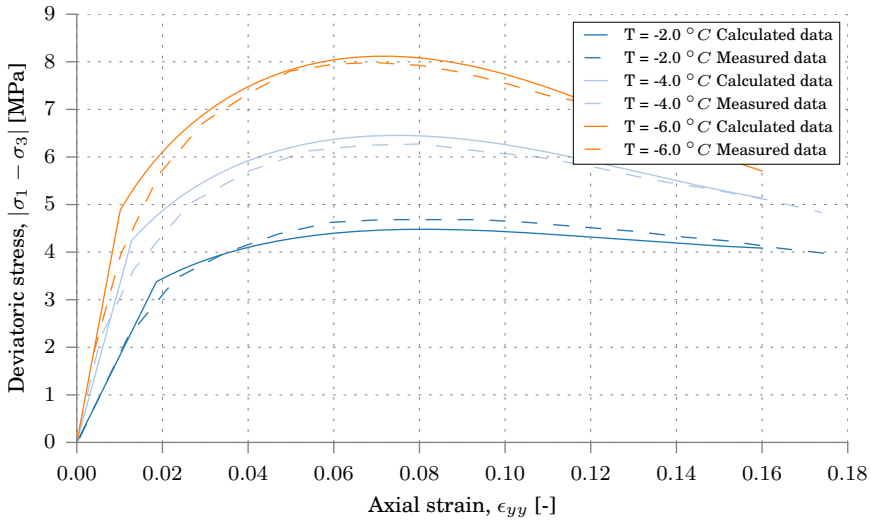

Figure 5.9: Comparison of stress-strain curves under constant confining pressure at −2, −4 and −6 °C obtained from Lai et al. (2010) and simulated results

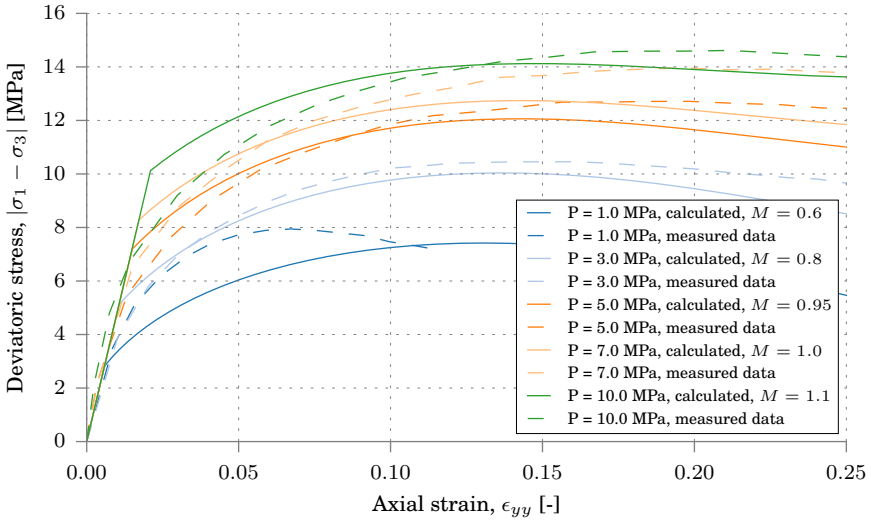

Figure 5.10: Comparison of stress-strain curves under a constant temperature of–6 °C and confining pressures of 1.0, 3.0, 5.0, 7.0, 10.0 MPa obtained from Lai et al. (2010) and simulated results

6

Verification of the model in a fully coupled THM finite element environment

In the following sections the constitutive model for frozen and unfrozen soil is verified regarding its applicability for practical uses. Simple boundary value problems, where changes in temperature and pressure are combined, are presented. More concrete applications complete this chapter. Two main features of the constitutive model, namely the ability to model frost heave and thaw settlements, can successfully be simulated. A chilled pipeline buried in unfrozen ground simulates the frost heave phenomenon. A footing placed on frozen ground subjected to a warming period shows the consequences of ice melting and the associated thaw settlements. To cope with the need of more insights in artificial ground freezing, an example of freeze pipes in tunnel construction finalises the verification of the model.

6.1. Boundary value problems

The boundary value problems performed try to cover and to present the main capabilities and limitations of the constitutive model in a thermo-hydro-mechanical finite element environment. The following cases are considered:

- Case 1: Temperature gradient under unconfined compression testing
- Case 2: Pressure melting
- Case 3: Freeze - thaw cycle
- Case 4: Frost heave analysis of a chilled pipeline
- Case 5: Foundation on frozen soil subjected to a warming period
- Case 6: Freeze pipes in tunnel construction

6.1.1. Soil parameter sets

The boundary value problems to investigate require the provision of soil parameter sets. The cases 1, 2, 3 and 6 are performed with only one soil parameter set. In cases 4 and 5 a two-layered stratigraphy is considered and two parameter sets are required. The reference soil clay, described in Section 5.2, and a new parameter set for a sandy soil are chosen. In the THM finite element environment, thermodynamic effects can now be considered. They are important for assessing the performance of the model. Thus, the initial segregation threshold value $(s_{c,seg})_{in}$ for the reference soil clay is set to 3.50 MPa, which is the default value for clay proposed in Section 4.3.4. A set of physical properties needed to obtain the SFCC and the saturated hydraulic conductivity as well as the hydraulic conductivity in a partially frozen state are given in Table 6.1. The complete parameter sets for clay and sand are presented in Table 6.2 and 6.3. The difference in yield surface of the two soil parameter sets is illustrated in Figure 6.1a and Figure 6.1b. The yield surfaces of both materials are only shown up to a mean net stress of 5MPa. This value is higher than the largest value of p^* envisaged in the following modelling exercises. The occurring differences in yield surface of the two soil materials are due to

two facts. On the one hand, the difference in chosen parameters (see Table 6.2) influences the yield surface. On the other hand, the influence of the unfrozen water content (see Equation 2.31 and Figure 6.2a and 6.2b) with a chosen yield parameter $m = 1.0$, are responsible for the major difference in shape.

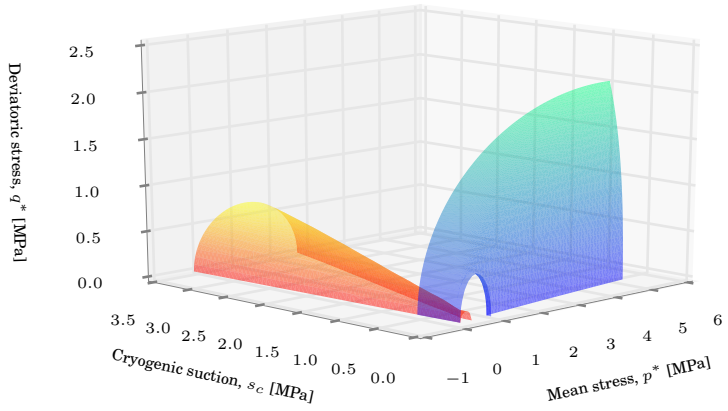

(a) Three dimensional yield surface of clay (orange) and sand (blue) - View 1

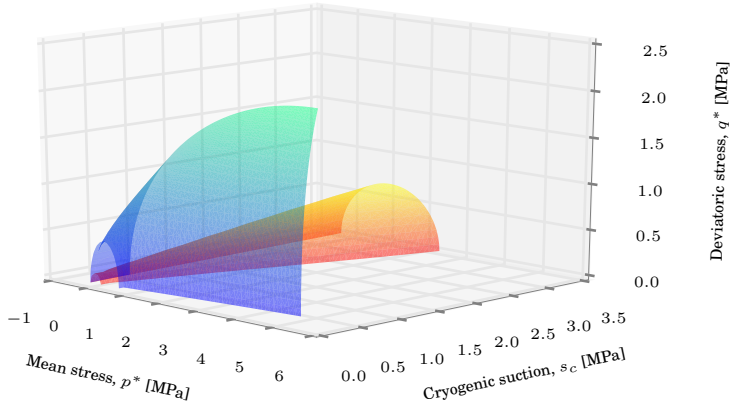

(b) Three dimensional yield surface of clay (orange) and sand (blue) - View 2

Figure 6.1: Three dimensional yield surfaces of clay and sand

Table 6.1: Physical properties clay and sand

Soil	Composite of particle diameters (%)			Void ratio	Solids density
	2.0 – 0.05 mm	0.05 – 0.002 mm	< 0.002 mm	[-]	[kg/m^3]
Clay	13	17	70	0.90	2700
Sand	92	4	4	0.35	2650

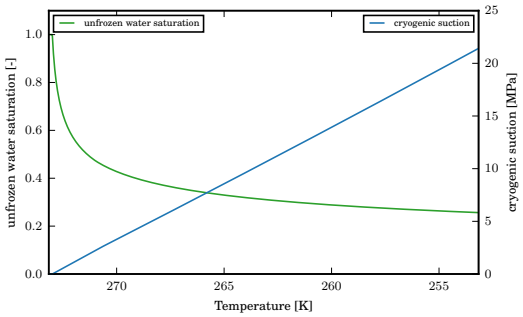

(a) Clay

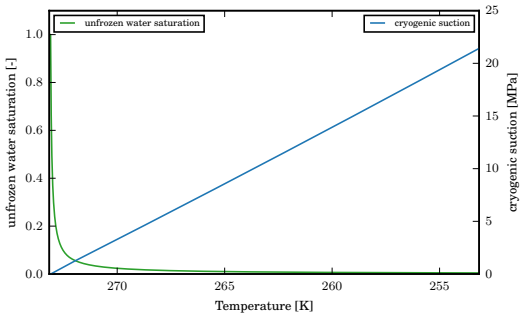

(b) Sand

Figure 6.2: SFCC and cryogenic suction with temperature of clay and sand

6.1.2. Temperature gradient under unconfined compression testing

The deformation and strength behaviour of frozen soils with thermal gradient is of great importance. Considering the temperature distribution in frozen soils, we are mostly facing non-uniform distributions. This can be regarded as a temperature field of different thermal gradients. Thus, a good understanding of the effects that thermal gradients cause to the strength and deformation behaviour is required. In order to examine the influence of a thermal gradient on deformation and uniaxial compression strength, three different thermal gradients (0.25 °C cm^{-1}, 0.50 °C cm^{-1}, 1.00 °C cm^{-1}) and two average temperatures (−10 °C, −15 °C) are applied on the soil sample. The reference soil clay is used (see 5.2). Figure 6.4 illustrates the set up and the temperature distribution which is kept constant during shearing. The finite element mesh and the fixities can be seen in Figure 6.3. Drainage is allowed. The obtained results are presented in Figure 6.5 where the applied vertical force over ΣMstage is diagrammed. Figure D.1 and Figure D.2 provide the evolution of deviatoric strains.

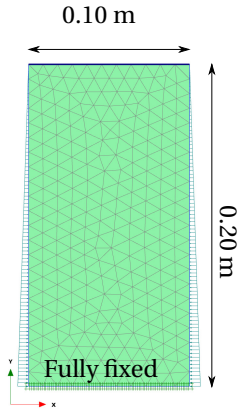

Figure 6.3: FE-model and mesh for case 1, 2 and 3 (492 elements, 4069 nodes)

From Figure 6.5 we can observe that the elastic modulus under constant average temperature shows little variation, but more at lower average temperatures. The hardening modulus and the uniaxial compression strength increase as the average temperature and the thermal gradient decrease. From Figure D.1 and D.2 we can note that at lower average temperatures and smaller temperature gradients, less deviatoric strains accumulate. Zhao et al. (2013) have carried out a series of uniaxial compression tests on frozen clay at various thermal gradients and average temperatures, and analysed the deformation and strength behaviours for frozen clay with thermal gradient. Our simulations are in accordance with the results obtained by Zhao et al. (2013) and cover the main behaviours of frozen soil subjected to a temperature gradient under unconfined compression.

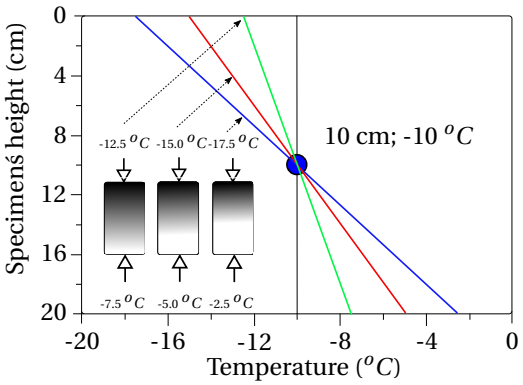

(a) Average temperature $T_{avg} = -10$°C

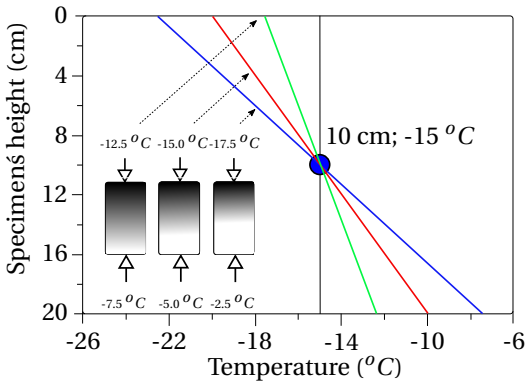

(b) Average temperature $T_{avg} = -15$°C

Figure 6.4: Applied temperature gradients

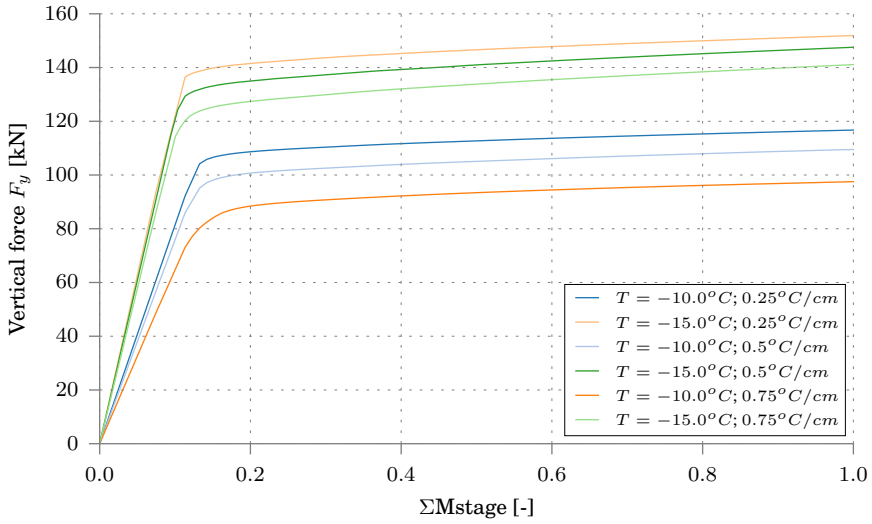

Figure 6.5: Vertical force vs. Σ Mstage

6.1.3. Pressure melting

Pressure melting is a phenomenon which occurs when high confining pressures cause the melting of ice crystals due to the reduction of the phase transition temperature (see Eq. 2.7). Higher amount of unfrozen water in the pores is expected. The high unfrozen water saturation and the low amount of ice lead to strength weakening of the soil. To simulate this behaviour, an undrained isotropic compression test on a clay sample is considered. The parameter set of the reference soil described in Section 5.2 is employed. The sample, defined by the FE model presented in Figure 6.3, is loaded with a confining pressure equal to 5 MPa. A constant temperature of −1 °C is considered during the simulation. Drainage is hindered, leading to an increase in pore water pressure and to the behaviour described before. The initial ice saturation is 41.06 % and the ice saturation after applying the confining pressure for a very long time ends up to be 29.13 %. The dependency of pore pressure and net mean stress with ice saturation, respectively, is presented in Figure 6.6. The behaviour of the pressure melting phenomenon in shearing considering an undrained triaxial test is illustrated in Ghoreishian Amiri et al. (2016).

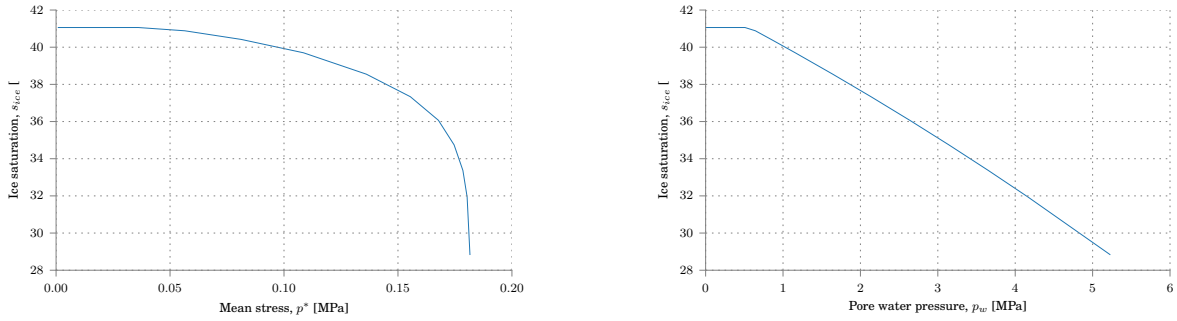

(a) Ice saturation vs. net mean stress

(b) Ice saturation vs. pore water pressure

Figure 6.6: Evolution of net mean stress and pore water pressure with decreasing ice saturation

6.1.4. Freeze - thaw cycles

The freeze - thaw cycles demonstrate the ability of the model to simulate the ice segregation phenomenon (frost heave) as well as the thaw settlement behaviour. With this application the coupling of the Grain Segregation yield surface and the Loading Collapse yield surface can be shown. In this regard, a clay sample with the set of parameters listed in Table 6.2 and 6.3 is subjected to two freeze-thaw cycles. Before the first cooling process starts, a confining pressure of 250 kPa is applied. The clay can therefore be considered as slightly

Table 6.2: Constitutive model parameters of clay and sand

Constitutive model parameters				
Parameter	Description	Clay	Sand	Unit
G_0	Unfrozen Soil shear modulus	2.22×10^6	5.00×10^6	N/m^2
κ_0	Unfrozen soil elastic compressibility coefficient	0.08	0.15	–
$E_{f,ref}$	Frozen soil Young's modulus at a reference temperature	6.00×10^6	20.00×10^6	N/m^2
$E_{f,inc}$	Rate of change in Young's modulus with temperature	9.50×10^6	100×10^6	$N/m^2/K$
ν_f	Frozen soil Poisson's ratio	0.35	0.30	–
m	Yield parameter	1.00	1.00	–
γ	Plastic potential parameter	1.00	1.00	–
$(p^*_{y0})_{in}$	Initial pre-consolidation stress for unfrozen condition	300×10^3	800×10^3	N/m^2
p^*_c	Reference stress	45.0×10^3	100×10^3	N/m^2
λ_0	Elasto-plastic compressibility coefficient for unfrozen state	0.40	0.50	–
M	Slope of the critical state line	0.77	1.20	–
$(s_{c,seg})_{in}$	Segregation threshold	3.50×10^6	0.55×10^6	N/m^2
κ_s	Elastic compressibility coefficient for suction variation	0.005	0.001	–
λ_s	Elasto-plastic compressibility coefficient for suction variation	0.80	0.10	–
k_t	Rate of change in apparent cohesion with suction	0.06	0.08	–
r	Coefficient related to the maximum soil stiffness	0.60	0.60	–
β	Rate of change in soil stiffness with suction	0.60×10^{-6}	1.00×10^{-6}	$(N/m^2)^{-1}$

Table 6.3: Thermal properties of clay and sand

Thermal properties				
c_s	Specific heat capacity	945	900	J/(kgK)
λ_{s1}	Thermal conductivity	1.50	2.50	W/(mK)
ρ_s	Density of the solid material	2700	2650	kg/m^3
α_x	Thermal expansion coefficient in x-direction	5.20×10^{-6}	5.00×10^{-6}	1/K
α_y	Thermal expansion coefficient in y-direction	5.20×10^{-6}	5.00×10^{-6}	1/K
α_z	Thermal expansion coefficient in z-direction	5.20×10^{-6}	5.00×10^{-6}	1/K

overconsolidated. The cooling process starts at a temperature higher than the freezing point (274.16 K). The soil temperature is then gradually reduced to a final temperature equal 263.16 K. During freezing two stages can be observed. In the elastic region, κ_s dominates the behaviour and acts by bonding the grains together and causing a volume decrease. When the GS-yield surface is hit and shifted upwards, dilative plastic strains start. The observed increase in volume is frost heave taking place. Additionally, the LC moves inward and is linked to a decrease in pre-consolidation pressure in the unfrozen state (Figure 2.7b). Once the whole soil sample is cooled down to 263.16 K, the thawing process starts. Upon the first thawing cycle an increase in confining pressure to 500 kPa is assumed. This increase secures that upon thawing, the LC-yield curve is hit at an early stage and plastic compression as well as thaw consolidation takes place. Figure 6.7 visualises that we end up with significant thaw settlements after the first freeze-thaw cycle. When hitting the LC-yield curve, a downward shift of the GS-yield surface is caused.

Once the sample is completely unfrozen, it can be considered as normally consolidated. The second freeze-thaw cycle is started. Although the GS-yield curve shifted downwards during the first thawing stage, it did not reach its initial position. This means that for the next freezing period, ice segregation will happen at lower temperatures. This can be seen when looking at the results of the second freezing period. The elastic part and, hence, the curvature induced premelting mechanism upon freezing dominate for a longer time than during the first freezing period. The GS-yield curve is hit at a lower temperature and less dilative plastic

strains can be accumulated than during the first freezing period. Once completely cooled down to 263.16 K, thawing of the soil sample is allowed, however, now without increasing the confining pressure. The pore water pressure in the soil sample is lower, thus, consolidation takes longer. Additionally the LC-yield curve is hit at a later stage than during the first thawing period. It can be observed that initially the influence of κ_s, causing a dilative behaviour upon thawing, dominates over the two other mechanisms. Once the LC-yield curve is hit, plastic compression takes place and the GS-yield curve moves downward. The resulting thaw-settlements due to the second thaw period are smaller than the dilative deformations due to the second freezing period.

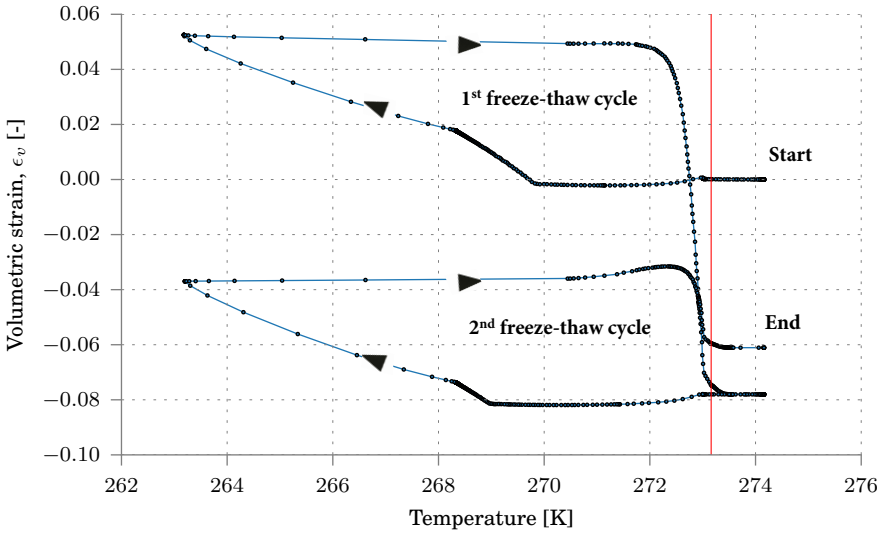

Figure 6.7: Volumetric strain ϵ_v vs. temperature T

6.1.5. Frost heave of a chilled pipeline

Frost heave and ice segregation can potentially cause many engineering problems, like cracking of pavements and fractures of pipelines. It is therefore of particular concern in highway and pipeline engineering. Frost heave can be explained as the ground expansion caused by water migration that supplies growing ice lenses. Frost heave is unrelated to the reduction in water density upon freezing (Taber, 1929, 1930). The water migration is driven by the cryogenic suction, but at the same time hindered by the reduced permeability developed in partially frozen soils.

Geometry and boundary conditions

A pipeline (∅ 0.60 m) is buried in a 1.30 m deep trench at a depth of 1.20 m. The excavated trench in the clay layer is then backfilled with sand. The pipeline has a bending stiffness of EI = 282,000 Nm^2/m. The modelled domain is 3.00 m wide and 3.00 m high. The symmetry of the investigated problem allows the modelling of only half of the pipeline cross-section. Due to symmetry reasons the left boundary is closed and no heat flux is allowed, whereas seepage is possible at the right boundary of the model. Relative fine meshing is used to account for the rapid change in unfrozen water saturation and hydraulic conductivity. A constant air temperature of 293 K with an assumed surface transfer of 300 W/m^2 is considered. The temperature at a depth of 3.00 m is set to 283 K. The geometry, the initial ground temperature and the boundary conditions are shown in Figure 6.8.

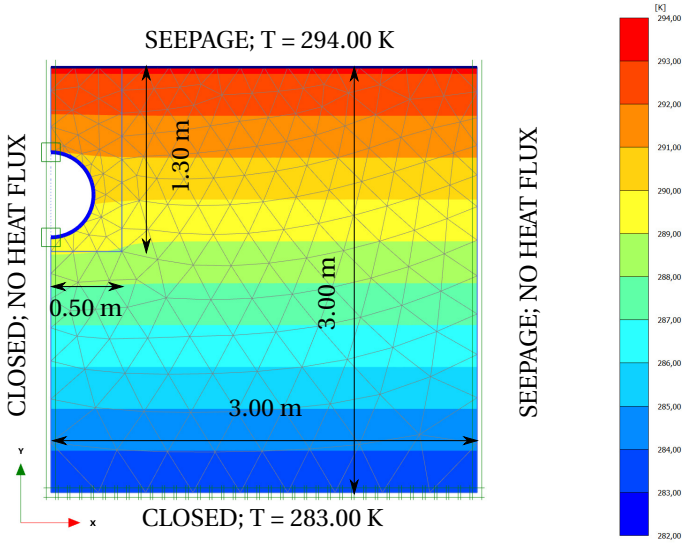

Figure 6.8: Geometry and boundary conditions - chilled pipeline

Simulation and results

After placing the pipeline and refilling the trench with the sand (see Table 6.2 and 6.3), the cooled fluid in the pipeline causes a decrease of the surrounding temperature. The temperature of the fluid is 253 K. It is assumed that it takes 10 days until the pipeline cools down to 253 K. During another 20 day period the temperature stays constant. The temperature regime after 30 days is shown in Figure D.3a. Stresses hit the Grain Segregation yield surface and cause the accumulation of dilative plastic strains. Figure D.4a shows the ice saturation and Figure D.5a the deformed mesh after the time period of 30 days. It is clearly visible that the frozen clay contains much more unfrozen water than the sand material does. A frost heave of about two centimetres takes place. After these 30 days of constant temperature a decrease in air temperature of 25 K over a period of 180 days is considered. The temperature at the bottom boundary stays constant. The purpose of this simulation is to demonstrate how frost heave evolves with time and changing temperatures. A new temperature distribution is reached (see Figure D.3b). The deformed mesh shows a frost heave of more than 7.0 cm and is illustrated in Figure 6.9 and D.5b, respectively. The final ice saturation after this cooling period is presented in Figure D.4b.

Temperature changes and the formation of frozen soil not only change the stress state in the ground, it also influences the stress state of the installed pipeline. An increase in the magnitude of the stress resultants, which may lead to the cracking of the pipeline, has to be considered when designing such structures. Figure D.6 exemplifies the increase of bending moments with time. If the surrounding soil is in an unfrozen state and if no chilled fluid flows through the pipeline, then the bending moments are relatively low. Once the pipeline starts cooling and the surrounding soil freezes, the induced deformations cause the adaption of the stress resultants. The bending moments increase dramatically: by a factor of 34 in this example.

6.1.6. A foundation on frozen soil subjected to a warming period

Settlements due to thawing of ice enclosed in frozen soil are of important consideration in frozen ground engineering. Embankments on permafrost and foundations in permafrost are two examples where thaw settlements may occur and lead to severe damage to the constructions.

Geometry and boundary conditions

A raft foundation with a width of 2.00 m is placed on a frozen clay layer of 1.00 m thickness. Under the clay layer there is a dense sand layer. In this layer, phase transition takes place, meaning that part of this layer is in a frozen state whereas the other part of the sand layer is in an unfrozen state. Again, the symmetry of the investigated problem is taken into account; plane strain is considered. The modelled domain is 6.00 m wide and 4.00 m high. Relative fine meshing is used. The initial ground temperature is set to a constant temperature of 270 K at the surface and 274 K at a depth of 4.00 m. The geometry, temperature distribution and boundary conditions are shown in Figure 6.10. Before applying the foundation load, it is important to

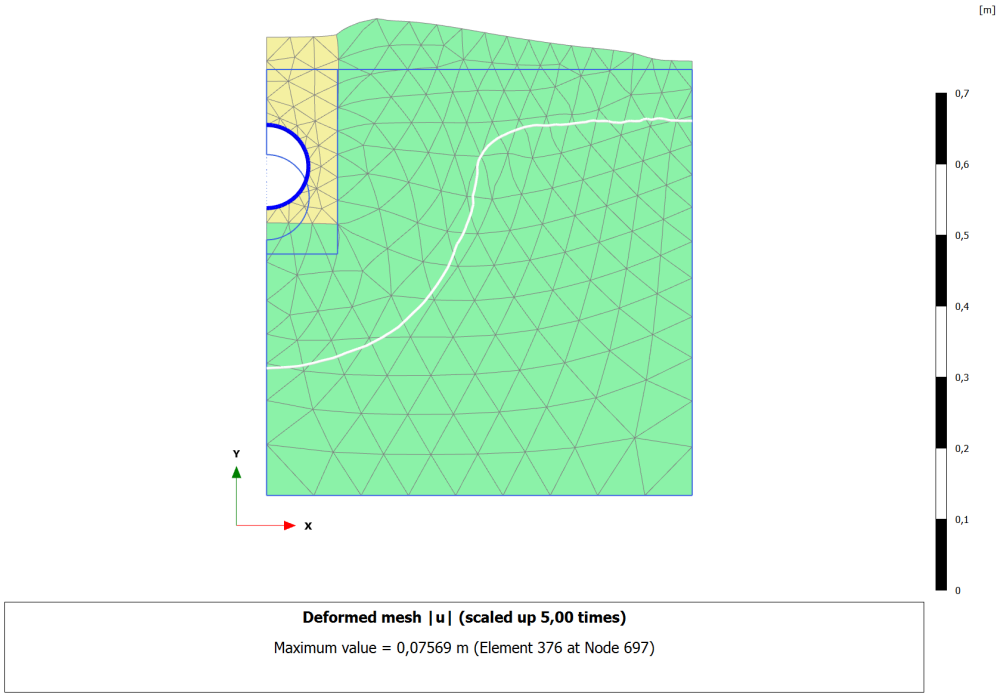

Figure 6.9: Deformed mesh on day 210

simulate the freezing period which led to the current temperature distribution. This also implies the correct stress state of the soil. The initial ice saturation is presented in Figure 6.11 and D.7a.

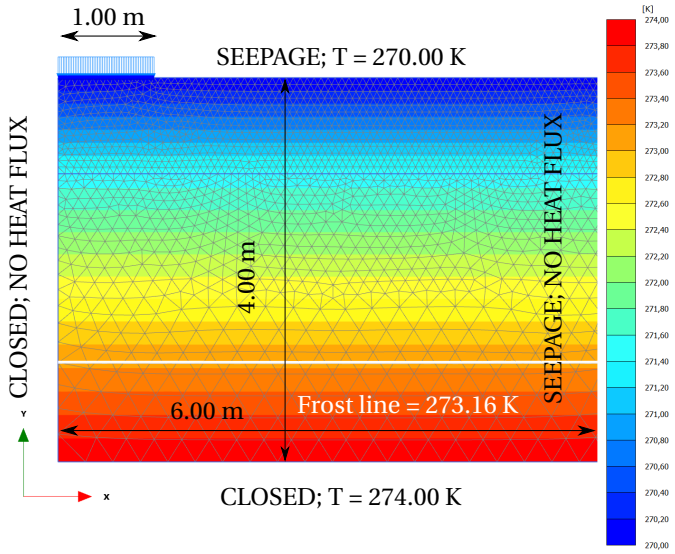

Figure 6.10: Geometry and boundary conditions - foundation on frozen soil

Simulation and results

Once the soil is loaded with the very high foundation load of 500 kPa, the soil underneath the foundation starts yielding. This outward shift of the Loading Collapse yield surface results in settlements up to 3.5 cm (see Figure D.9a). Both the clay layer and the sand layer, experience deformations due to the increase of the surcharge. Although such a high foundation load is probably unrealistic, it shows that frozen ground with

its beneficial properties like high strength and stiffness is able to bear very high loads. Pressure melting by means of the resulting excess pore water pressures at the early stage of loading the soil is not an issue. The load is not high enough to cause this phenomenon to happen. Ice saturation only changes in a range of 1 %.

Next, a linear increase of 2 K in the surface temperature over a long period of time is assumed. This can be related to the climate warming most likely to occur over the next few decades. A new temperature distribution develops. The frost line shifts upward. The cryogenic suction and the ice saturation in both soil layers decrease (see Figure 6.11 and D.7b). The decrease in cryogenic suction and the increase in unfrozen water and therefore also in pore water pressure lead to a new stress state which, at some point, might hit the LC-yield curve. Once the stress hits the LC-yield curve, significant compressive strains and thaw settlements are generated (see also Section 6.1.4). Next to this mechanism, consolidation and, hence, the dissipation of excess pore water pressure with time, result in thaw settlements. The influence of the increase in temperature clearly can be seen in Figure D.8b, where most of the displacements occur in the upper clay layer. The lower dense sand layer is still strong enough to bear the change in temperature, the decrease in ice saturation and the related loss in strength.

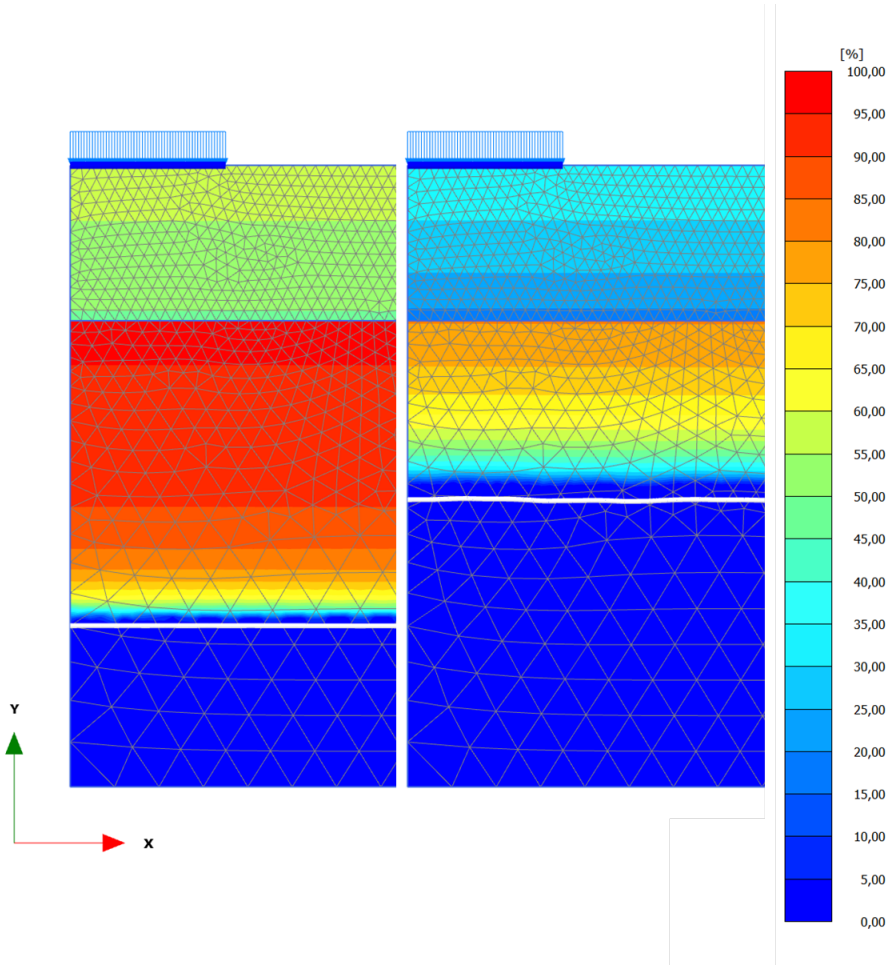

Figure 6.11: Initial ice saturation (left) and ice saturation after the warming period (right)

6.1.7. Freezing pipes in tunnel construction

Artificial ground freezing is an essential element in ground engineering. Many engineering problems are solved by taking advantage of the properties of saturated soil once frozen. By installing freezing pipes and circulating fluid with temperature below the freezing point of water through them, the surrounding soil freezes. An increase in strength and decrease in permeability occurs in freezing soils, thus providing temporary stabilisation of soils and hydraulic seal. However, freezing can cause significant changes in the soil structure. Frost heave while freezing and adverse settlement during thawing may be expected. This small case is adapted

from Brinkgreve et al. (2016), where a tunnel is constructed with the use of freeze pipes in order to stabilise the soil during excavation. Firstly, the soil is frozen by means of the installed freeze pipes. Watertightness and an increase in strength of the soil are achieved. Once the soil has frozen sufficiently, tunnel construction can take place.

Geometry and boundary conditions

A tunnel with a radius of 3.0 m is constructed in a 30.0 m deep sand layer, whose input parameters are defined in Table 6.2 and 6.3. The soil is fully saturated, groundwater flow is not considered. Although it is a symmetric problem we decide to model the whole geometry which is presented in Figure 6.12. The SFCC is calculated by means of the approach described in Section 2.1.2 and illustrated in Figure 6.2b. The freeze pipes are modelled by defining lines with a length similar to the freeze pipe diameter (10.0 cm). Although a convective boundary condition would represent a fluid giving its temperature to the surrounding pipe very accurate, the temperature of the pipe (line) itself is specified. Twelve cooling elements are defined. In reality the amount and the location of the installed freeze pipes may differ. The initial temperature of the soil is set to 283 K. This temperature is kept constant during the entire cooling process at the outer boundaries of the model. Seepage is allowed at the left and right side of the model. The behaviour of the top and bottom groundwater flow conditions is set to closed. The boundary conditions as well as the generated mesh can be seen in Figure 6.12. The tunnel is created with the help of the *Tunnel designer*. Because deformations are considered in this example, a plate material is assigned to the tunnel. The plate (shell) element is defined in Table 6.4 (Brinkgreve et al., 2016).

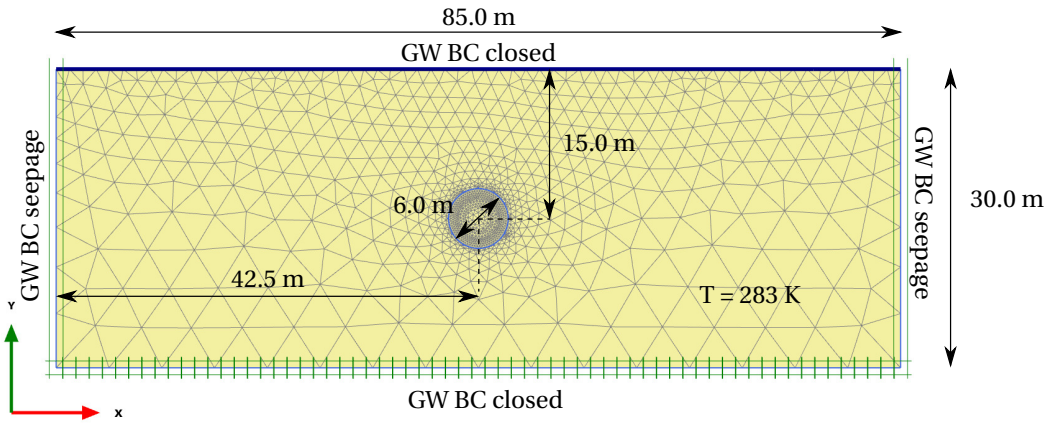

Figure 6.12: Geometry, boundary conditions and mesh - freezing pipes in tunnel construction

Table 6.4: Lining properties

Axial stiffness	Flexural rigidity	Plate thickness	Specific weight	Poisson's ratio	Maximum bending moment	Maximum axial force
EA	EI	d	w_{plate}	ν_{plate}	M_p	N_p
N/m	Nm^2/m	m	N/(mm)	-	Nm/m	N/m
14×10^9	143×10^6	0.35	8400	0.15	1×10^{18}	10×10^{12}

Simulation and results

After a time period of 10 days the freezing pipes reach the temperature of 250 K. For another 170 days this temperature is kept constant. In Figure 6.13 the temperature distribution is captured. The consequences of the artificial ground freezing action is presented in Figure D.10a and D.10b. We observe that a small frost heave of 8 mm occurs and that almost all the soil to be excavated is frozen. Constructing the tunnel requires

the excavation of part of the frozen soil body. This process is carried out in two different ways, namely without and with applying a surcharge at ground level. The freezing period is stopped and both cases are investigated over a time period of one day. Figure D.11 indicates that when excavating the frozen soil body where the future tunnel lining will be installed, an upward force of the underlying unfrozen and frozen soil cause considerable frost heave (2.3 cm). This rigid upward movement is due to buoyancy forces when removing the heavy frozen ice body. When applying a surcharge of 70 kPa this upward movement is not just hindered, but settlements at the ground surface take place (up to 6.8 cm), see Figure D.12 We clearly observe that the resulting displacements in the ground search their way around the strong and stiff frozen 'toroid'. Both investigated cases show that the excavation is safe and stable, a stand-up time of several days is guaranteed.
After one day of unsupported tunnel excavation, the lining is installed. A 15 day period is considered without the operation of the freezing pipes. A new temperature distribution develops, ice starts melting and a reduction in strength can be observed. The displacements after a period of 15 days without operating freeze pipes are shown in Figure D.13 and D.14. Thaw settlements of 0.6 and 1.8 cm are observed, respectively. The total displacements are presented in Figure D.15. The case where a surcharge has been applied provides final settlements of 8.1 cm whereas the one without surcharge ends up with a heave of the ground surface of 1.9 cm.

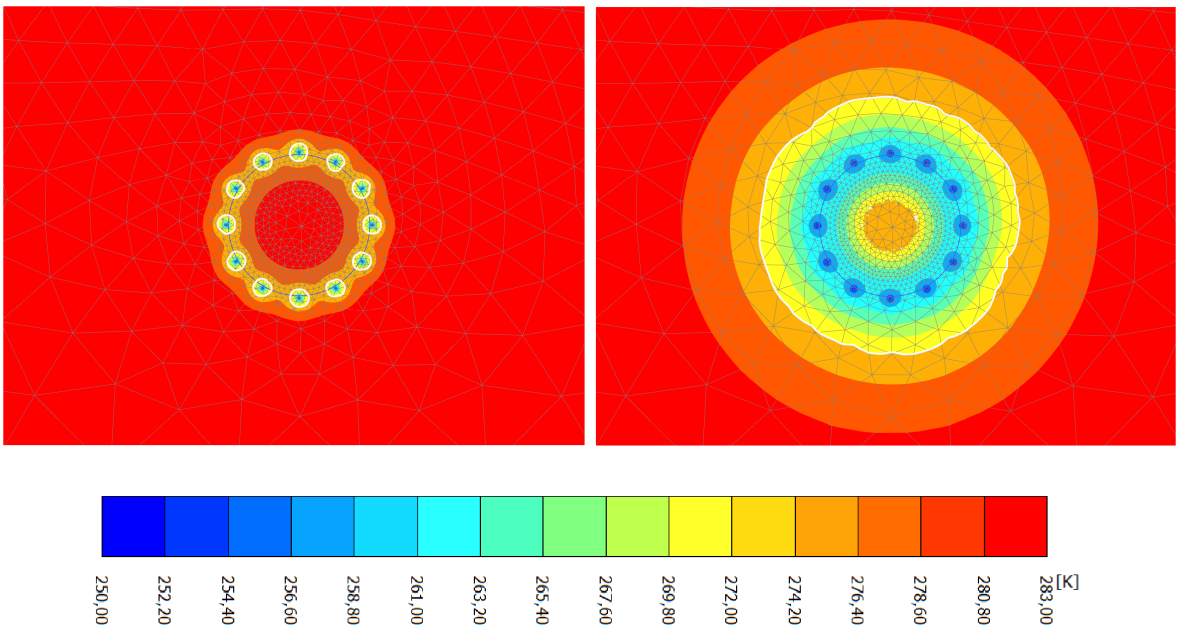

Figure 6.13: Temperature distribution after a time period of 10 days (left) and 180 days (right)

7

Discussion and conclusions

7.1. Discussion

In this section, the proposed approaches, parameter determination procedures and obtained results from verification and validation calculations are reflected and discussed. The limitations of my research and the ones of the constitutive model are highlighted.

7.1.1. Determination of the soil freezing characteristic curve and hydraulic soil properties

This straightforward approach shows that it is possible to obtain crucial frozen soil properties by means of limited input data. Time-consuming field tests and laboratory tests can be sidestepped. Furthermore, the use of other approaches to relate the water retention curve to the SFCC and to estimate the hydraulic properties of frozen soil, like the ones from van Genuchten (1980) or Fredlund et al. (1994), require the determination of additional parameters and can be avoided. One has to keep in mind that the determination of these parameters to many engineers is not daily engineering practice.

Our proposed approach provides budding results regarding the determination of the SFCC for different types of soil subjected to different pressure levels. In the empirical equation used to calculate the unfrozen water content the specific surface area represents the soil type dependence. The fact that many physical and chemical soil processes in soil are closely related to the SSA justifies using this soil parameter. The use of the empirical relation of Sepaskhah et al. (2010) to estimate the specific surface area by means of the geometric mean of the soil particle diameter d_g has been examined by Fooladmand (2011) and was found to provide good approximations of the SSA for different soils. The determination of the geometric mean of the soil particle diameter (Shirazi and Boersma, 1984), however, requires some assumptions. Firstly, the soil has to have a lognormal particle size distribution within each size fraction. Secondly, it is based on the U.S.D.A. classification scheme and sticks to its particle size limits. Finally, an important limitation of the determination of d_g, and consequently the SSA, is the fact that the specific surface area differs largely between types of clay minerals and this cannot be taken into account using the textural information approach.

When considering the pressure dependence of the SFCC and the related depression of the freezing/thawing point the pressure melting phenomena plays a key role. The comparison values used in 3.1.2 are results from SFCC measurements under high pressure levels conducted by Zhang et al. (1998). We are sure that the conducted tests can be classified as tests in undrained conditions, leading to the development of excess pore water pressure in the soil sample almost equal to the applied pressure. By using the pressure-dependent formulation for the freezing/melting point the high pore water pressures lead to the depression of the freezing/melting point. The simulated results in 3.1.2 show conformity with the test results. The assumption that most tests on frozen soil can be classified as undrained tests, is supported by Andersland and Ladanyi (2004).

Obviously there is no perfect conformity of the estimated hydraulic conductivities in an unfrozen and frozen state with direct measurements. Factors which influence the accuracy of the simulated results are the empirical estimation of the volumetric unfrozen water content as well as the use of Campbell's model which is again empirical and originally formulated for unsaturated soil. Other points are the quality of direct measurements and the influence of ice lenses in the soil samples (see the results of densely lensed Leda clay in Fig 3.6c). They highly influence the hydraulic conductivity. The drop in hydraulic conductivity occurring within

a very small temperature range of less than 0.50 °C, however, can be reproduced by using the proposed approach. One has to keep in mind that all these equations are estimations and will never correctly predict, for instance, the saturated hydraulic conductivity of a soil which contains large, interconnected cracks or root channels. Furthermore, the effect of overburden pressure and pressure in general is not investigated. In qualitative terms, an increase in pressure causes a freezing point depression. The result is a bigger availability of unfrozen water and considering double porosity networks a higher hydraulic conductivity at constant temperature. Reversely, as pressure (or temperature) decreases, the hydraulic conductivity of frozen soil sharply decreases. This is commonly observed in frozen soil (Stähli et al., 1999; McCauley et al., 2002). Summing up, the pressure dependence also can be achieved using the proposed empirical approach. Benson and Othman (1993) explain, however, that an increase in overburden pressure may also decrease the hydraulic conductivity of the frozen fringe, by compressing the pores and the cracks which consequently restricts the conduits for flow. This effect, causing a decrease in voids, cannot be taken into account using this approach.

Keeping in mind the simplicity, the user-friendliness, the low expenditure of time and the obtained conformity between model predictions and measured data of many soil types, it is worth considering this approach as the initial estimation of the SFCC, the freezing/melting point of a soil-water system and its hydraulic conductivity. First boundary value problems performed in a THM-FE environment considering unfrozen and frozen soil have shown that the numerical implementation of this approach is stable.

7.1.2. Parameter determination

The parameter determination comprises a great part of this report. Proposed soil tests, correlations, default values and a calibration method are discussed. The proposed soil tests should be conducted in order to obtain reliable input parameters. Correct sampling and execution of the test programme is of great importance. Strain rates and stress levels should be chosen in a way that they correspond with the ones to be envisaged in the modelling exercise. Thus, the default values proposed in 4.3 should be used cautiously. Although proper testing might have been executed, still, it may prove impossible to come up with a perfect parameter set. In other words, it may be impossible to matching accurately the behaviour of some frozen soils under isotropic or one-dimensional stress states with the constitutive model, irrespective of the choice of model parameter values. The parameters controlling virgin loading under isotropic stress state are the most difficult ones to determine. Significant reasons for this current difficulty are the determination of these parameters in general and the uncertainty whether the model is actually able to represent frozen soil accurately enough or not. The lack of experimental data on hydrostatic testing and/or oedometer testing on frozen soil at different constant temperatures impedes this validation. The proposed calibration method using oedometer test results can be a starting point to fit parameters controlling virgin loading under isotropic stress state to real test data.

7.1.3. Interpretation of results

The verification and validation of the constitutive model have the intention to check for the correctness of its theoretical implementation and for its correct representation of the behaviour of frozen soil found in nature. The simulated tests on the reference soil clay as well as the outcome of the boundary value problems are generally in accordance with the expected behaviour described by many researchers. However, the presented tests cannot demonstrate the entire sensitivity of frozen soil response to various effects.

The behaviour of a frozen soil under an increase of isotropic compression is considered to be the result of combined mechanical and thermodynamic effects. Mechanical effects govern the stress sharing, and thermodynamic effects the pressure melting phenomenom, respectively. Considering an increase in confining pressure, the strength of frozen soil increases to a peak value. The general increase in strength caused by the increase in confining pressure can be observed in all simulated tests which are mainly conducted as drained tests. In order to observe the decrease in strength with a further increase of confining pressure, fast loading (undrained behaviour) and high confining pressures have to be applied. The decrease in strength with further increase in confining pressure is due to the increasing amount of unfrozen water in the samples as a result of pressure melting, see Parameswaran and Jones (1981) and Yang et al. (2010). They consider that the initial increase in strength with increase in hydrostatic confining pressure could be due to the closure of voids and microcracks. Ma et al. (1999) explain that the effect of pressure melting causes a decrease of the cementing leverage between the soil skeleton and the ice matrix, thus increasing the effective stress applied to the soil skeleton. Due to the low hydraulic conductivity of frozen soil (see 3.2.2), water migration toward lower stress regions and the time necessary to transfer applied stresses to the grain structure is extremely long. Meanwhile, the increasing amount of unfrozen water reduces friction among particles and accelerates the adjustment in the structure. With the breakdown of the coarse particles in frozen soils, the particles are

rearranged, the stresses are redistributed and a new equilibrium system is formed, causing the strength of the frozen soils to begin to decrease. With further increases in the confining pressure, the above process goes on repeatedly until the pore ice begins to melt. When the effective stress applied to the soil skeleton surpasses its limiting strength, micro-cracks start causing a decrease in the strength of the frozen soils. The incorporation of the pressure melting phenomenon is definitely a nice feature, and is important when designing projects like mines, underground railways and across-river tunnels (Lai et al., 2009).

When we consider shear testing, a very important assumption of the model is the independence of Young's modulus with a change in confining pressure. The simulated results compared to results from Lai et al. (2010) illustrated in Figure 5.10 showed that this assumption is not necessarily wrong. In contrary, the bulk modulus is partly pressure-dependent and is in accordance with observed results in an isotropic compression test conducted by Lee et al. (2002).

The comparison of results of triaxial compression tests on frozen silt obained by Lai et al. (2010) and simulated results in a single stress point environment show that a best fit can only be achieved when two slightly different parameter sets are chosen to represent the temperature and the confining pressure dependence. To obtain conformable results regarding the pressure dependency, the critical slope line M had to be changed with pressure. It is not completely clear to the author if this is a limitation of the model or if it is caused by an inappropriate parameter set and the non incorporation of thermodynamic effects in single stress point environment tests. Despite this discrepancy, it is notable that parameter sets can be found to represent temperature dependency and pressure dependency very accurately.

The temperature is probably the most important factor affecting the behaviour of frozen soil. In nature it directly influences the strength of intergranular ice, the bonding strength of the interface between soil particles and ice, and the amount of unfrozen water in a frozen soil. In general, a decrease in temperature results in an increase in strength of a frozen soil, but at the same time it increases its brittleness, which is manifested by a larger drop of strength after the peak. When looking at the simulation results compared to the results of frozen silt tested under triaxial compression by Lai et al. (2010), this behaviour can clearly be achieved with the current constitutive model. It is remarkable how accurate the interaction between chosen parameter set and the estimated SFCC can represent the behaviour of the tested frozen silt.

The right elastic behaviour of a frozen soil is quite straightforward to simulate. Only few parameters control this behaviour. When it comes to plastic behaviour, controlling the amount of plastic strains arising is difficult. Almost all parameters are more or less influencing the plastic behaviour of the partially frozen soil. The sensitivity of each single parameter hasn't been investigated in detail. Certainly we can conclude that the direction of plastic strain increments, associated with the LC-yield surface, is highly dependent on the unfrozen water saturation S_{uw}. The plastic potential parameter γ gives us the possibility to steer the volumetric behaviour. However, a better understanding and a detailed investigation of the influence of each single parameter on the plastic behaviour is necessary.

When soil is subjected to a freezing period, frost heave and ice segregation may occur. Depending on the frost susceptibility of the soil and the availability of water and overburden pressure, soils vary in their proneness to undergo frost heave actions. In sand, the surface contact is relatively low, so the unfrozen water saturation will decrease very fast, then the relative permeability will decrease rapidly, so water movement to the frozen fringe is hindered. No considerable frost heave can therefore be observed in sand. This behaviour is also obtained considering the simulated cases of the chilled pipeline and the freezing pipes in tunnel construction. The sand layer shows a low proneness to undergo frost heave. When we consider clay, although the specific surface area is high and water saturation decreases slowly, the intrinsic permeability is very low and prevents excessive frost heaving action. The chilled pipeline example illustrates that with the chosen clay parameter set, the accumulation of dilative plastic strains is much higher than the ones occurring in sand. The pipeline and the trench filled with sand are literally pushed up due to the frost heave action arising in the clay layer. Silt is not tested in any of the performed boundary value problems, but its specific surface area is not as low as the one of sand and the unfrozen water saturation will actually decrease moderately with decreasing temperature. Furthermore, the relative permeability doesn't decrease very fast and, hence, its intrinsic permeability is not low enough to prevent the movement of water. Regarding frost heave, silts can be considered as probably the most problematic soils. Despite this generalisation, other soil types may also indicate excessive frost heave. Before actual frost heave and the related formation of ice lenses are allowed to occur, the constitutive model requires to pass an elastic region in the $s_c : p^*$ plane. In this region ice starts forming but causes the attraction of soil grains and elastic compressive strains. This simulated behaviour can be related to a phenomenon of the macroscopic behaviour of freezing soils, namely the curvature induced premelting mechanism. This mechanism is a result of the existence of surface tension of the water meniscus

formed between soil particles and is is very similar to the capillary suction by bonding grains together. It is a reason why not all of the water in a frozen soil transforms to ice. The arising elastic compressive strains are controlled by the parameter κ_s and the segregation threshold value $s_{c,seg}$. Once the temperature reaches the value where the related cryogenic suction hits the GS-yield surface ($s_{c,seg}$) the accumulation of dilative plastic strains is allowed and frost heave takes place. The proposed initial segregation threshold values are related to the water saturation of the soil. Because of the rapid increase in ice saturation in a sandy sample, the formation of ice lenses starts at a lower $s_{c,seg}$ value than for silt and clay. Rempel (2007) demonstrates that the initiation of a new second ice lens occurs at a different temperature than the first one and that ice lenses continuously grow until a limiting temperature is reached. The constitutive model, however, cannot distinguish whether it is the first ice lens or any successive one. Furthermore, no actual limiting value can be considered stopping ice lens growth, but with decreasing temperature and decreasing availability of water the increase in $s_{c,seg}$ and the decrease in S_{uw} reduce the accumulation of dilative plastic strains gradually. One has to keep in mind that the term ice lens formation is only linked to the occurrence of dilative plastic strains in this constitutive model. The actual theory behind ice lens formation in nature is very difficult to implement.

The freeze-thaw cycles and the practical application of a foundation on frozen soil subjected to a warming period show the ability of the model to simulate the thaw consolidation and settlement behaviour, respectively. Due to the disappearance of ice upon increasing temperature or very high confining pressures, the soil skeleton must adapt itself to a new equilibrium void ratio (Andersland and Ladanyi, 2004). The increase in unfrozen water content may cause the occurrence of excessive pore water pressures. During thaw consolidation these excessive pore water pressures abate. The rate of the thaw consolidation depends on both the melting rate of the ice and the hydraulic properties of the soil (Zhang, 2014). Volume change will then result from the phase change, the flow of excess water out of the soil and due to applied loads. In both examples this behaviour can be observed. The right choice of parameters, the length of the thawing period and the stress state of the soil play a vital role in achieving this behaviour. In more explanatory words this means that upon thawing three different behaviours influence the volumetric behaviour of the soil. The first one is the parameter κ_s, which upon freezing causes compressive elastic strains but on thawing dilative elastic strains due to the negative increment of cryogenic suction. The second one is consolidation, which like previously mentioned depends on both the hydraulic properties of the soil and the rate of temperature increase. Finally, the stress state plays a key role. Upon freezing the GS-yield curve moves upward, consequently the LC-yield curve moves inward and reduces the pseudo-preconsolidation pressure at any negative temperature. Upon thawing the stress may hit the LC-yield curve and plastic compressive strains accumulate. Whether or when this occurs, depends on the initially chosen preconsolidation pressure of the soil in unfrozen state, the confining pressure and the rate at which consolidation takes place. All three behaviours are competing and influencing each other during the whole thawing period. Therefore, if these principles of the constitutive model are not well understood and inappropriate parameters are chosen, unexpected behaviour might be encountered when simulating thawing periods. However, ending up with smaller displacements than the displacements caused by frost heave is not necessarily wrong (Konrad, 1989). Real soil behaviour shows that it depends primarily on the history of loading prior to freezing and the number of freeze-thaw cycles the soil has been subjected to.

Considering a situation where the LC-yield curve is not hit at all upon thawing, we most probably end up with an increase in volume. Furthermore, the GS-yield curve will not be activated and stays at its maximum experienced cryogenic suction value. A second freeze-thaw cycle to the same negative temperature would only result in pure elastic compressive strains upon freezing and elastic dilative strains upon thawing. The user has to exercise with caution.

7.1.4. Limitations of the constitutive model and my research

Some issues which have to be regarded with suspicion are mentioned in the previous section. This section gives a summary of the limitations of the constitutive model regarding its theoretical formulation and the delimitations of my research activities.

Limitations of the constitutive model

The presented constitutive model is not able to demonstrate the entire sensitivity of frozen soil response to various effects. Probably the most important feature not incorporated is the deformation behaviour with time of frozen soils. Ice and consequently frozen soil is highly rate dependent. A decrease in peak strength values as well as in residual values can be observed for decreasing strain rates (Haynes, 1978; Andersland

and Ladanyi, 2004; Arenson and Springman, 2005). Figure 1.7b illustrates that for a given temperature the compressive strength increases with increasing strain rate. Additionally, Arenson and Springman (2005) note that as axial strain rates decrease, the peak value approaches the value of the residual shear strength. Their explanation is that the material starts to creep at the lower strain rates and therefore stresses redistribute and relaxation occurs, suppressing the tendency for dilation, so no additional shear resistance of the frozen soil is activated as the sample undergoes increasing strain. Considering creep behaviour of frozen soil, Andersland and Ladanyi (2004) show that primary, secondary, and tertiary creep can be distinguished. Creep in frozen soils is influenced not only by temperature but also by the magnitude of applied stress, soil type, and its density. An enhanced constitutive model with the incorporation of creep and rate dependence behaviour is in development at NTNU in Norway.

Once water in the pores starts to freeze, the ice together with the soil grains form the so called solid phase. The definition of the solid phase stress, hence, cannot distinguish between the actual stress-strain behaviour of ice and the soil skeleton. However, in reality both materials show different strain dependences and start yielding at different axial strains. The yielding of ice starts at much lower strains than the yielding of the soil skeleton.

Investigating cyclic behaviour and the related hysteresis effects is not possible with the current implementation of the model, even if the actual formulation of the model allows it. Experimental observations have revealed that the variation of the unfrozen water content of a soil is hysteretic during freezing-thawing cycles (Spaans and Baker, 1996). However, in order to incorporate this feature in the hydrodynamic part of the THM-model, a better understanding of this mechanism is required. Moreover, the model itself also has difficulties when cooping with more than one freeze-thaw cycle (see Section 6.1.4). Generally the author proposes to only use the current model for not more than one freeze-thaw cycle.

Although a linear increase in tensile strength with increasing ice saturation is considered in the formulation of the constitutive model, test data have shown a different evolution of the tensile strength of freezing soil (Haynes, 1978; Akagawa and Nishisato, 2009; Wu et al., 2010; Azmatch et al., 2011; Zhou et al., 2015). At temperatures close to the freezing point, an initial high increase in tensile strength is expected. With decreasing temperature the increase flattens. The major part of tensile strength a freezing soil obtains at temperatures close to the freezing point. The evolution of apparent cohesive strength is chosen to be a simplification of real soil behaviour. Whether this simplification can be seen as limitation is not clear. The use of a critical state line with constant inclination is another simplification of the model. Lai et al. (2009) propose to use a curved critical state line rather than a linear one. In addition, Lai et al. (2010) show that the CSL curve of frozen silt could be approximately considered as a straight line under low confining pressures, but with the increase of confining pressures the CSL curve begins to bend downwards. When considering a further increase of confining pressures, the CSL curve even drops because of the pressure melting and the crushing phenomena. The current model uses the Drucker-Prager surface in the three dimensional principal stress space (π-plane), which is an attempt to approximate the irregular hexagonal cross-section of Mohr-Coulomb by a smooth circular cone that is independent of the Lode angle, θ. More advanced strength criterion could be considered, like the Mohr-Coulomb or the extended Lade-Duncan strength function.

The anisotropy and the non-uniformity of ice distribution in naturally frozen soils like permafrost cannot be taken into consideration. Yang et al. (2015) have reported that the ultimate compressive strength of naturally frozen horizontal specimens is substantially higher than that of vertical specimens at the same testing temperature. This strength anisotropy is likely due to ice wedge formation, commonly observed in permafrost.

7.2. Conclusions and recommendations

7.2.1. Conclusions

What are the main features of the new constitutive model for frozen and unfrozen soil developed by NTNU and Plaxis bv and how does it differ from other constitutive models for frozen soil?

The new constitutive model describes the mechanical behaviour of frozen soil as a function of temperature, all the way to the unfrozen state, and vice versa. It has been implemented in a fully coupled THM finite element code. This allows the study of a variety of geotechnical issues involving freezing and thawing soils. The constitutive model is a critical-state elasto-plastic mechanical soil model formulated within the framework of two-stress state variables. The stress state variables are the cryogenic suction and the solid phase stress. The latter is considered as the combined stress of the soil grains and ice, whereas the cryogenic suction is defined as the difference between the ice pressure and the pore water pressure, taking the effects of

ice content and temperature variation into account. In its unfrozen state, the model becomes a conventional critical state model. The simple modified Cam clay model is adopted for the unfrozen state. Considering the frozen state, two suction-dependent yield functions are applied. The Loading Collapse yield surface considers the variation of solid phase stress and takes the influence of the bonded water in frozen soil into account. In contrary the Grain Segregation yield criterion covers the variation in cryogenic suction and captures the phenomenon of grain segregation and ice lens formation upon freezing.

There is no well-known and generally accepted constitutive model for frozen soil yet. Researchers have come up with a variety of approaches to describe frozen soil over the last decades and hence a comparison to all of them is difficult to make. To name the most important differences to other models the following can be said: Total stress-based models (Arenson and Springman, 2005; Lai et al., 2008, 2009, 2010; Zhu et al., 2010; Xu, 2014) place less emphasis on the influence of factors like temperature and ice content, hence, they cannot simulate deformations under the variation of ice content and/or temperature during a freezing or thawing period. Effective stress-based models (Thomas et al., 2009; Nishimura et al., 2009; Zhou, 2014; Zhang, 2014) may use different definitions of pore water pressure and, if applicable, a different second state variable than the cryogenic suction. Zhou (2014) considers the temperature during freezing whereas Zhang and Michalowski (2015) employ the pore ice ratio as the independent second state variable. To simulate the frost heave phenomenon Nishimura et al. (2009) apply a segregation potential theory, Thomas et al. (2009) adopt a stress criterion for initiating a new ice lens and Zhang and Michalowski (2015) a porosity growth function.

Is the numerical model implemented according to its theoretical formulation and is the simulated mechanical behaviour in accordance with the observed behaviour in nature?
The theoretical implementation of the model and its ability to represent the behaviour of frozen soil has been investigated in the chapters verification and validation (Chapter 5 and 6). The simulated tests on the reference soil clay as well as the outcome of the boundary value problems show accordance with the theoretical formulation and with the expected frozen soil behaviour found in nature. Phase transition and further changes in temperature and confining pressure provide the expected change in mechanical properties and stress-strain behaviour. A decrease in temperature results in an increase in strength of a frozen soil, but at the same time increases its brittleness. Considering an increase in confining pressure, the strength of frozen soil increases to a peak value and decreases with a further increase of confining pressure. The decrease in strength with further increase in confining pressure is due to the increasing amount of unfrozen water in the samples as a result of pressure melting (Parameswaran and Jones, 1981; Yang et al., 2010). The phenomena of frost heave, thaw settlements and pressure melting can successfully be simulated for the investigated cases. However, not the entire sensitivity of frozen soil response to various effects can be represented.

Is it possible to model frost heave appropriately?
Rempel (2007) demonstrates that the initiation of a first ice lens occurs for different soils at different negative temperature and that ice lenses continuously grow until a limiting temperature is reached. The constitutive model requires an initial segregation threshold value as input parameter which can be seen as the initiation of the first ice lens to grow. Once the temperature drops to the temperature causing a cryogenic suction equal to the initial segregation threshold value, the Grain Segregation yield surface is hit and the accumulation of dilative plastic strains is allowed. Frost heave takes place. The amount of plastic dilative strains accumulating depends on the availability of water. With decreasing temperature and decreasing availability of water the accumulation of dilative plastic strains gradually decreases and stops. The plastic resistance of the soil increases and a limiting value is reached when the water saturation reduces to zero. Hence, the model is able to simulate frost heave in a correct qualitative manner.

How accurate can settlements due to thawing processes be modelled?
Three different behaviours influence the volumetric behaviour of the soil upon thawing. The parameter κ_s causes dilative elastic strains due to the negative increment of cryogenic suction upon thawing. Next, consolidation affects the volumetric behaviour when frozen ground is subjected to a warming period. The consolidation is dependent on the hydraulic properties of the soil and the increase rate of temperature. Finally, the stress state plays a key role. Upon freezing the GS-yield curve is shifted upward and due to coupling effects the LC-yield curve moves inward. Due to this inward shift, stresses may hit the LC-yield curve upon thawing and plastic compressive strains accumulate. Whether or when this occurs depends on the initially chosen preconsolidation pressure of the soil in unfrozen state, the confining pressure and the rate at which consolidation takes place. All three behaviours are in a constant competition and influence each other during the thawing period. Therefore, the right choice of parameters, the length of the thawing period and the stress state are important. The model has to be fully understood when simulating thawing periods, otherwise unexpected behaviour might be encountered. However, ending up with smaller displacements than the

displacements caused by frost heave is not always wrong (Konrad, 1989).

Is the model appropriate to forecast the long term behaviour of an engineering structure?
The presented constitutive model is not able to demonstrate one of the most important features considering long term behaviour. The deformation behaviour with time of frozen soil is not incorporated. Ice and consequently frozen soil is highly rate dependent. Furthermore, the creep behaviour of frozen soils is not negligible and is influenced not only by the temperature but also by the magnitude of applied stress, soil type, and its density (Andersland and Ladanyi, 2004). When considering long term behaviour, the simulation of cyclic behaviour (multiple freeze-thaw cycles) may lead to unexpected results. Furthermore, hysteresis effects on the unfrozen water content due to freeze-thaw cycles (Spaans and Baker, 1996) are not possible to consider with the current implementation of the model. Generally the author proposes to only use the current model for not more than one freeze-thaw cycle. Forecasting the long term behaviour is not yet possible, but is part of the ongoing research at NTNU.

What are the shortcomings and limitations of the constitutive model?
The investigated constitutive model cannot demonstrate the entire sensitivity of frozen soil response to various effects. The non-incorporation of the deformation behaviour with time is a major shortcoming. Furthermore, the difficulty to simulate multiple freeze-thaw cycles and the non consideration of related hysteresis effects make the model not appropriate to forecast long term behaviour of engineering structures. The definition of the solid phase stress cannot distinguish between the actual stress-strain behaviour of ice and the soil skeleton. The yielding of ice starts at much lower strains than yielding of the soil skeleton. The anisotropy and the non-uniformity of ice distribution in naturally frozen soils like permafrost cannot be taken into account. Strength anisotropy is likely to occur due to ice wedge formation, commonly observed in permafrost.

The constitutive model requires several parameters of which quite a few are not very common to geotechnical engineers. Although some correlations and default values can be provided, the number of parameters needed remains high. Thus, the user-friendliness recedes. However, empirical approaches to obtain the soil freezing characteristic curve and hydraulic properties for freezing soil as well as a calibration method to determine the Barcelona Basic Model parameters explained in 4.4 are provided to countervail this shortcoming.

Simplifications, like the assumption that the tensile strength of a freezing soil increases linearly with decreasing temperature, that the critical state line is a straight line rather than a curved one and that the current model uses the Drucker-Prager surface in the three dimensional principal stress space (π-plane) are no real shortcomings, but are starting points to improve and enhance the model.

7.2.2. Recommendations for further research

The main research objective was to verify the implementation of the new numerical model and to test it in practical applications by validating whether it represents real data sufficiently and may be used for design and forecast approaches. Some important topics, however, haven't been investigated in detail.

Further research has to focus on the influence and the sensitivity of the different model parameters. Although it is explained what the single parameters stand for and what their physical meaning is, their influence on the yield surface and on the elasto-plastic behaviour should be researched in more detail. Especially the exact influence of parameters controlling virgin loading under isotropic stress state and the ones considering cryogenic suction variation, the yield parameter and the plastic potential parameter should be investigated thoroughly. Parameter variation studies and sensitivity analyses should be carried out. Part of this research could also be the validation of the proposed parameter calibration method using oedometer tests to calibrate parameters controlling virgin loading under isotropic stress state. Oedometer tests on frozen soil at different constant temperatures below the freezing point and at least one in an unfrozen state should be performed. The results should be used to calibrate the parameters for the current constitutive model and to validate the suitability of the proposed calibration method. It would be of great importance to further increase the user-friendliness of the constitutive model.

This research has verified boundary value problems and simplified applications which might represent real case studies. In further research, more advanced case studies, like the degradation of permafrost underneath a road embankment, the occurrence of slope failure due to the exposure of an ice rich cut slope or the development of stresses and deformations due to a buried pipeline in permafrost could be investigated. However, in order to perform a more advanced case study, the influence and the sensitivity of the model parameters have to be fully understood and the robustness of the THM finite element modelling has to be guaranteed. The incorporation of the time dependent behaviour of frozen soil is a plus.

Bibliography

All about frozen ground. https://nsidc.org/cryosphere/frozenground. Accessed 2 June 2016.

Akagawa, S. and K. Nishisato (2009). Tensile strength of frozen soil in the temperature range of the frozen fringe. *Cold Regions Science and Technology 57*(1), 13 – 22.

Alfaro, M., G. Ciro, K. Thiessen, and T. Ng (2009). Case study of degrading permafrost beneath a road embankment. *Journal of Cold Regions Engineering 23*(3), 93–111.

Alkire, B. D. (1973). The effect of confining pressure on the mechanical properties of sand-ice materials. *Journal of Glaciology 12*(66), 469–481.

Alonso, E., A. Gens, and A. Josa (1990). A constitutive model for partially saturated soils. *Géotechnique 40*(3), 405–430.

Andersland, O. and B. Ladanyi (2004). *Frozen Ground Engineering (2nd Edition)*. John Wiley & Sons.

Andersland, O. B., D. C. Wiggert, and S. H. Davies (1996). Hydraulic conductivity of frozen granular soils. *Journal of Environmental Engineering 122*(3), 212–216.

Anderson, D. M. and A. R. Tice (1972). Predicting unfrozen water content in frozen soils from surface area measurements. In *Highway Research Record*, Volume 393, pp. 12–18.

Arenson, L. and S. Springman (2005). Mathematical descriptions for the behaviour of ice-rich frozen soils at temperature close to $0^o c$. *Canadian Geotechnical Journal 42*(2), 431–442.

Azmatch, T. F., D. C. Sego, L. U. Arenson, and K. W. Biggar (2011). Tensile strength and stress-strain behaviour of devon silt under frozen fringe conditions. *Cold Regions Science and Technology 68*(1-2), 85 – 90.

Azmatch, T. F., D. C. Sego, L. U. Arenson, and K. W. Biggar (2012a). New ice lens initiation condition for frost heave in fine-grained soils. *Cold Regions Science and Technology 82*, 8 – 13.

Azmatch, T. F., D. C. Sego, L. U. Arenson, and K. W. Biggar (2012b). Using soil freezing characteristic curve to estimate the hydraulic conductivity function of partially frozen soils. *Cold Regions Science and Technology 83 - 84*, 103 – 109.

Baker, T. (1979). Strain-rate effect on the compressive strength of frozen sand. *Engineering Geology 13*, 223–231.

Bear, J. and A. Verruijt (1987). *Modeling Groundwater Flow and Pollution*, Volume 2. D. Reidel Publishing Company.

Bekele, Y. (2014, 18–20 June). On thermo-hydro-mechanically (thm) coupled finite element modeling of ground freezing and thawing. In M. A. Hicks, R. B. Brinkgreve, and A. Rohe (Eds.), *Numerical Methods in Geotechnical Engineering*, Volume 2, Delft, The Netherlands, pp. 959–964. CRC Press/Balkema.

Benson, C. and M. Othman (1993). Hydraulic conductivity of compacted clay frozen and thawed in situ. *Journal of Geotechnical Engineering 119*(2), 276–294.

Black, P. and A. Tice (1989). Comparison of soil freezing curve and soil water curve data for windsor sandy loam. *Water Resources Research 25*(10), 2205–2210.

Brinkgreve, R., S. Kumarswamy, and W. Swolfs (2016). *PLAXIS 2D Tutorial Manual*.

Burt, T. and P. Williams (1976). Hydraulic conductivity of frozen soils. *Earth Surf. Processes 1*(4), 349–360.

Campbell, G. S. (1985). *Soil Physics with Basic*. Elsevier.

Chamberlain, E., C. Groves, and R. Perham (1972). The mechanical behaviour of frozen earth materials under high pressure triaxial test conditions. *Géotechnique 22*(3), 469–483.

Coussy, O. (2005). Poromechanics of freezing marterials. *Journal of Mechanics and Physics of Solids 53*, 1689–1718.

de Grandpré, I., D. Fortier, and E. Stephani (2012). Degradation of permafrost beneath a road embankment enhanced by heat advected in groundwater. *Canadian Journal of Earth Sciences 49*(8), 953–962.

DiMillio, A. (1999, June). A quarter century of geotechnical research. Technical report, Federal Highway Administration, Washington, DC.

D'Onza, F., D. Gallipoli, and S. J. Wheeler (2012). *Unsaturated Soils: Research and Applications: Volume 2*, Chapter A New Procedure for Determining Parameter Values in the Barcelona Basic Model, pp. 93–102. Berlin, Heidelberg: Springer Berlin Heidelberg.

D'Onza, F., S. Wheeler, D. Gallipoli, M. B. Bucio, M. Hofmann, M. Lloret-Cabot, A. L. Morancho, C. Mancuso, J.-M. Pereira, E. R. Morales, M. Sánchez, W. Solowski, A. Tarantino, D. Toll, and R. Vassallo (2015). Benchmarking selection of parameter values for the barcelona basic model. *Engineering Geology 196*, 99 – 118.

Fooladmand, H. R. (2011). Estimating soil specific surface area using the summation of the number of spherical particles and geometric mean particle-size diameter. *African Journal of Agricultural Research 6*(7), 1758–1762.

Fortier, R., A.-M. LeBlanc, and W. Yu (2011). Impacts of permafrost degradation on a road embankment at umiujaq in nunavik (quebec), canada. *Canadian Geotechnical Journal 48*(5), 720–740.

Fredlund, D. and A. Xing (1994). Equations for the soil-water characteristic curve. *Canadian Geotechnical Journal 31*(4), 521–532.

Fredlund, D., A. Xing, and S. Huang (1994). Predicting the permeability function for unsaturated soils using the soil-water characteristic curve. *Canadian Geotechnical Journal 31*(4), 533–546.

Gallipoli, D., F. D'Onza, and S. J. Simon Wheeler (2010). A sequential method for selecting parameter values in the barcelona basic model. *Canadian Geotechnical Journal 47*(11), 1175–1186.

Ghoreishian Amiri, S. A., G. Grimstad, M. Kadivar, and S. Nordal (2016). A constitutive model for rate-independent behavior of saturated frozen soils. *Canadian Geotechnical Journal*.

Glendinning, M. C. (2007). *Modelling the Freezing and Thawing Behaviour of Saturated Soils*. Ph. D. thesis, Cardiff University.

Hansen-Goos, H. and J. S. Wettlaufer (2010, March). Theory of ice premelting in porous media. *Physical Review E 81*(3).

Haynes, F. (1978, July). Strength and deformation of frozen silt. In *Proc. 3rd Int. Conf. on Permafrost*, Volume 1, Edmonton, Alberta, Canada, pp. 656 – 661. National Research Council of Canada.

Henry, K. (2000, September). A review of the thermodynamics of frost heave. Technical Report ERDC/CRREL TR-00-16, US Army Corps of Engineers.

Hohmann, M. (1997). Soil freezing - the concept of soil water potential. state of the art. *Cold Regions Science and Technology 25*(2), 101 – 110.

Horiguchi, K. and R. Miller (1983). Hydraulic conductivity functions of frozen material. In *Proc. 4th Int. Conf. on Permafrost*, pp. 504–508. National Academy Press, Washington, D.C.

Johnston, G. H. (1981). *Permafrost Engineering Design and Construction*. Toronto: Wiley.

Kechin, V. V. (1995). Thermodynamically based melting-curve equation. *Journal of Physics: Condensed Matter 7*(3), 531.

Kennedy, J. and R. Eberhart (1995). Particle swarm optimization. In *Proceedings of IEEE International Conference on Neural Networks*, Volume IV, pp. 1942 – 1948.

Konrad, J. M. (1989). Effect of freeze-cycles on the freezing characteristics of a clayey silt at various overconsolidation ratios. *Canadian Geotechnical Journal 26*(2), 217–226.

Kozlowski, T. (2004). Soil freezing point as obtained on melting. *Cold Regions Science and Technology 38*, 93 – 101.

Kozlowski, T. (2009). Some factors affecting supercooling and the equilibrium freezing point in soil-water systems. *Cold Regions Science and Technology 59*(1), 25 – 33.

Kozlowski, T. (2016). A simple method of obtaining the soil freezing point depression, the unfrozen water content and the pore size distribution curves from the dsc peak maximum temperature. *Cold Regions Science and Technology 122*, 18 – 25.

Ladanyi, B. (1981). Mechanical behaviour of frozen soils. In *Proc. Int. Symp. on Mechancial Behavior of Structured Media*, Volume B, Ottawa, pp. 205–245. Carleton Univ.: New York: Elsevier.

Lai, Y., L. Jin, and X. Chang (2009). Yield criterion and elasto-plastic damage constitutive model for frozen sandy soil. *International Journal of Plasticity 25*(6), 1177 – 1205.

Lai, Y., S. Li, J. Qi, Z. Gao, and X. Chang (2008). Strength distributions of warm frozen clay and its stochastic damage constitutive model. *Cold Regions Science and Technology 53*(2), 200 – 215.

Lai, Y., Y. Yang, X. Chang, and S. Li (2010). Strength criterion and elastoplastic constitutive model of frozen silt in generalized plastic mechanics. *International Journal of Plasticity 26*(10), 1461 – 1484.

Lal, R. and M. K. Shukla (2004). *Principles of Soil Physics*. Marcel Dekker, Inc.

Lay, R. D. (2005). Development of a frost heave test apparatus. Master's thesis, Brigham Young University.

Lee, M. Y., A. Fossum, L. S. Costin, and D. Bronowski (2002). Frozen soil material testing and constitutive modeling. Technical report, Sandia Noational Laboratories.

Lemke, P., J. Ren, R. Alley, I. Allison, J. Carrasco, J. Flato, Y. Fujii, G. Kaser, P. Mote, R. Thomas, and T. Zhang (2007). *Climate Change 2007: The Physical Science Basis. Contribution of Working Group I to the Fourth Assessment Report of the Intergovernmental Panel on Climate Change*. Cambridge, United Kingdom and New York, NY, USA: Cambridge University Press.

Li, G., Q. Yu, W. Ma, Z. Chen, Y. Mu, L. Guo, and F. Wang (2016). Freeze-thaw properties and long-term thermal stability of the unprotected tower foundation soils in permafrost regions along the qinghai-tibet power transmission line. *Cold Regions Science and Technology 121*, 258 – 274.

Li, N., B. Chen, F. X. Chen, and X. Z. Xu (2000). The coupled heat-moisture-mechanic model of the frozen soil. *Cold Regions Science and Technology 31*(3), 199–205.

Liu, Z. and X. Yu (2011). Coupled thermo-hydro-mechanical model for porous materials under frost action: theory and implementation. *Acta Geotechnica 6*(2), 51–65.

Low, P. F., D. M. Anderson, and P. Hoekstra (1968). Some thermodynamic relationships for soils at or below the freezing point: 1. freezing point depression and heat capacity. *Water Resources Research 4*(2), 379–394.

Ma, T., C. Wei, X. Xia, J. Zhou, and P. Chen (2015). Soil freezing and soil water retention characteristics: Connection and solute effects. *Journal of Performance of Constructed Facilities*.

Ma, W., Z. Wu, L. Zhang, and X. Chang (1999). Analyses of process on the strength decrease in frozen soils under high confining pressures. *Cold Regions Science and Technology 29*(1), 1 – 7.

Madan, M. (2012, May). Artificial ground freezing for water infested tunnel strata and weak rock mass having high seepage water. `http://mmmhydropower.blogspot.nl/2012/05/artificial-ground-freezing-for-water.html`. Accessed 5 June 2016.

McCauley, C., D. White, M. Lilly, and D. Nyman (2002). A comparison of hydraulic conductivities, permeabilities and infiltration rates in frozen and unfrozen soils. *Cold Regions Science and Technology 34*(2), 117–125.

Michalowski, R. L. and M. Zhu (2006). Frost heave modelling using porosity rate function. *International journal for numerical and analytical methods in geomechanics 30*(8), 703–722.

Mu, S. and B. Ladanyi (1987). Modeling of coupled heat, moisture and stress-field in freezing soil. *Cold Regions Science and Technology 14*(3), 237–246.

Muir Wood, D. (1991). *Soil Behaviour and Critical State Soil Mechanics*. Cambridge University Press.

Nakano, Y. (1990). Quasi-steady problems in freezing soils. i. analysis on the steady growth of an ice layer. *Cold Regions Science and Technology 17*(3), 207–226.

Neaupane, K. M., T. Yamabe, and R. Yoshinaka (1999). Simulation of a fully coupled thermo-hydro-mechanical system in freezing and thawing rock. *International Journal of Rock Mechanics and Mining Sciences 36*(5), 613–637.

Nishimura, S., A. Gens, S. Olivella, and R. Jardine (2009). Thm-coupled finite element analysis of frozen soil: formulation and application. *Géotechnique 59*, 159–171.

Oliphant, J., A. Tice, and Y. Nakano (1983). Water migration due to a temperature gradient in frozen soil. In *Proc. 4th Int. Conf. on Permafrost*, pp. 951–956. National Academy Press, Washington, D.C.

Ortiz, J., J. Serra, and C. Oteo (1986). *Curso Aplicado de Cimentaciones* (Third Edition ed.). Madrid: Colegio de Arquitectos de Madrid.

Parameswaran, V. and S. Jones (1981). Triaxial testing of frozen sand. *Journal of Glaciology 27*(95), 147 – 155.

Peng, X. M., X. B. Chen, and Y. Q. Wang (1991). A model coupled heat, moisture and stress-field of saturated soil during freezing. *Ground Freezing 91 1*(1), 77–82.

Peppin, S. S. L. and R. W. Style (2012). The physics of frost heave and ice-lens growth. Preprint 12/35, Oxford Centre for Collaborative Applied Mathematics.

Petersen, L. W., P. Moldrup, O. H. Jacobsen, and D. E. Rolston (1996). Relation between specific surface area and soil physical and chemical properties. *Soil Science 161*(1), 9–21.

Qi, J., X. Yao, and F. Yu (2013). Consolidation of thawing permafrost considering phase change. *KSCE Journal of Civil Engineering 17*(6), 1293–1301.

Ratkje, S. K., H. Yamamoto, T. Takashi, T. Ohrai, and J. Okamoto (1982). The hydraulic conductivity of soils during frost heave. In *Proc. of the 3d Intern. Symp. on Ground Freezing*.

Rempel, A. W. (2007). Formation of ice lenses and frost heave. *Journal of Geophysical Research: Earth Surface 112*, F02S21.

Rempel, A. W. (2010). Frost heave. *Journal of Glaciology 56*(200).

Rempel, A. W., J. S. Wettlaufer, and M. Grae Worster (2004). Premelting dynamics in a continuum model of frost heave. *J. Fluid Mech. 498*, 227–244.

Sayles, F. H. and D. L. Carbee (1981). Strength of frozen silt as a function of ice content and dry unit weight. *Engineering Geology 18*, 55–66.

Sepaskhah, A. R., A. Tabarzad, and H. R. Fooladmand (2010). Physical and empirical models for estimation of specific surface area of soils. *Archives of Agronomy and Soil Science 56*(3), 325–335.

Shirazi, M. A. and L. Boersma (1984). A unifying quantitative analysis of soil texture. *Soil Sci. Soc. Am. J. 48*, 142–147.

Simon, F. and G. Glatzel (1929). Bemerkungen zur schmelzdruckkurve. *Zeitschrift für anorganische und allgemeine Chemie 178*(1), 309–316.

Smith, M. W. and A. R. Tice (1988). Measurement of the unfrozen water content of soils. Technical report, Cold Regions Research and Engineering Laboratory (U.S.), & United States. Army.Corps of Engineers, Hanover, N.H.

Spaans, E. J. A. and J. M. Baker (1996). The soil freezing characteristic: Its measurement and similarity to the soil moisture characteristic. *Soil Science Society of America Journal 60*(1), 13–19.

Springman, S. and L. U. Arenson (2008, June 29 - July 3). Recent advances in permafrost geotechnics. In D. L. Kane and K. M. Hinkel (Eds.), *Ninth International Conference on Permafrost*, Volume 2, pp. 1685–1694. University of Alaska Fairbanks.

Stähli, M., P.-E. Jansson, and L.-C. Lundin (1999). Soil moisture redistribution and infiltration in frozen sandy soils. *Water Resources Research 35*(1), 95–103.

Taber, S. (1916). The growth of crystals under external pressure. *American Journal of Science 41*(246), 532–556. Ser. 4.

Taber, S. (1929). Frost heaving. *Journal of Geology 37*(5), 428–461.

Taber, S. (1930). The mechanics of frost heaving. *Journal of Geology 38*(4), 303–317.

Tarnawski, V. R. and B. Wagner (1996). On the prediction of hydraulic conductivity of frozen soils. *Canadian Geotechnical Journal 33*(1), 176–180.

Thomas, H., P. Cleall, Y.-C. LI, C. Harris, and M. Kern-Luetschg (2009). Modelling of cryogenic processes in permafrost and seasonally frozen soils. *Géotechnique 59*(3), 173–184.

Tice, A. R., D. M. Anderson, and A. Banin (1976). The prediction of unfrozen water contents in frozen soils from liquid limit determinations. CRREL Report 76-8, Cold Regions Research and Engineering Laboratory.

Ting, J. M., R. T. Martin, and C. C. Ladd (1983). Mechanisms of strength for frozen sand. *J. Geotech. Eng. ASCE 109*(10), 1286–1302.

Tsytovich, N. A. (1975). *The Mechanics of Frozen Ground (trans.)*. Washington : Scripta Book Co.

U.S.D.A. Saturated hydraulic conductivity. Website. accessed on 04.03.2016.

van Genuchten, M. T. (1980). A closed-form equation for predicting the hydraulic conductivity of unsaturated soils. *Soil Sci. Soc. Am. J. 44*, 892–898.

Wagner, W., T. Riethmann, R. Feistel, and A. H. Harvey (2011). New equations for the sublimation pressure and melting pressure of h2o ice ih. *Journal of Physical and Chemical Reference Data 40*(4).

Watanabe, K. and M. Flury (2008). Capillary bundle model of hydraulic conductivity for frozen soil. *Water Resources Research 44*(12), n/a–n/a. W12402.

Watanabe, K. and T. Wake (2009). Measurement of unfrozen water content and relative permittivity of frozen unsaturated soil using {NMR} and {TDR}. *Cold Regions Science and Technology 59*(1), 34 – 41.

Wettlaufer, J. and M. G. Worster (2006). Premelting dynamics. *Annual Review of Fluid Mechanics 38*(1), 427–452.

Wheeler, S. J., D. Gallipoli, and M. Karstunen (2002). Comments on use of the barcelona basic model for unsaturated soils. *International Journal for Numerical and Analytical Methods in Geomechanics 26*(15), 1561–1571.

Williams, P. (1963). Specific heat and unfrozen water content of frozen soils. In *1st Canadian Conference on Permafrost*, Ottawa, pp. 109–126. Assoc. Com. on Soil and Snow Mechs.: National Research Council of Canada. Tech. Memo. No. 76.

Wu, Y., Y. Sheng, Y. Wang, H. Jin, and W. Chen (2010). Stresses and deformations in a buried oil pipeline subject to differential frost heave in permafrost regions. *Cold Regions Science and Technology 64*(3), 256 – 261. China-Russia Crude Oil Pipeline in Permafrost Regions in Northeastern China.

Xia, K., Y. Luo, and W. Li (2011). Simulation of freezing and melting of soil on the northeast tibetan plateau. *Chinese Science Bulletin 56*(20), 2145–2155.

Xu, G. (2014, January). *Hypoplastic constitutive models for frozen soil*. Ph. D. thesis, University of Natural Resources and Life Sciences, Vienna.

Yang, Y., Y. Lai, Y. Dong, and S. Li (2010). The strength criterion and elastoplastic constitutive model of frozen soil under high confining pressures. *Cold Regions Science and Technology 60*(2), 154 – 160.

Yang, Z. J., B. Still, and X. Ge (2015). Mechanical properties of seasonally frozen and permafrost soils at high strain rate. *Cold Regions Science and Technology 113*, 12 – 19.

Yasufuku, N., S. Springman, L. Arenson, and T. Ramholt (2003). Stress-dilatancy behaviour of frozen sand in direct shear. In M. Phillips, S. Springman, and L. Arenson (Eds.), *Eighth International Conference on Permafrost*, Volume 2, Zurich, Switzerland, pp. 1253–1258. A.A. Balkema.

Zhang, L.-X., X.-Z. Xu, Z.-X. Zhang, and Y.-S. Deng (1998). Experimental study of the relationship between the unfrozen water content of frozen soil and pressure. *Journal of Glaciology and Geocryology 20*(2), 124–127.

Zhang, X. (2010). Analytical solution of the barcelona basic model. In *GeoShanghai 2010 international conference*, Shanghai, China, pp. 96–103. ASCE Special Publication 376: Experimental and applied modeling of unsaturated soils.

Zhang, X., E. E. Alonso, and F. Casini (2016). Explicit formulation of at-rest coefficient and its role in calibrating elasto-plastic models for unsaturated soils. *Computers and Geotechnics 71*, 56 – 68.

Zhang, X. and R. Lytton (2009a). Modified state-surface approach to the study of unsaturated soil behavior. part i: Basic concept. *Canadian Geotechnical Journal 46*(5), 536–552.

Zhang, X. and R. Lytton (2009b). Modified state-surface approach to the study of unsaturated soil behavior. part ii: General formulation. *Canadian Geotechnical Journal 46*(5), 553–570.

Zhang, X. and R. Lytton (2012). Modified state-surface approach to the study of unsaturated soil behavior. part iii: Modeling of coupled hydromechanical effect. *Canadian Geotechnical Journal 49*(1), 98–120.

Zhang, Y. (2014). *Thermal-hydro-mechanical model for freezing and thawing of soils*. Ph. D. thesis, University of Michigan.

Zhang, Y. and R. L. Michalowski (2015). Thermal-hydro-mechanical analysis of frost heave and thaw settlement. *Journal of Geotechnical and Geoenvironmental Engineering 141*(7), 04015027.

Zhao, X., G. Zhou, and J. Wang (2013). Deformation and strength bbehavior of frozen clay with thermal gradient under uniaxial compression. *Tunnelling and Underground Space Technology 38*, 550–558.

Zhou, G., K. Hu, X. Zhao, J. Wang, H. Liang, and G. Lu (2015). Laboratory investigation on tensile strength characteristics of warm frozen soils. *Cold Regions Science and Technology 113*, 81 – 90.

Zhou, M. and G. Meschke (2013). A three-phase thermo-hydro-mechanical finite element model for freezing soils. *International Journal for Numerical and Analytical Methods in Geomechanics 37*(18), 3173–3193.

Zhou, M. M. (2014). *Computational simulation of freezing: Multiphase modeling and strength upscaling*. Ph. D. thesis, Ruhr University Bochum.

Zhu, Z., J. Ning, and W. Ma (2010). A constitutive model of frozen soil with damage and numerical simulation for the coupled problem. *Science China Physics, Mechanics and Astronomy 53*(4), 699–711.

A

Influence of selected input parameters

The focus is put on the influence of the four parameters β, λ_0, r and p_c^* which control isotropic virgin loading of the soil (together with $N(0)$). Isotropic compression tests, or one-dimensional compression tests should be conducted to obtain the magnitude of these input parameters. In Chapter 4 this is described in more detail. To illustrate the influence of the selected input parameters in a clear manner, it is assumed that the elastic parameter κ_s is known. We now define the mapped specific volume as follows (Wheeler et al., 2002):

$$v^* = v + \kappa_s \ln \frac{s_c + p_{at}}{p_{at}} \tag{A.1}$$

Normal compression lines obtained from constant temperature isotropic compression tests can now be presented in the $v^* - \ln p^*$ plane. This representation makes it possible to investigate the four controlling parameters. The graphs in Figure A.1 show the effects of the variation of β, λ_0, r and p_c^* and are borrowed from Gallipoli et al. (2010).

The influence on the shape of the LC yield curves for selected values of parameters p_{y0}^*, r and β is shown in Figure A.2. Other parameters used are $p_c^* = 0.1$ MPa, $\lambda_0 = 0.2$ and a constant $\kappa = 0.02$ for demonstration purpose. Although these graphs are obtained by Alonso et al. (1990), and thus related to unsaturated soil, the qualitative influence is the same for the frozen and unfrozen BBM when $m = 0$.

In Section 4.4.4 it is mentioned that when the normal compression lines for different values of cryogenic suction diverge with decreasing mean net stress the coefficient related to the maximum soil stiffness r should be chosen smaller than 1.0. Furthermore, when $r < 1.0$, the reference stress p_c^* has to be chosen smaller than the initial preconsolidation pressure $(p_{y0}^*)_{in}$. The effect of $r < 1.0$ on the expansion of the LC yield curve is shown in Figure A.3a. However, if the normal compression lines converge with increasing p^* (see Figure) a value greater than 1.0 for the model parameter r should be chosen. With r greater than 1, a very large value must be selected for the reference stress p_c. Figure A.3b shows the expansion of the LC yield curve for values of $r > 1.0$ and large values for p_c^*.

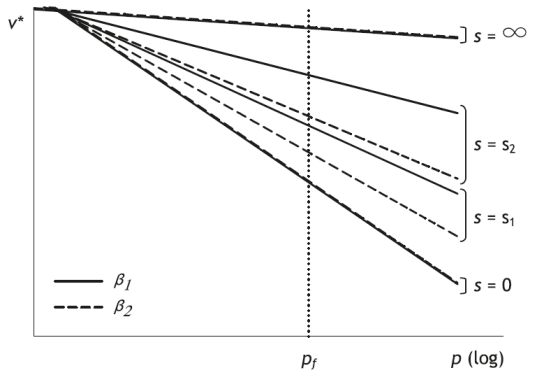

(a) Effect of variation of relative spacing (i.e. parameter β) on position of constant cryogenic suction normal compression lines

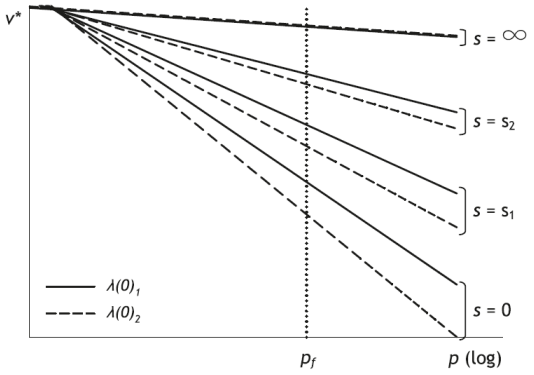

(b) Effect of variation of slope of normal compression line in an unfrozen state (zero cryogenic suction) by varying the parameter λ_0

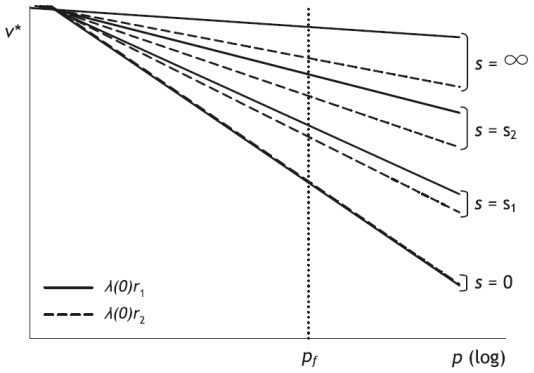

(c) Effect of variation of slope of normal compression line in a fully frozen state (infinite cryogenic suction) by varying the parameter $r \times \lambda_0$

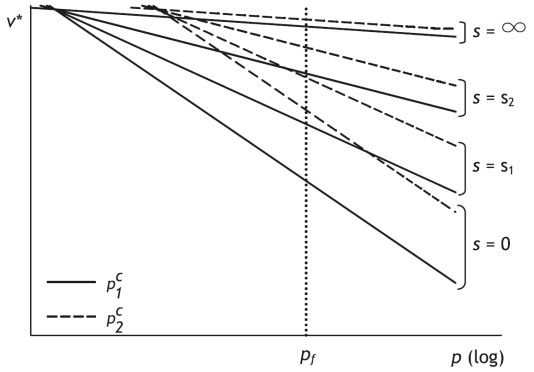

(d) Effect of variation of abscissa at the intersection point (i.e., variation of parameter p_c^*)

Figure A.1: Effects of selected parameters on constant cryogenic suction normal compression lines (after Gallipoli et al. (2010))

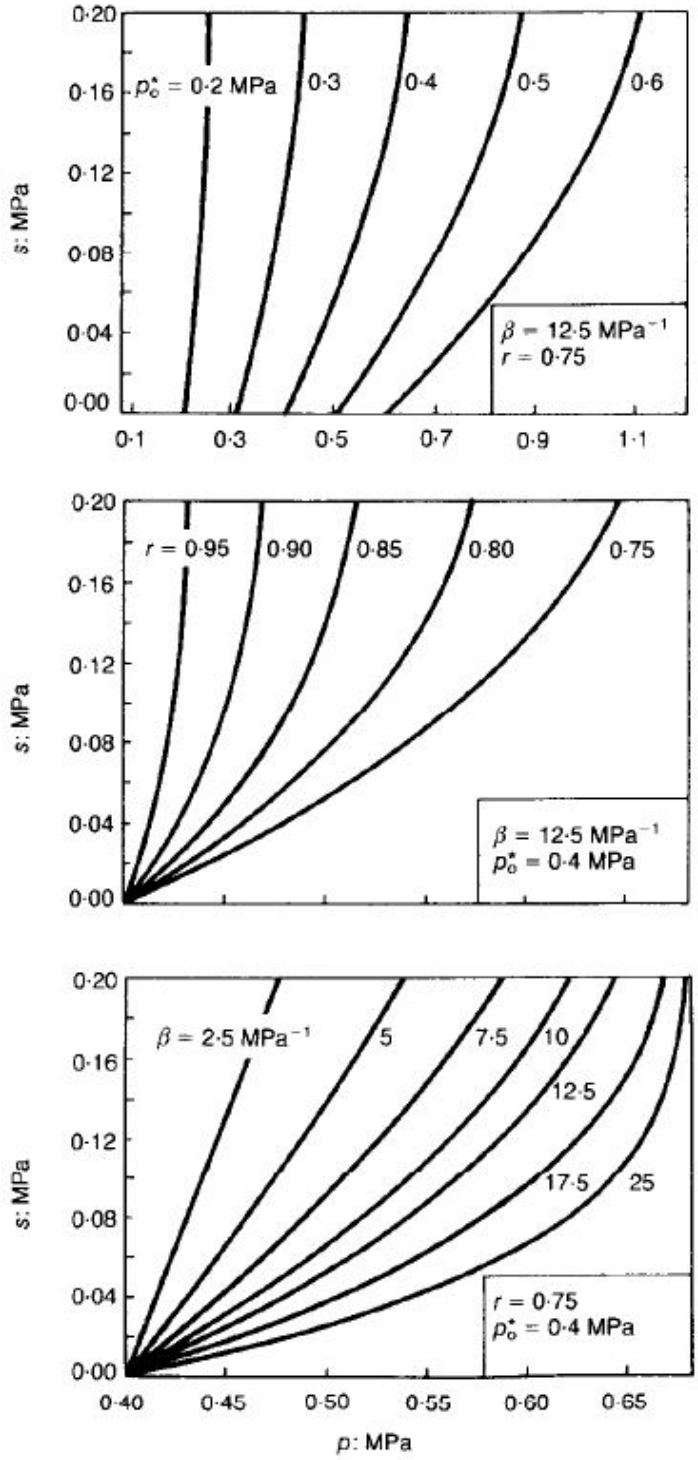

Figure A.2: Shapes of the LC yield curve for different values of the parameters p^*_{y0}, r and β (after Alonso et al. (1990))

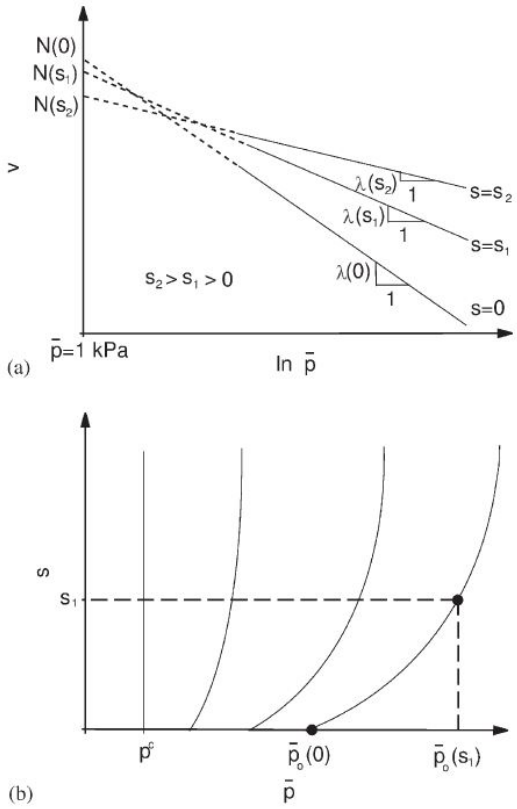

(a) Model predictions with $r < 1.0$: (a) isotropic compression lines; (b) expansion of LC yield curve

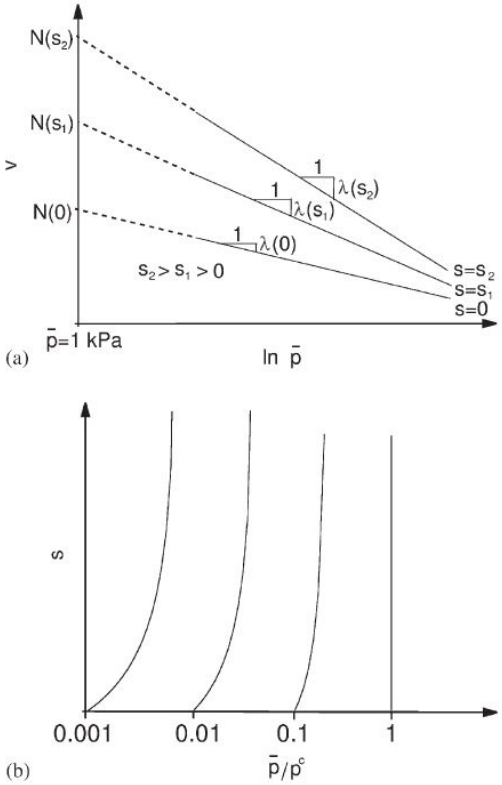

(b) Model predictions with $r > 1.0$: (a) isotropic compression lines; (b) expansion of LC yield curve

Figure A.3: Model predictions for values of r smaller and larger than 1.0 (after Wheeler et al. (2002))

B

Derivation of the explicit formulation of the at-rest coefficient K_0

B.0.1. Input parameters

The following parameters are input values for the calibration of the frozen / unfrozen Barcelona Basic Model parameters :

- Initial void ratio, e_0
- Initial pre-consolidation stress for unfrozen condition, $(p^*_{y0})_{in}$
- Reference Frozen Soil Young's Modulus, $E_{f,ref}$
- Rate of change in Young's modulus with temperature, $E_{f,inc}$
- Frozen Soil Poisson's ratio, ν_f
- Slope of the critical state line, M
- Rate of change in apparent cohesion with suction, k_t
- Shear modulus in an unfrozen state, G_0
- Elastic compressibility coefficient for suction variation, κ_s
- Elasto-plastic compressibility coefficient for unfrozen state, λ_0

The temperatures at which the oedometer tests are conducted are seen as input parameters as well. Considering the temperature-dependent behaviour of ice:

$$E_f = E_{f,ref} - E_{f,inc}(T - T_{ref}) \tag{B.1}$$

where $E_{f,ref}$ is the value of E_f at the reference temperature T_{ref} and $E_{f,inc}$ is considered as the rate of change in E_f with temperature.

$$K = (1 - S_i)\frac{(1 + e_0)p^*_{y0}}{\kappa_0} + \frac{S_i E_f}{3(1 - 2\nu_f)} \tag{B.2}$$

$$G = (1 - S_i)G_0 + \frac{S_i E_f}{2(1 + 2\nu_f)} \tag{B.3}$$

where G (Eq. B.3)and K (Eq. B.2) are the equivalent stress-dependent shear modulus and bulk modulus of the mixture, respectively.
In order to conduct this derivation in terms of κ and μ, we define them as follows:

$$\kappa = \frac{1+e_0}{K} p^*_{y0} \tag{B.4}$$

$$\mu = \frac{3K-2G}{6K+2G} \tag{B.5}$$

B.0.2. Derivation of the explicit formulation of the at-rest coefficient K_0

Based on the BBM the so called loading collapse (LC) yield surface due to variation of solid phase stress is expressed as:

$$F_1 = (p^* + k_t s_c)[(p^* + k_t * s_c){S_{uw}}^m - (p^*_y + k_t s_c)] + \frac{(q^*)^2}{M^2} = 0 \tag{B.6}$$

where

$$p^*_y = {p_c}^* (\frac{p^*_{y0}}{{p_c}^*})^{\frac{\lambda_0-\kappa}{\lambda_s-\kappa}} \tag{B.7}$$

with

$$\lambda_s = \lambda_0[(1-r)exp(-\beta s_c) + r] \tag{B.8}$$

Taking the natural log on both sides of Eq. (B.7) and rearrange results in

$$[\lambda_0-\kappa]\ln(p^*_{y0}) = [\lambda_s-\kappa][\ln(p^*_y) - \ln({p_c}^*)] + [\lambda_0-\kappa]\ln({p_c}^*) \tag{B.9}$$

Solving Eq. (B.6) in terms of p^*_y, we obtain

$$p^*_y = \frac{(q^*)^2}{M^2(p^* + k_t s_c)} + (p^* + k_t s_c){S_{uw}}^m - k_t s_c \tag{B.10}$$

Combining Eq. (B.9) and (B.10) results in

$$[\lambda_0-\kappa]\ln(p^*_{y0}) = f = [\lambda_s-\kappa][\ln(\frac{(q^*)^2}{M^2(p^* + k_t s_c)} + (p^* + k_t s_c){S_{uw}}^m - k_t s_c) - \ln({p_c}^*)] + [\lambda_0-\kappa]\ln({p_c}^*) \tag{B.11}$$

Where f is a function equal to the right-hand side, $f(p^*, q^*, s_c)$. By taking the derivative on both sides of Eq. (B.11), we can write

$$[\lambda_0-\kappa]\frac{dp^*_{y0}}{p^*_{y0}} = \frac{\partial f}{\partial p^*}dp^* + \frac{\partial f}{\partial q^*}dq^* + \frac{\partial f}{\partial s_c}ds_c \tag{B.12}$$

where,

$$\frac{\partial f}{\partial p^*}dp^* = \frac{[\lambda_s-\kappa]}{(q^*)^2 + M^2(p^* + k_t s_c)[(p^* + k_t s_c){S_{uw}}^m - k_t s_c]} \frac{{S_{uw}}^m M^2(p^* + k_t s_c)^2 - (q^*)^2}{p^* + k_t s_c} = AB \tag{B.13}$$

$$\frac{\partial f}{\partial q^*}dq^* = \frac{[\lambda_s-\kappa]}{(q^*)^2 + M^2(p^* + k_t s_c)[(p^* + k_t s_c){S_{uw}}^m - k_t s_c]} 2q = 2Aq \tag{B.14}$$

$$\frac{\partial f}{\partial s_c} ds_c = \frac{(-\frac{(q^*)^2 k_t}{M^2(k_t s_c + p^*)^2} + k_t {S_{uw}}^m - k_t)(\lambda_0(\frac{1-r}{\exp \beta s_c} + r) - k_t)}{\frac{(q^*)^2}{M^2(k_t s_c + p^*)} + {S_{uw}}^m (k_t s_c + p^*) - k_t s_c} + \\ - \frac{\beta \lambda_0 (1-r)(\ln(\frac{(q^*)^2}{M^2(p^* + k_t s_c)} + (p^* + k_t s_c){S_{uw}}^m - k_t s_c) - \ln({p_c}^*))}{\exp \beta s_c} = -C \tag{B.15}$$

with

$$A = \frac{[\lambda_s - \kappa]}{(q^*)^2 + M^2(p^* + k_t s_c)[(p^* + k_t s_c){S_{uw}}^m - k_t s_c]}$$

$$B = \frac{{S_{uw}}^m M^2 (p^* + k_t s_c)^2 - (q^*)^2}{p^* + k_t s_c}$$

The plastic volumetric strain is defined as follows:

$$d\epsilon_v^{mp} = \frac{\lambda_0 - \kappa}{1+e} \frac{dp_{y0}^*}{p_{y0}^*} = \frac{1}{\nu}(ABdp^* + 2Aq^* dq^* - Cds_c) \tag{B.16}$$

The non associated flow rule is used to calculate the deviatoric plastic strain rate:

$$\frac{d\epsilon_s^p}{d\epsilon_v^p} = \frac{2q^*}{M^2 {S_{uw}}^\gamma (2p^* + k_t s_c - p_y^*)} = \frac{1}{d} \tag{B.17}$$

where d is referred to the dilatancy. Substituting Eq. (B.10) into Eq. (B.17) we get

$$\frac{d\epsilon_s^p}{d\epsilon_v^p} = \frac{2q^*}{M^2 {S_{uw}}^\gamma (2p^* + k_t s_c - \frac{(q^*)^2}{M^2(p^* + k_t s_c)} - (p^* + k_t s_c){S_{uw}}^m + k_t s_c} \\ = \frac{2q^*(p^* + k_t s_c)}{{S_{uw}}^\gamma [M^2(p^* + k_t s_c)^2 \ (2 - {S_{uw}}^m) - (q^*)^2]} \tag{B.18}$$

For one dimensional oedometer test, the lateral stress is defined by the constraint that the lateral strain is always equal zero:

$$d\epsilon_2 = d\epsilon_3 = 0 \tag{B.19}$$

As a result, the volumetric strain is equal to the vertical strain:

$$d\epsilon_v = d\epsilon_1 + d\epsilon_2 + d\epsilon_3 = d\epsilon_1 \tag{B.20}$$

The deviatoric strain is defined as follows:

$$d\epsilon_s = \frac{2}{3}(d\epsilon_1 - d\epsilon_3) = \frac{2}{3} d\epsilon_1 = \frac{2}{3} d\epsilon_v \tag{B.21}$$

Thus, one has

$$(\frac{\partial \epsilon_v}{\partial \epsilon_s})_{K_0} = (\frac{\partial \epsilon_v^e + \partial \epsilon_v^p}{\partial \epsilon_s^e + \partial \epsilon_s^p})_{K_0} = \frac{3}{2} \tag{B.22}$$

In the elastic zone of the unfrozen/frozen BBM, the volumetric and shear strains are calculated as follows:

$$d\epsilon_v^e = \frac{\kappa}{\nu} \frac{dp^*}{p^*} + \frac{\kappa_s}{\nu} \frac{ds}{(s + p_{at})} \tag{B.23}$$

$$d\epsilon_s^e = \frac{2(1+\mu)}{9(1-2\mu)} \frac{\kappa}{\nu p^*} dq^* \tag{B.24}$$

Substituting Eq. (B.16), (B.18), (B.23) and (B.24) into Eq. (B.22) the following expression is obtained:

$$\begin{aligned}(\frac{\partial\epsilon_v}{\partial\epsilon_s})_{K_0} = \frac{3}{2} = (\frac{\partial\epsilon_v^e+\partial\epsilon_v^p}{\partial\epsilon_s^e+\partial\epsilon_s^p})_{K_0} &= \frac{[\frac{\kappa}{\nu}\frac{dp^*}{p^*}+\frac{\kappa_s}{\nu}\frac{ds_c}{s_c+p_{at}}]+[\frac{\lambda_0-\kappa}{\nu}\frac{dp_{y0}^*}{p_{y0}^*}]}{[\frac{2(1+\mu)}{9(1-2\mu)}\frac{\kappa}{\nu p^*}dq^*]+[\frac{1}{d}\frac{\lambda_0-\kappa}{\nu}\frac{dp_{y0}^*}{p_{y0}^*}]} \\ &= \frac{\kappa\frac{dp^*}{p^*}+\kappa_s\frac{ds_c}{s_c+p_{at}}+(ABdp^*+2Aq^*dq^*-Cds_c)}{\frac{2(1+\mu)}{9(1-2\mu)}\frac{\kappa}{p^*}dq^*+\frac{2q^*(p^*+k_ts_c)}{S_{uw}{}^{\gamma}[M^2(p^*+k_ts_c)^2\ (2-S_{uw}{}^m)-(q^*)^2]}*(ABdp^*+2Aq^*dq^*-Cds_c)}\end{aligned} \tag{B.25}$$

For constant suction oedometer tests, $ds_c = 0$ and Eq. (B.25) becomes:

$$\frac{3}{2} = \frac{\kappa\frac{dp^*}{p^*}+ABdp^*+2Aq^*dq^*}{\frac{2(1+\mu)}{9(1-2\mu)}\frac{\kappa}{p^*}dq^*+\frac{2q^*(p^*+k_ts_c)}{S_{uw}{}^{\gamma}[M^2(p^*+k_ts_c)^2\ (2-S_{uw}{}^m)-(q^*)^2]}*(ABdp^*+2Aq^*dq^*)} \tag{B.26}$$

Further rearranging results in

$$\begin{aligned}\frac{2(1+\mu)}{3(1-2\mu)}\frac{\kappa}{p^*}dq^*+\frac{6q^*(p^*+k_ts_c)}{S_{uw}{}^{\gamma}[M^2(p^*+k_ts_c)^2\ (2-S_{uw}{}^m)-(q^*)^2]}(ABdp^*+2Aq^*dq^* \\ = \frac{2\kappa}{p^*}dp^*+2ABdp^*+4Aq^*dq^*\end{aligned} \tag{B.27}$$

$$\begin{aligned}&[\frac{2(1+\mu)}{3(1-2\mu)}\frac{\kappa}{p^*}+\frac{6q^*(p^*+k_ts_c)}{S_{uw}{}^{\gamma}[M^2(p^*+k_ts_c)^2\ (2-S_{uw}{}^m)-(q^*)^2]}*2Aq^*-4Aq^*]dq^* \\ &+[\frac{6q^*(p^*+k_ts_c)}{S_{uw}{}^{\gamma}[M^2(p^*+k_ts_c)^2\ (2-S_{uw}{}^m)-(q^*)^2]}AB-\frac{2\kappa}{p^*}-2AB]dp^*=0 \\ &[\frac{2(1+\mu)}{3(1-2\mu)}\frac{\kappa}{p^*}-2Aq^*(2-\frac{6q^*(p^*+k_ts_c)}{S_{uw}{}^{\gamma}[M^2(p^*+k_ts_c)^2\ (2-S_{uw}{}^m)-(q^*)^2]})]dq^* \\ &-[AB(2-\frac{6q^*(p^*+k_ts_c)}{S_{uw}{}^{\gamma}[M^2(p^*+k_ts_c)^2\ (2-S_{uw}{}^m)-(q^*)^2]})+\frac{2\kappa}{p^*}]dp^*=0\end{aligned} \tag{B.28}$$

To simplify the equations, we now can express

$$D = \frac{2(1+\mu)}{3(1-2\mu)}\frac{\kappa}{p^*} \tag{B.29}$$

and

$$E = (2-\frac{6q^*(p^*+k_ts_c)}{S_{uw}{}^{\gamma}[M^2(p^*+k_ts_c)^2\ (2-S_{uw}{}^m)-(q^*)^2]}). \tag{B.30}$$

Furthermore we can take into account the net mean solid phase stress and the deviatoric stress, defined as:

$$dp = \frac{d(\sigma_1-S_{uw}p_w)+2d(\sigma_3-S_{uw}p_w)}{3} = \frac{d\sigma_1^*+2d\sigma_3^*}{3} \tag{B.31}$$

$$dq = d(\sigma_1-S_{uw}p_w)-(\sigma_3-S_{uw}p_w) = d\sigma_1^*-d\sigma_3^* \tag{B.32}$$

By substituting Eq. (B.31) and Eq. (B.32) into Eq. (B.28) we obtain the following expression:

$$(D-2Aq^*(E))(d\sigma_1^*-d\sigma_3^*)-(AB(E)+\frac{2\kappa}{p^*})\frac{d\sigma_1^*+2d\sigma_3^*}{3}=0 \tag{B.33}$$

Rearranging results leads to:

$$d\sigma_3^*(-D+2Aq^*E-\frac{2}{3}ABE-\frac{4\kappa}{3p^*})=d\sigma_1^*(\frac{ABE}{3}+\frac{2\kappa}{3p^*}-D+2Aq^*E) \tag{B.34}$$

$$d\sigma_3^*=\frac{\frac{ABE}{3}+\frac{2\kappa}{3p^*}-D+2Aq^*E}{-D+2Aq^*E-\frac{2}{3}ABE-\frac{4\kappa}{3p^*}}=K_0 d\sigma_1^* \tag{B.35}$$

And the explicit formulation of the at-rest coefficient K_0 is finally obtained:

$$K_0=\frac{((D-2Aq^*E)-(\frac{2\kappa}{3p^*}+\frac{ABE}{3})}{2(\frac{2\kappa}{3p^*}+\frac{ABE}{3})+(D-2Aq^*E)} \tag{B.36}$$

C

Verification results in a single stress point environment

C.0.1. Shear test results

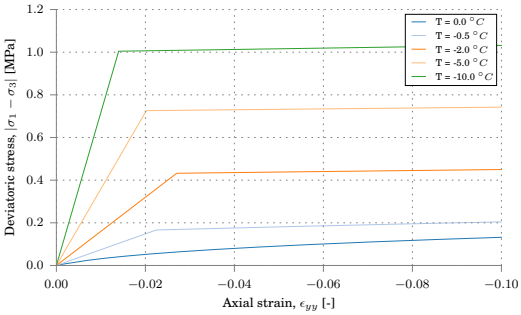

(a) $|\sigma_1 - \sigma_3|$ over ϵ_{yy} for all temperatures at constant confining pressure of $(p^*_{y0})_{init}$

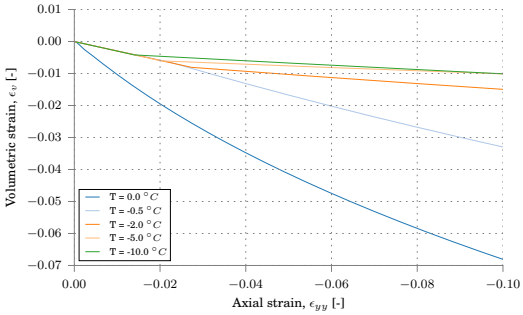

(b) ϵ_v over ϵ_{yy} for all temperatures at constant confining pressure of $(p^*_{y0})_{init}$

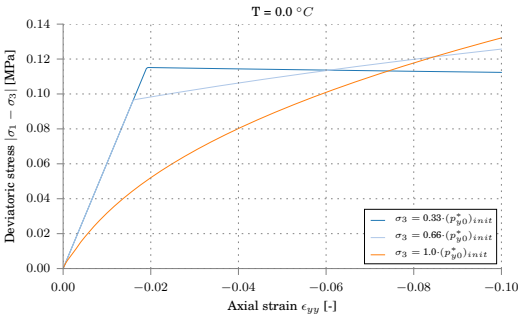

(c) $|\sigma_1 - \sigma_3|$ over ϵ_{yy} at 0°C at varying confining pressure

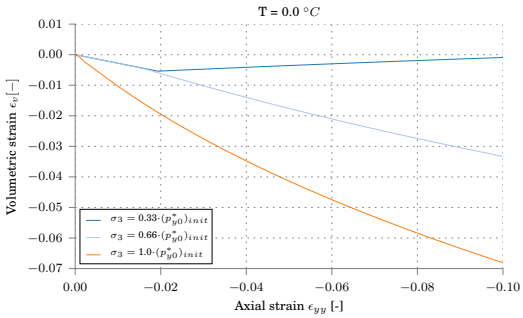

(d) ϵ_v over ϵ_{yy} at 0°C at varying confining pressure

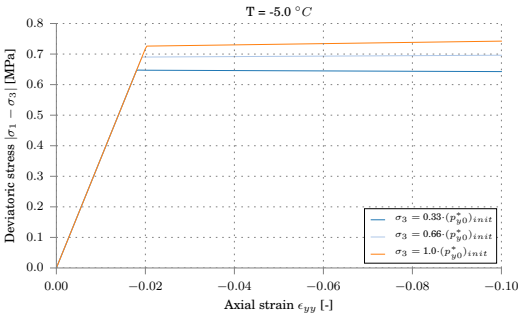

(e) $|\sigma_1 - \sigma_3|$ over ϵ_{yy} at −5°C at varying confining pressure

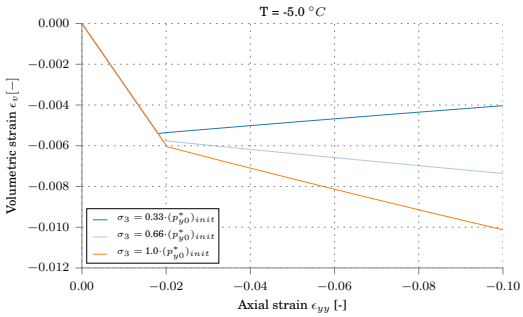

(f) ϵ_v over ϵ_{yy} at −5°C at varying confining pressure

Figure C.1: Triaxial compression test results at different temperatures and confining pressures of the reference soil: Clay

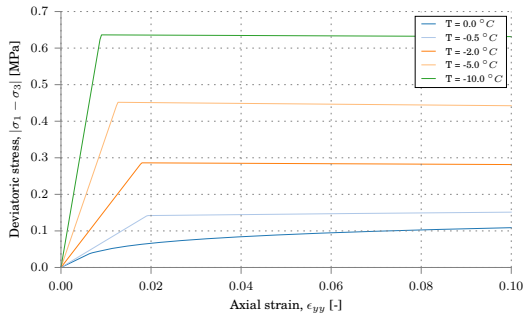

(a) $|\sigma_1 - \sigma_3|$ over ϵ_{yy} for all temperatures at constant confining pressure of $(p^*_{y0})_{init}$

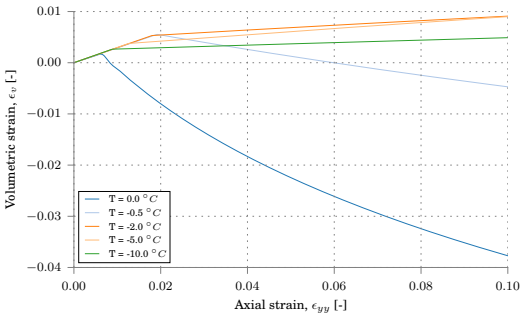

(b) ϵ_v over ϵ_{yy} for all temperatures at constant confining pressure of $(p^*_{y0})_{init}$

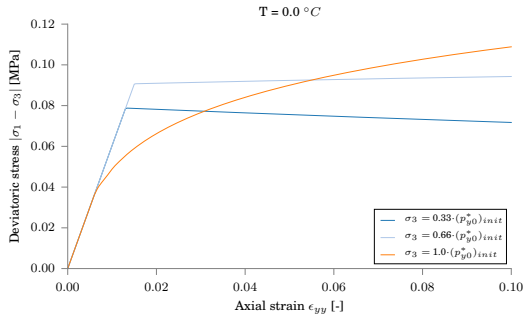

(c) $|\sigma_1 - \sigma_3|$ over ϵ_{yy} at 0°C at varying confining pressure

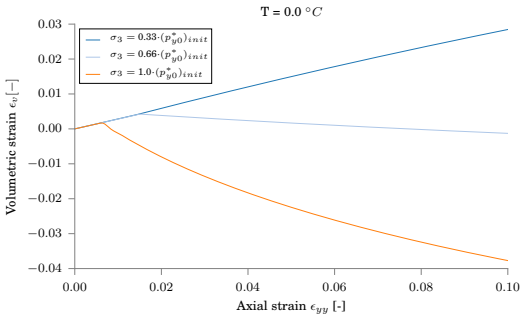

(d) ϵ_v over ϵ_{yy} at 0°C at varying confining pressure

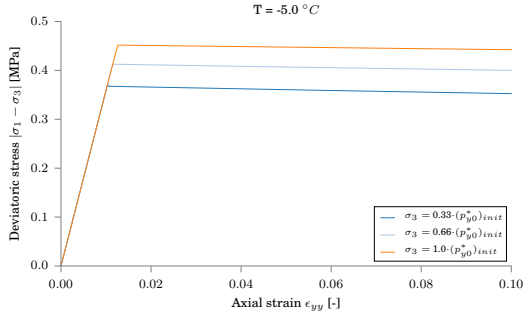

(e) $|\sigma_1 - \sigma_3|$ over ϵ_{yy} at −5°C at varying confining pressure

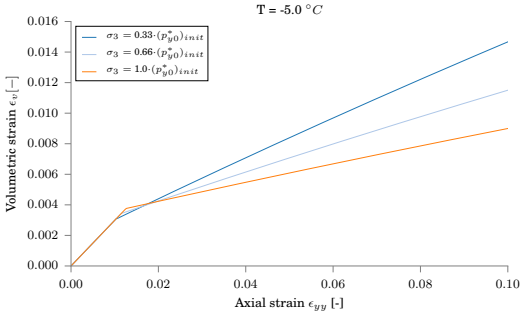

(f) ϵ_v over ϵ_{yy} at −5°C at varying confining pressure

Figure C.2: Triaxial extension test results at different temperatures and confining pressures of the reference soil: Clay

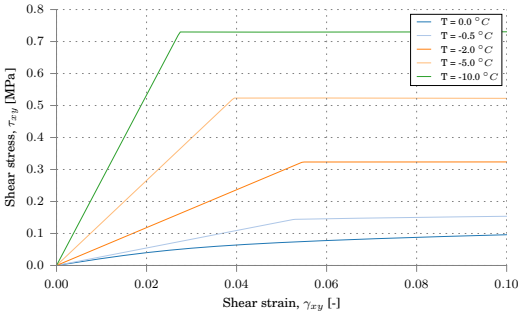

(a) τ_{xy} over γ_{xy} for all temperatures at constant vertical pressure of $(p^*_{y0})_{init}$

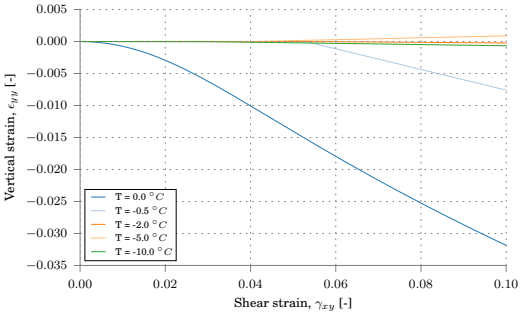

(b) γ_{xy} over ϵ_{yy} for all temperatures at constant vertical pressure of $(p^*_{y0})_{init}$

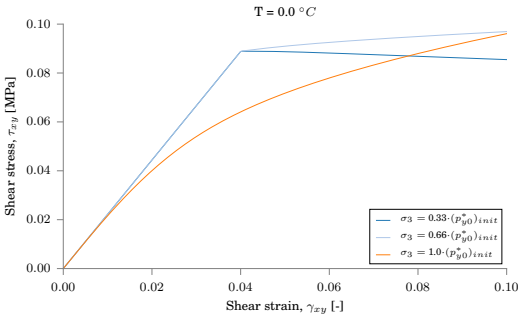

(c) τ_{xy} over γ_{xy} at 0°C at varying vertical pressure

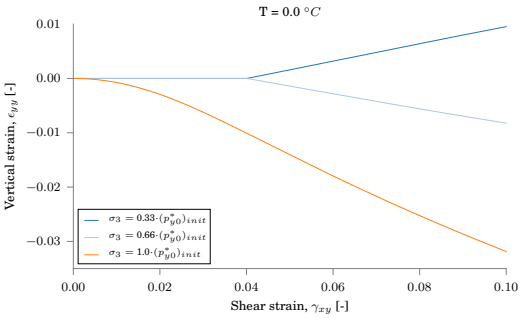

(d) γ_{xy} over ϵ_{yy} at 0°C at varying vertical pressure

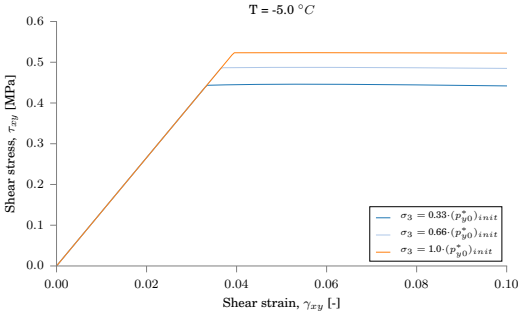

(e) τ_{xy} over γ_{xy} at −5°C at varying vertical pressure

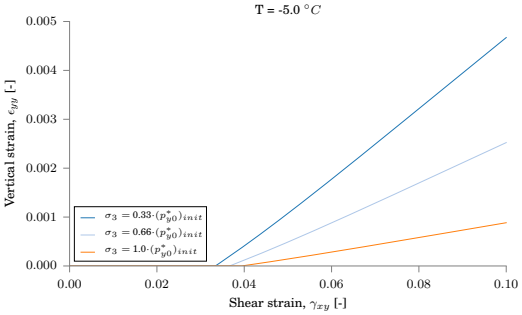

(f) γ_{xy} over ϵ_{yy} at −5°C at varying vertical pressure

Figure C.3: Direct simple shear test results at different temperatures and vertical pressures of the reference soil: Clay

D

Verification results in a fully coupled THM finite element environment

D.0.1. Temperature gradient under uniaxial compression
D.0.2. Frost heave of chilled pipeline
D.0.3. A foundation on frozen soil subjected to a warming period
D.0.4. Freezing pipes in tunnel construction

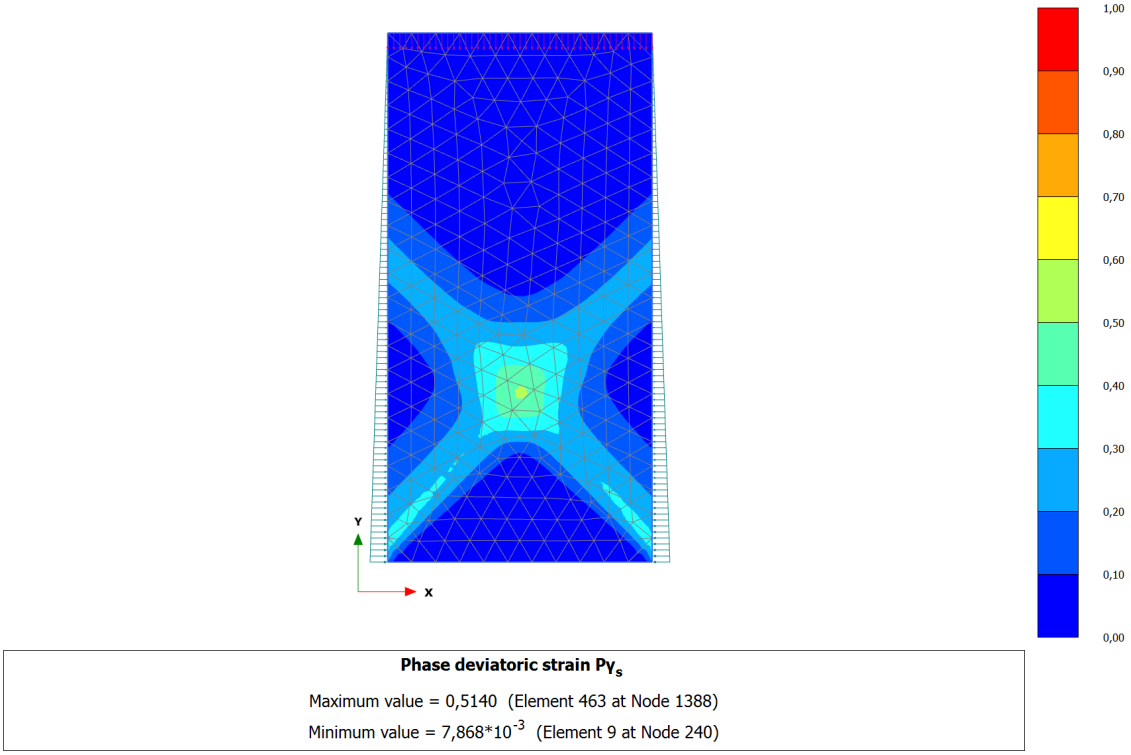

(a) $T_{avg} = -10°C$; Thermal gradient: $0.25°C cm^{-1}$

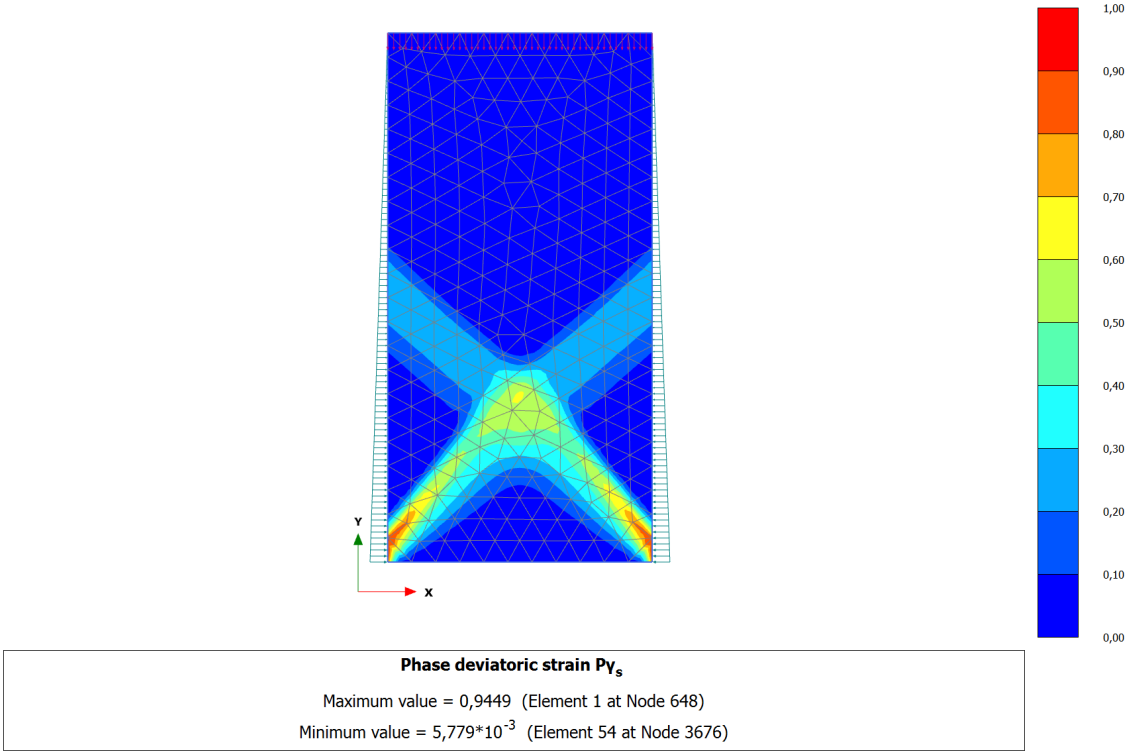

(b) $T_{avg} = -10°C$; Thermal gradient: $0.75°C cm^{-1}$

Figure D.1: Deviator strains - 1

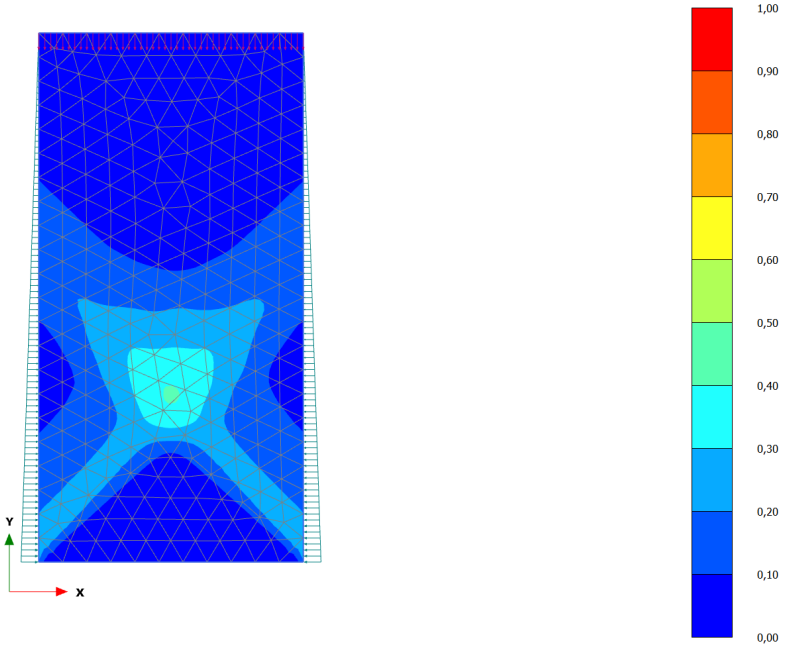

Phase deviatoric strain $P\gamma_s$

Maximum value = 0,4105 (Element 463 at Node 1388)

Minimum value = 5,985*10^{-3} (Element 9 at Node 240)

(a) $T_{avg} = -15°C$; Thermal gradient: $0.25°C\,cm^{-1}$

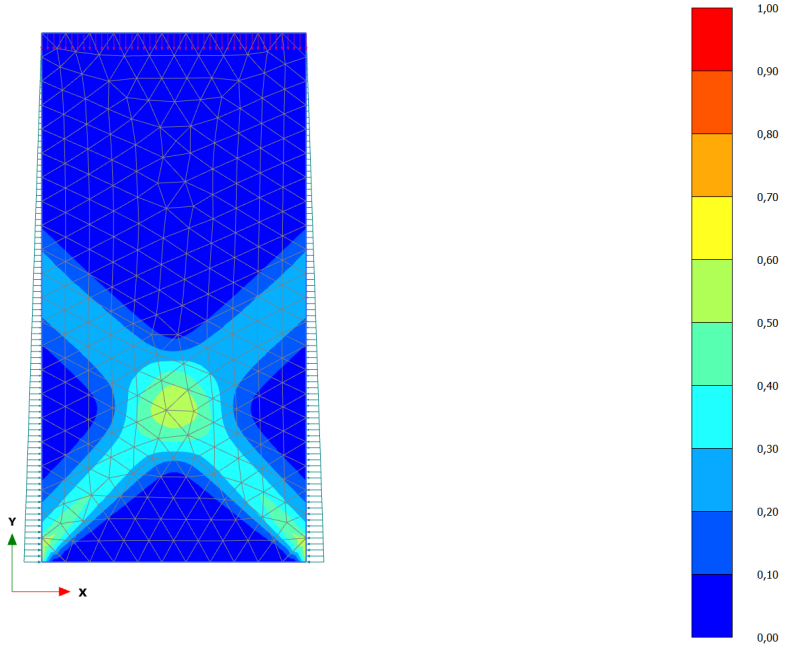

Phase deviatoric strain $P\gamma_s$

Maximum value = 0,6202 (Element 19 at Node 6)

Minimum value = 6,477*10^{-3} (Element 54 at Node 3676)

(b) $T_{avg} = -15°C$; Thermal gradient: $0.75°C\,cm^{-1}$

Figure D.2: Deviator strains - 2

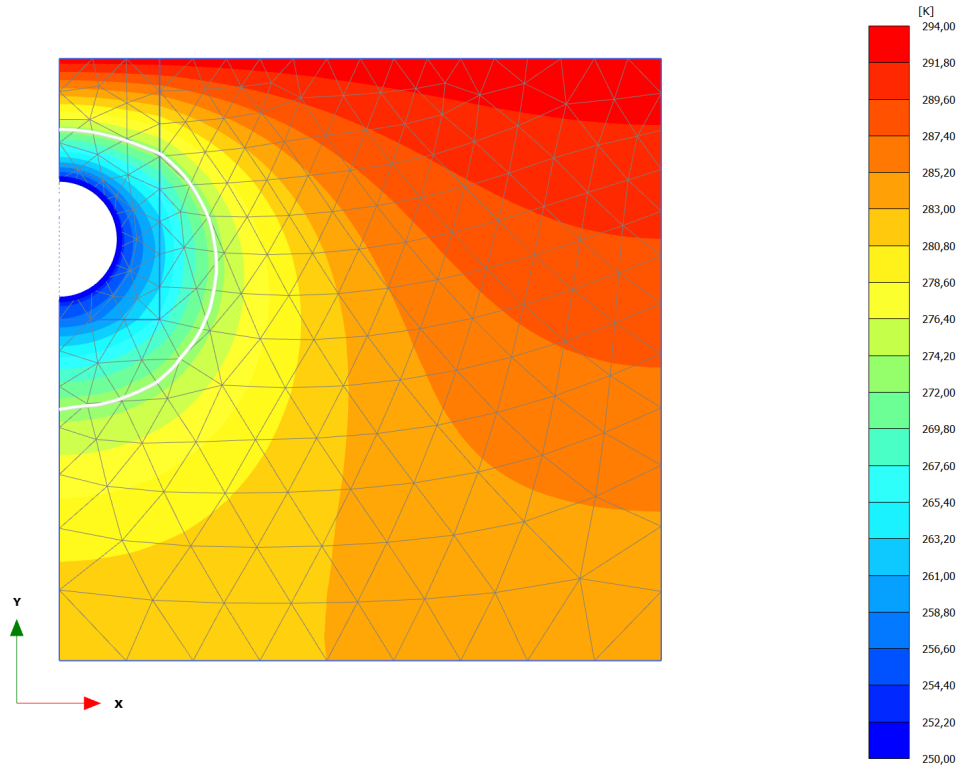

(a) Temperature distribution after 30 days

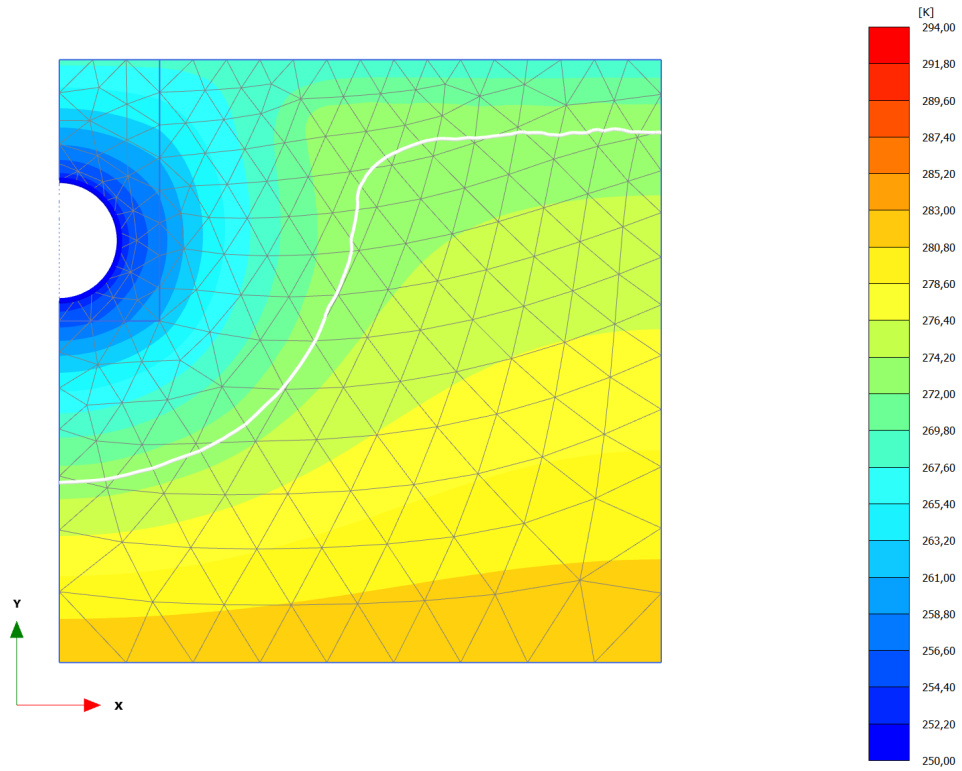

(b) Temperature distribution after 210 days

Figure D.3: Temperature distribution on day 30 and 210, respectively

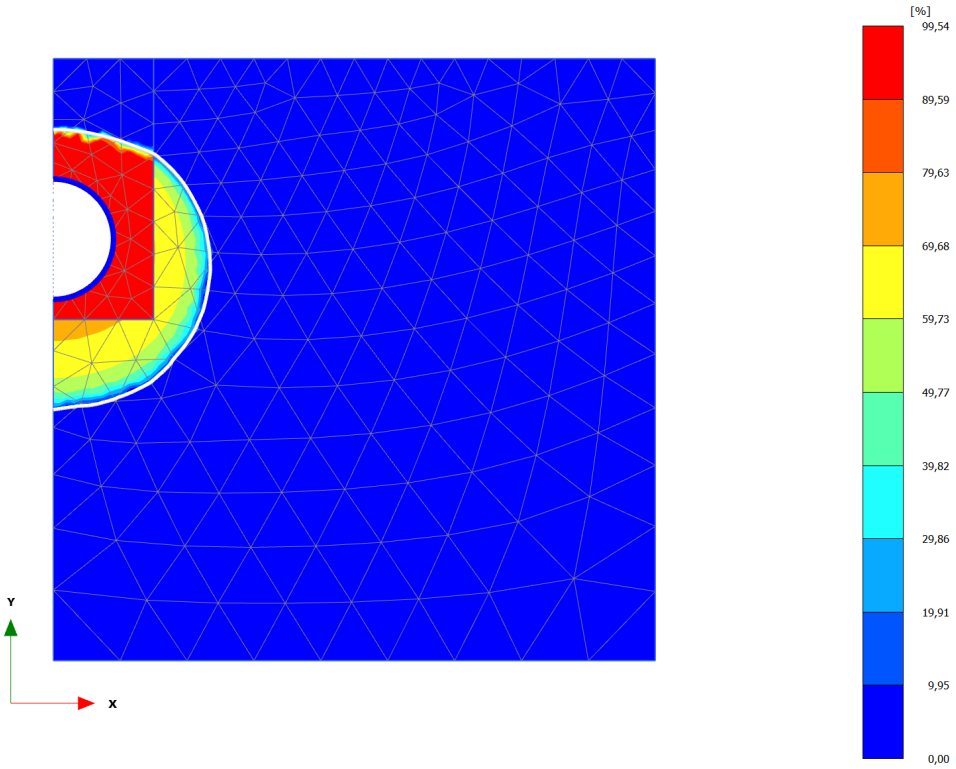

(a) Ice saturation on day 30 day

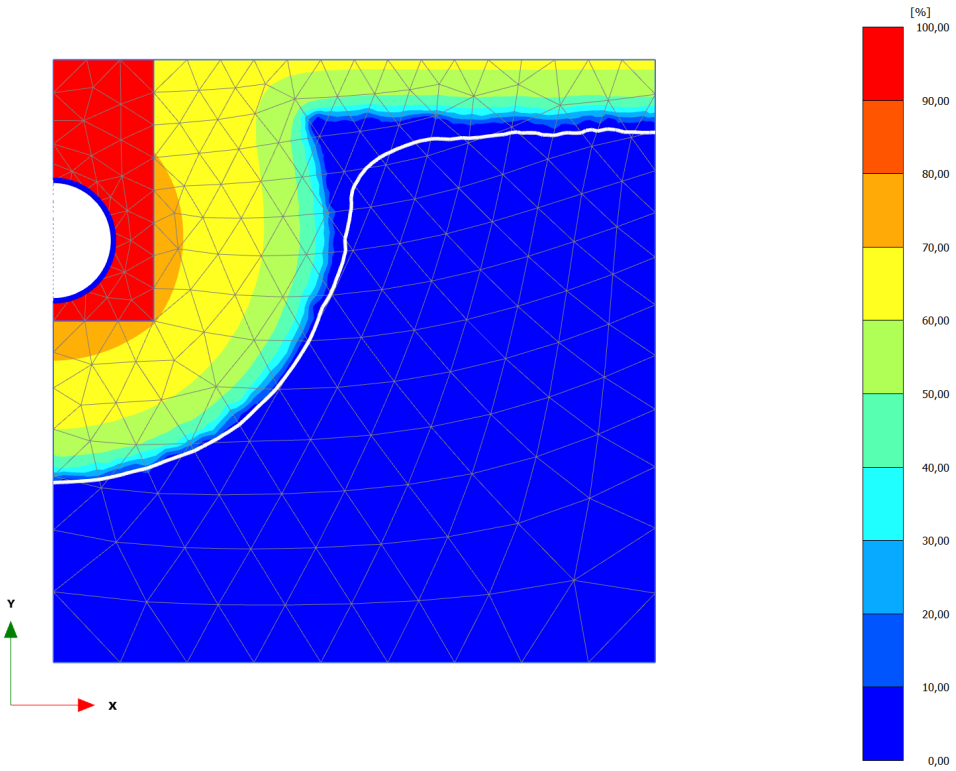

(b) Ice saturation on day 210

Figure D.4: Ice saturations on day 30 and 210, respectively

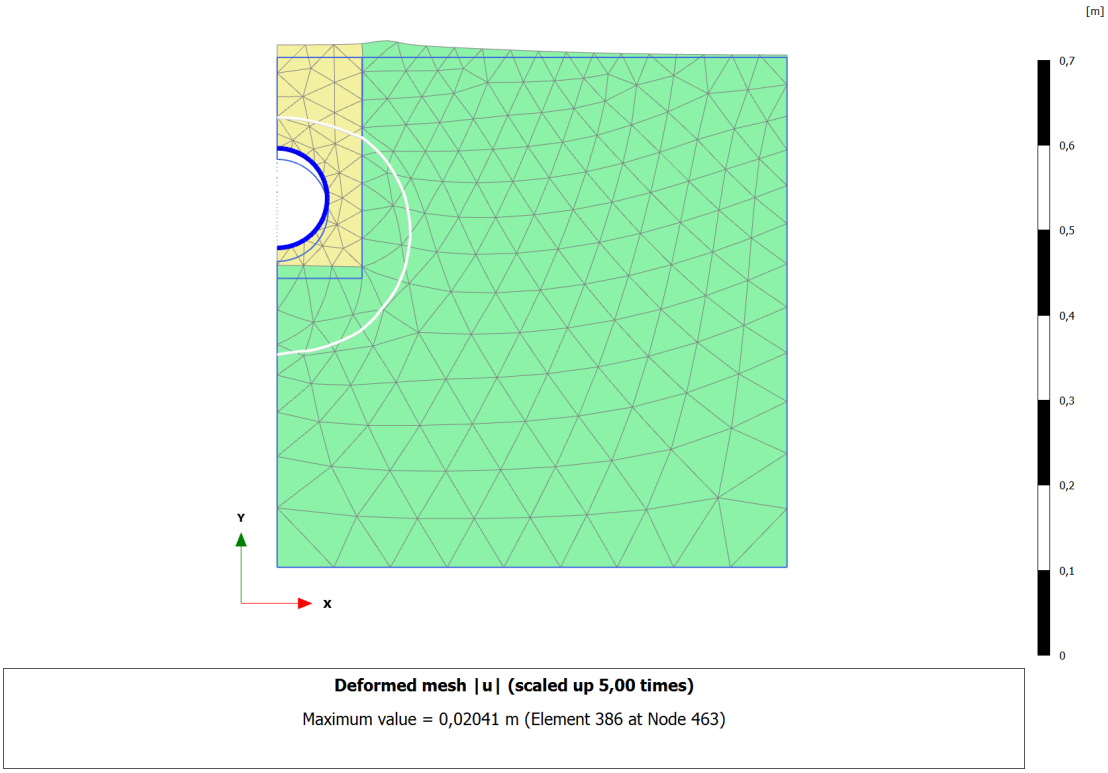

(a) Deformed mesh on day 30 day (maximum value $\bar{2}$.00 cm)

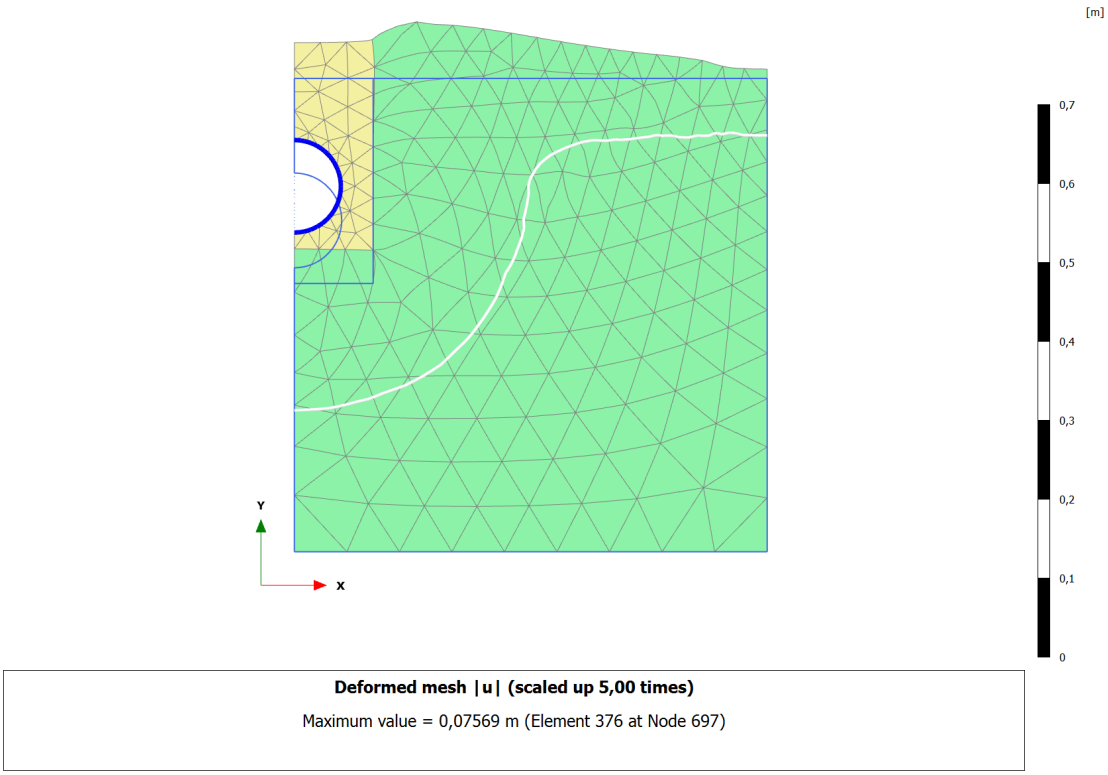

(b) Deformed mesh on day 210 (maximum value $\bar{7}$.60 cm)

Figure D.5: Deformed meshes on day 30 and 210, respectively

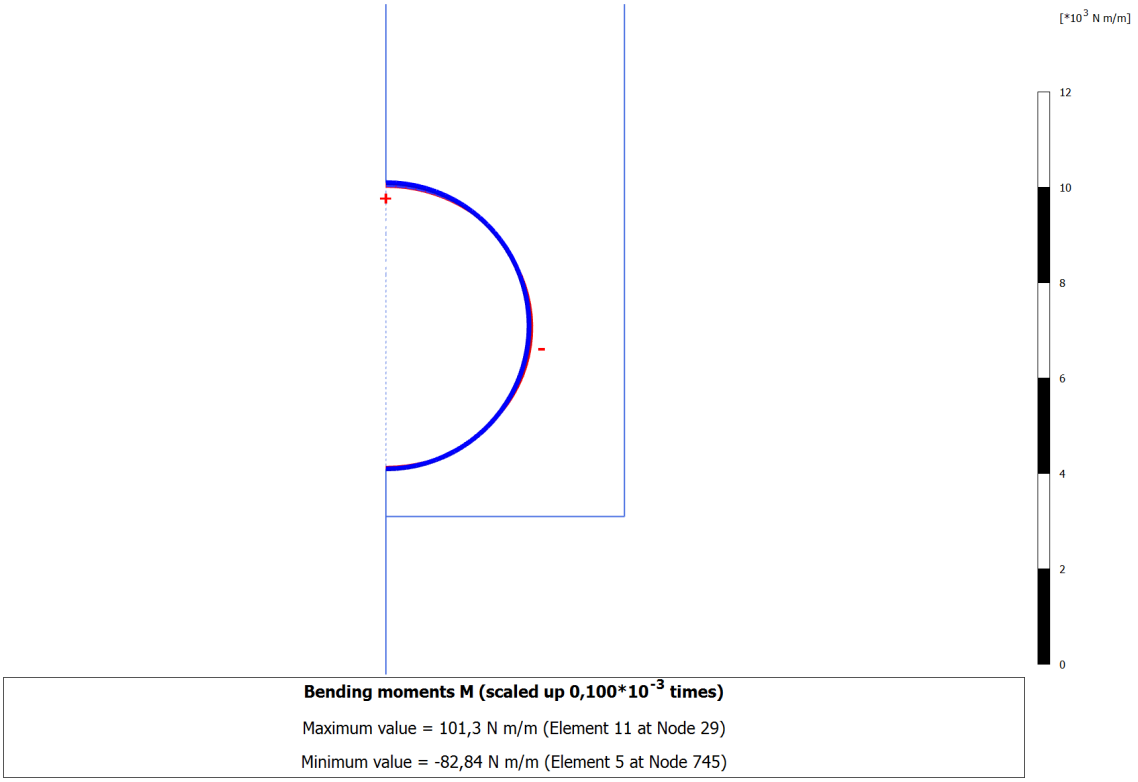

(a) Bending moments of the installed pipeline after construction ($M_{max} = 101.3\,\mathrm{N\,m^{-1}\,m^{-1}}$)

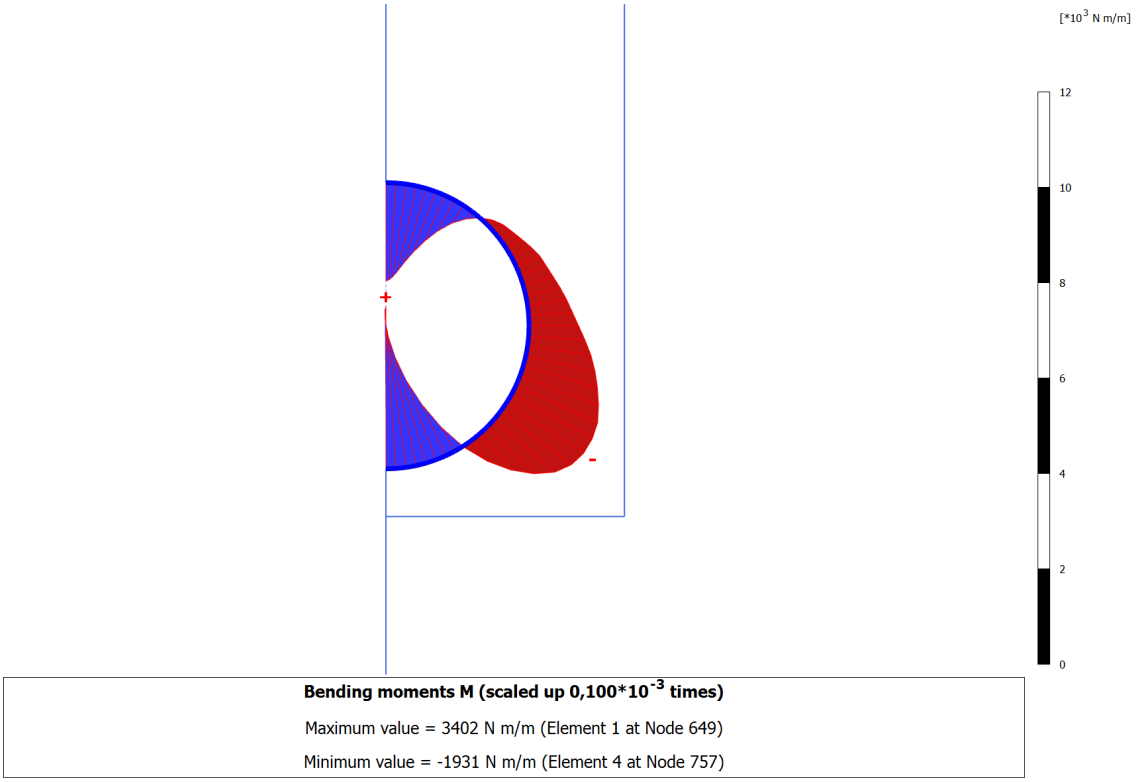

(b) Bending moments of the installed pipeline after 210 days ($M_{max} = 3402\,\mathrm{N\,m^{-1}\,m^{-1}}$)

Figure D.6: Bending moments after installation and on day 210, respectively

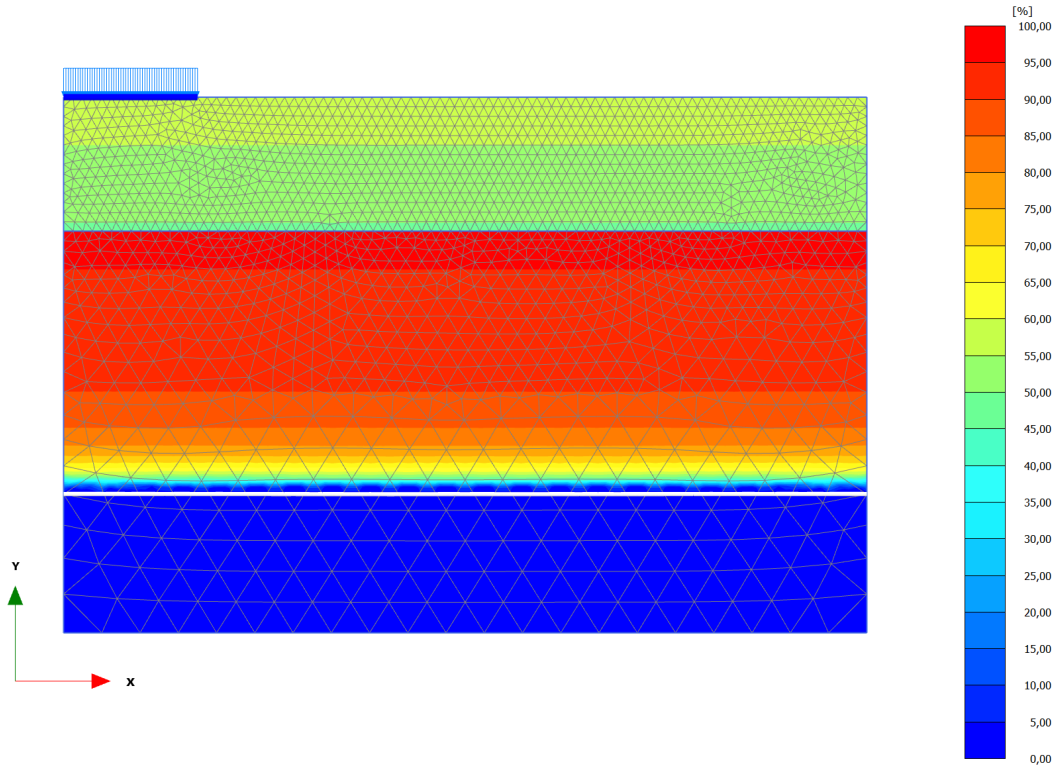

(a) Initial ice saturation

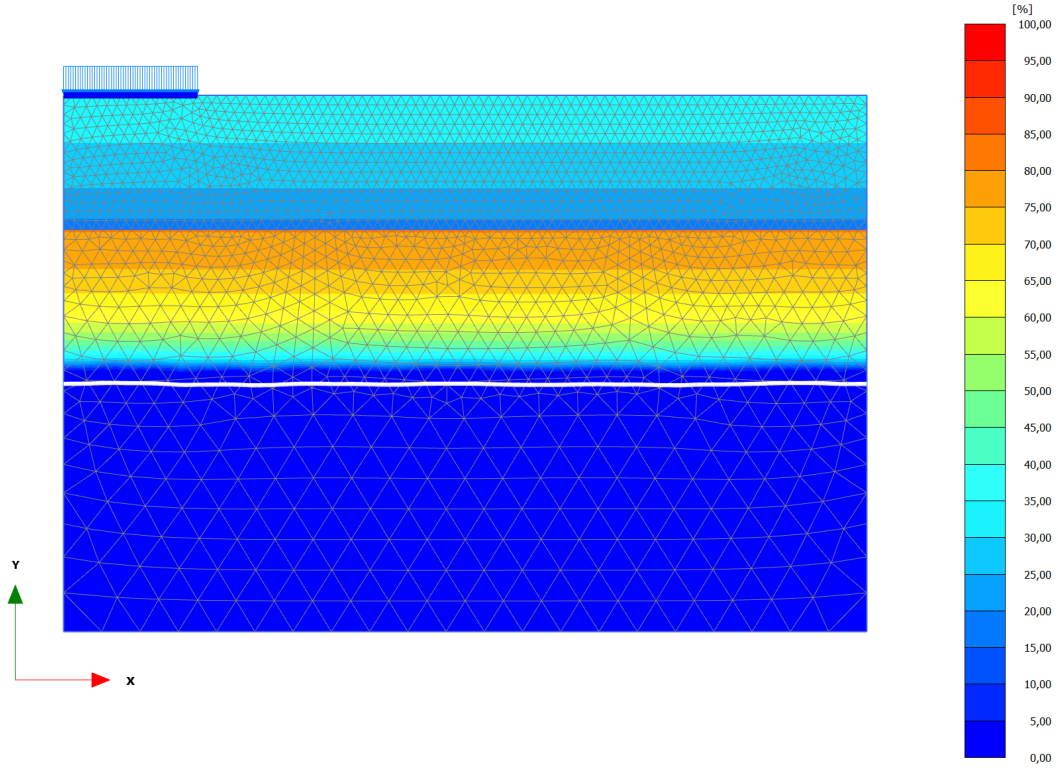

(b) Ice saturation after an increase in air temperature

Figure D.7: Initial ice saturations and after an increase in air temperature

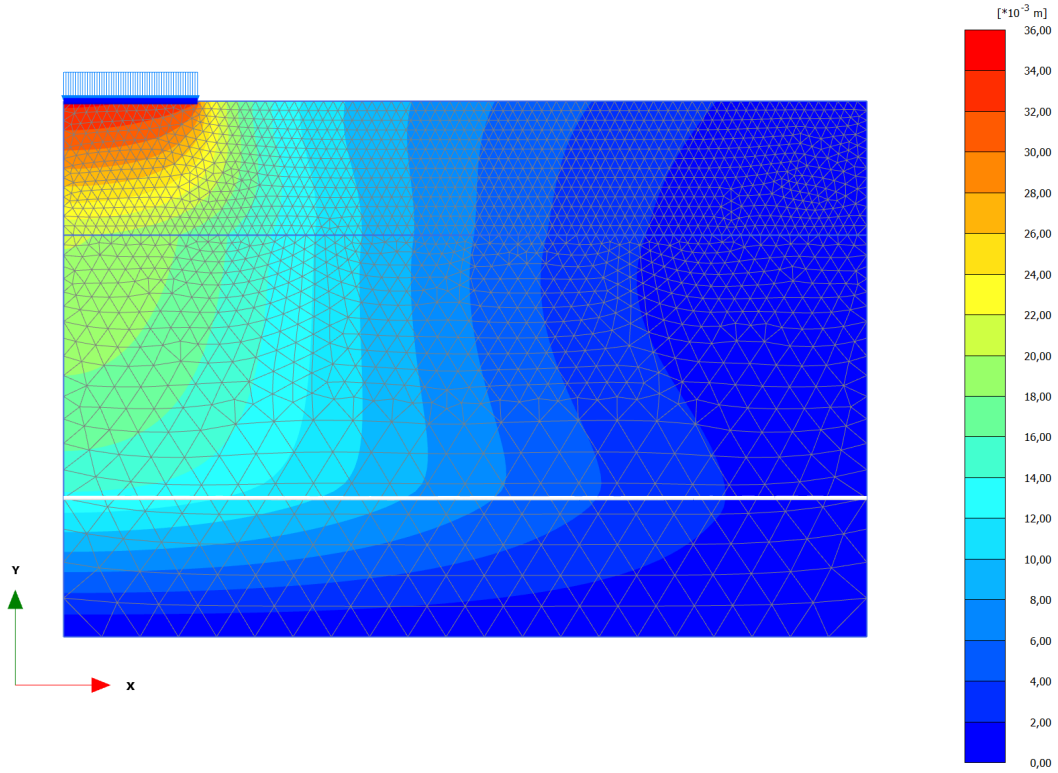

(a) Phase displacements due to the foundation loading (maximum value = 3.50 cm)

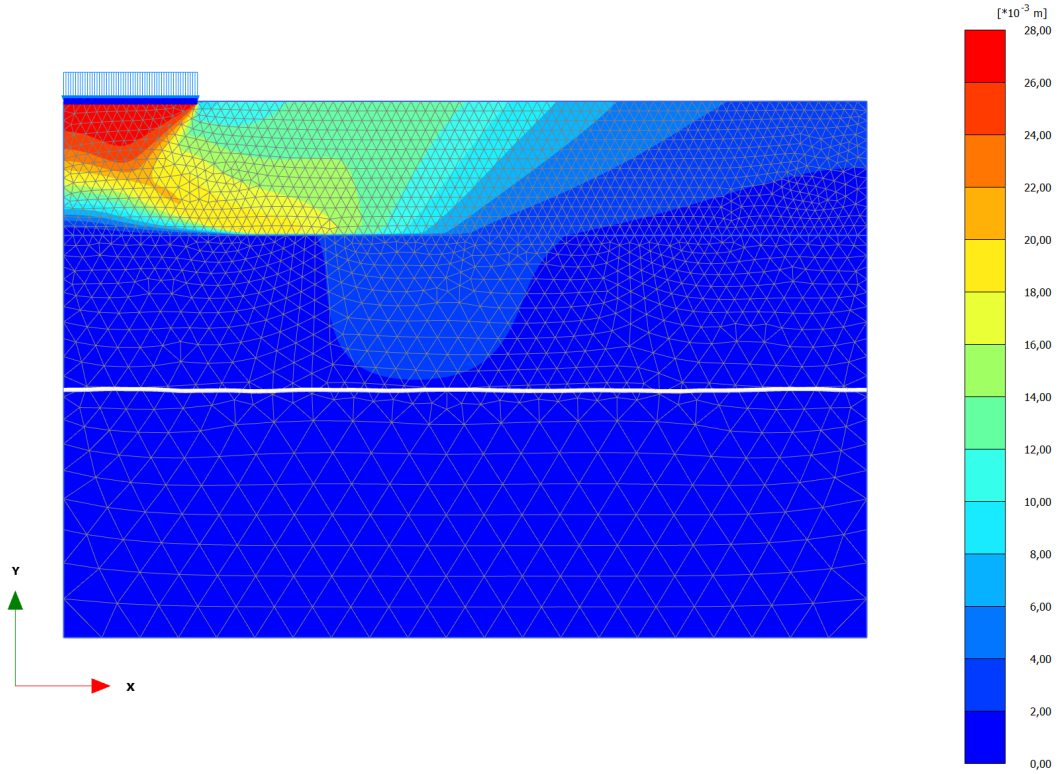

(b) Phase displacements due to climate warming (maximum value = 2.80 cm)

Figure D.8: Phase displacements due to foundation loading and climate warming

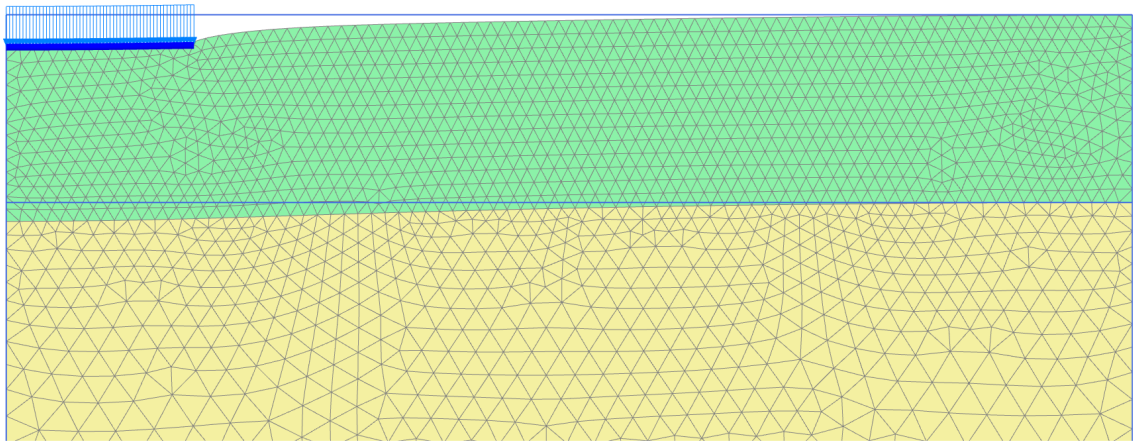

(a) Deformed mesh due to foundation loading (maximum value = 3.50 cm)

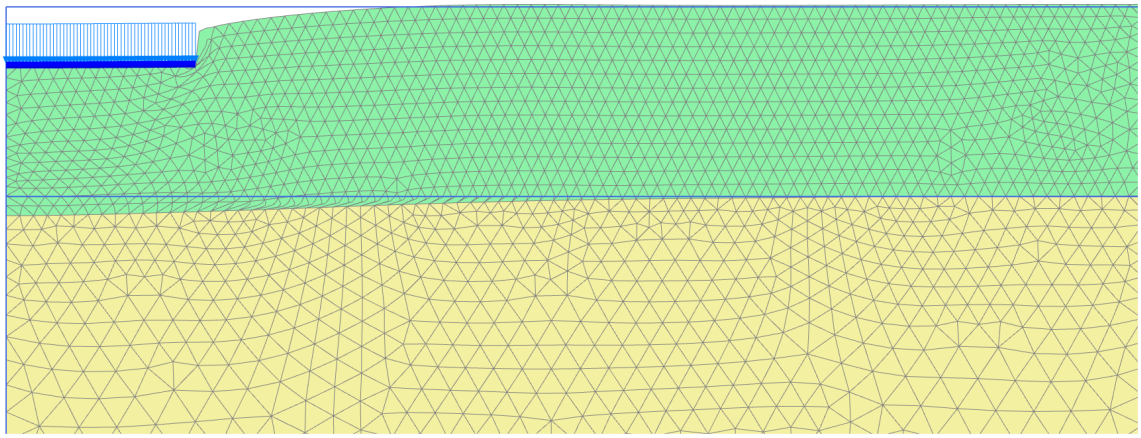

(b) Deformed mesh due to foundation loading and climate warming (maximum value = 6.10 cm)

Figure D.9: Deformed meshes due to foundation loading and climate warming

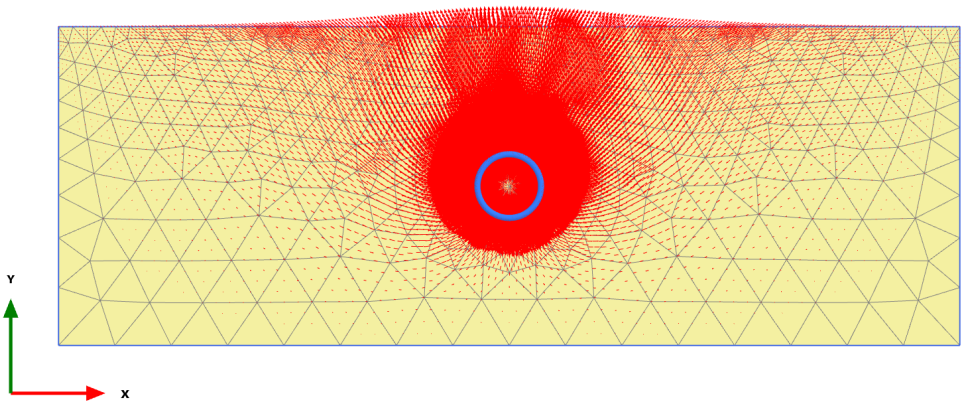

(a) Displacements after 180 days of freezing (arrows) with a maximum value of 0.80 cm (scaled up 500 times)

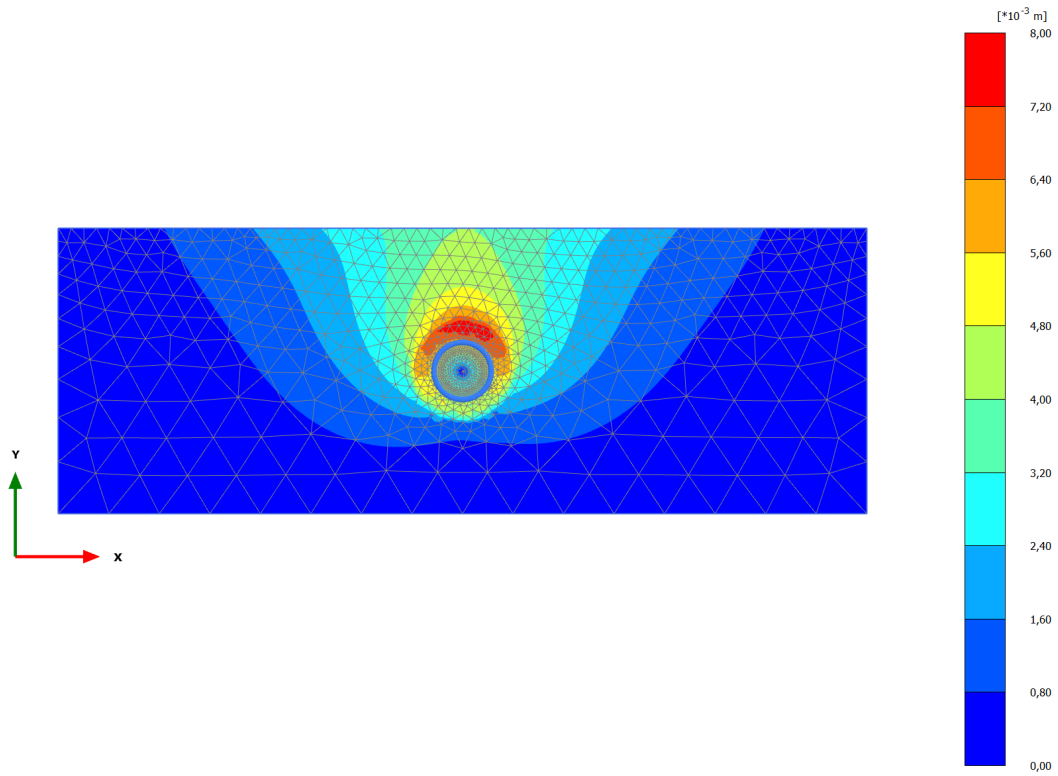

(b) Displacements after 180 days of freezing (shading) with a maximum value of 0.80 cm

Figure D.10: Deformations after a time period of 180 days

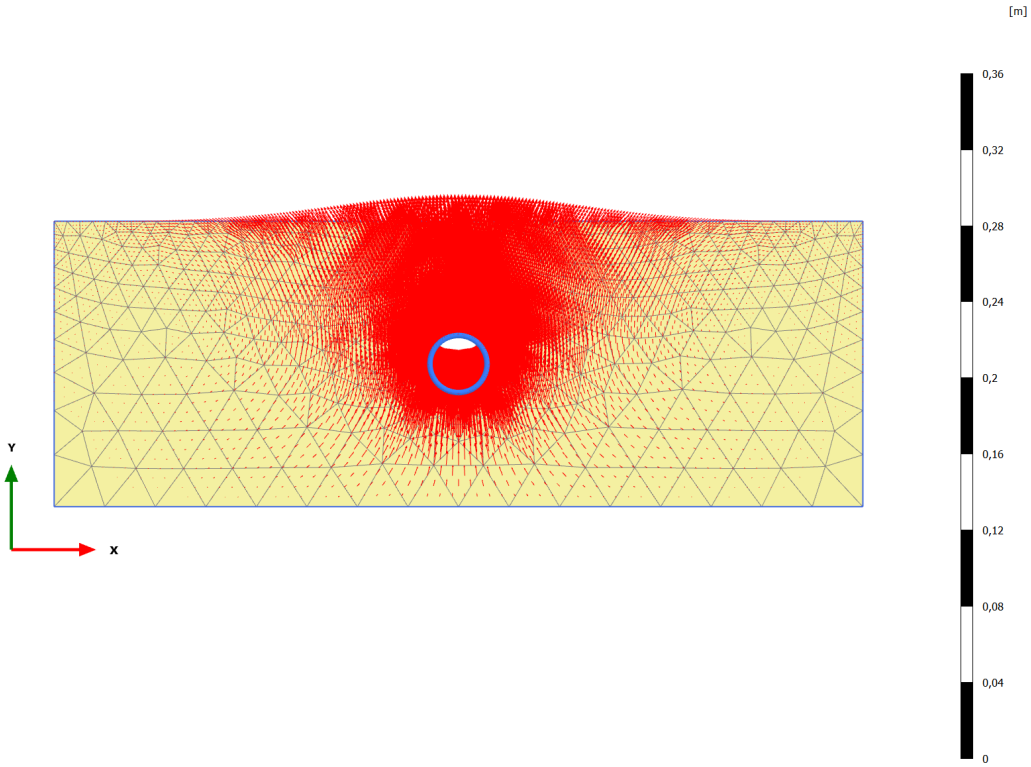

(a) Phase displacements (arrows) due to tunnel excavation (maximum displacement = 2.30 cm)

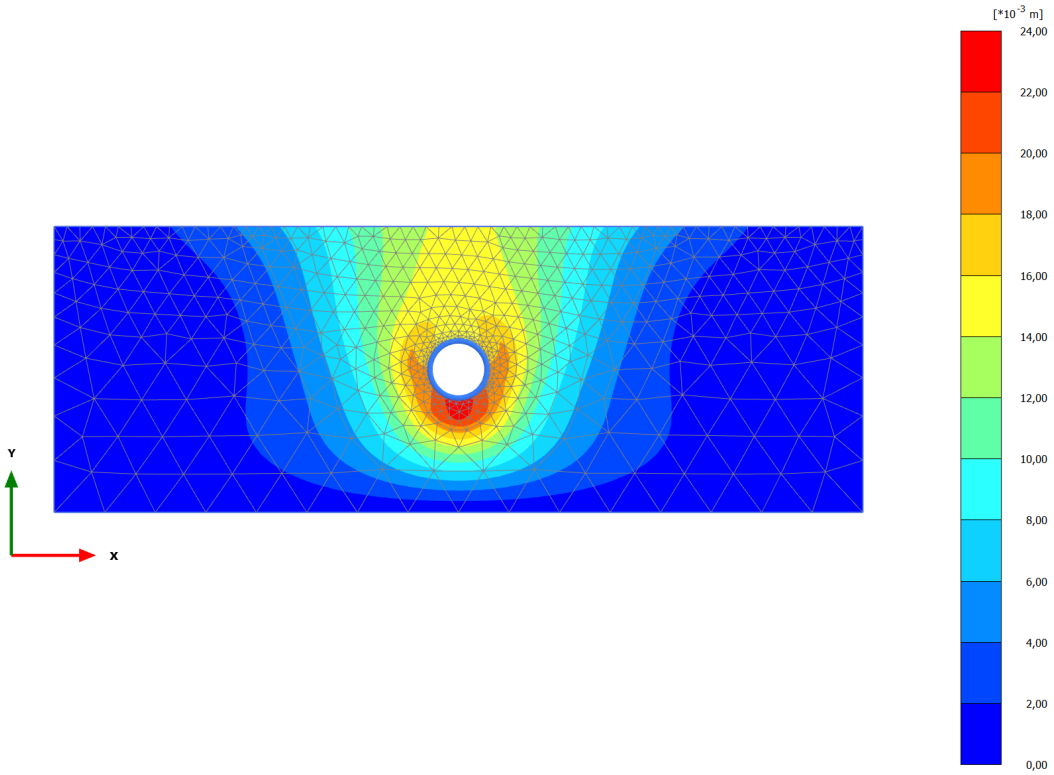

(b) Phase displacements (shading) due to tunnel excavation (maximum displacement = 2.30 cm)

Figure D.11: Phase displacements due to tunnel excavation

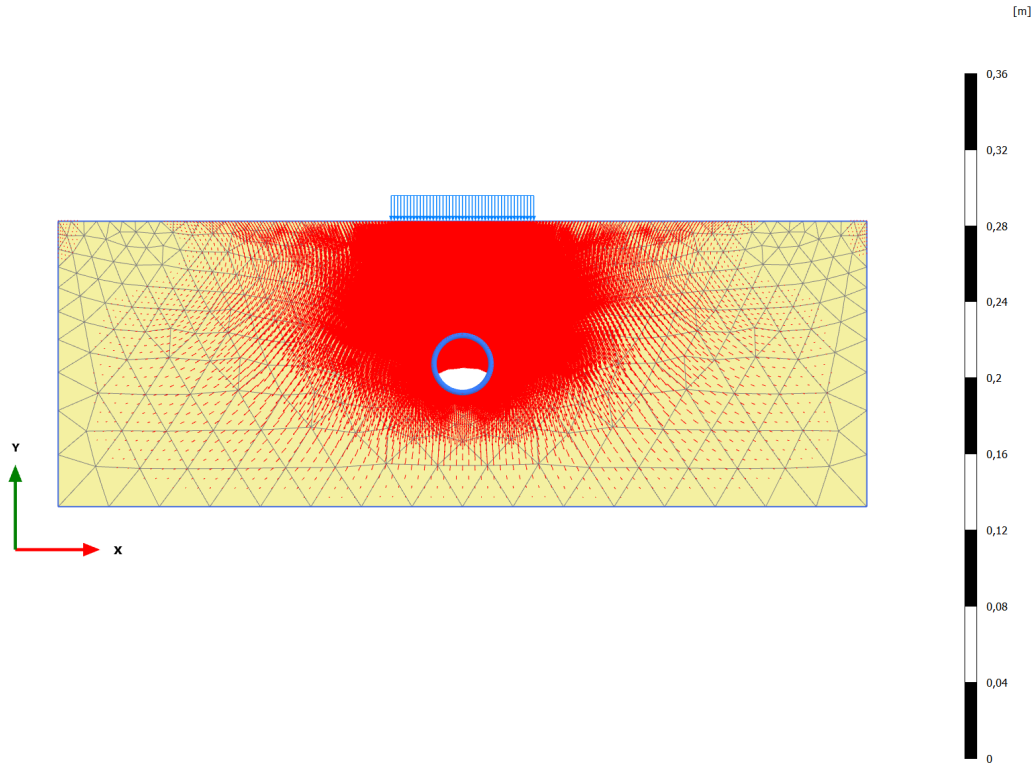

(a) Phase displacements (arrows) due to tunnel excavation and surcharge (maximum displacement = 6.80 cm)

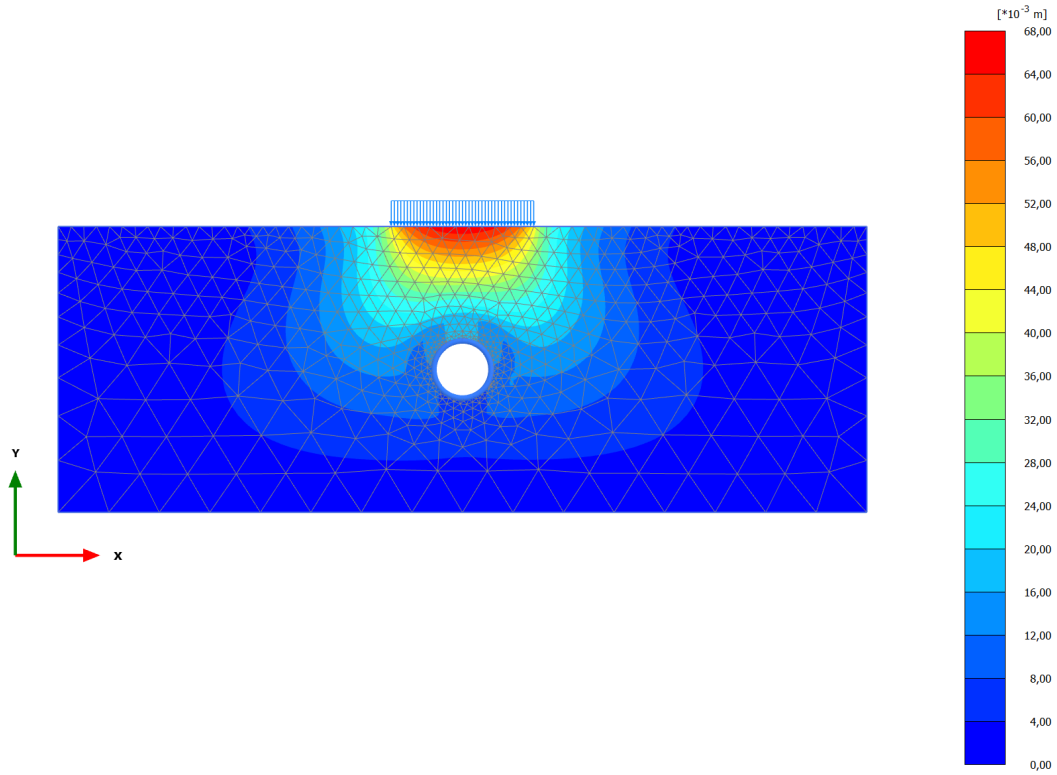

(b) Phase displacements (shading) due to tunnel excavation and surcharge (maximum displacement = 6.80 cm)

Figure D.12: Phase displacements due to tunnel excavation and surcharge

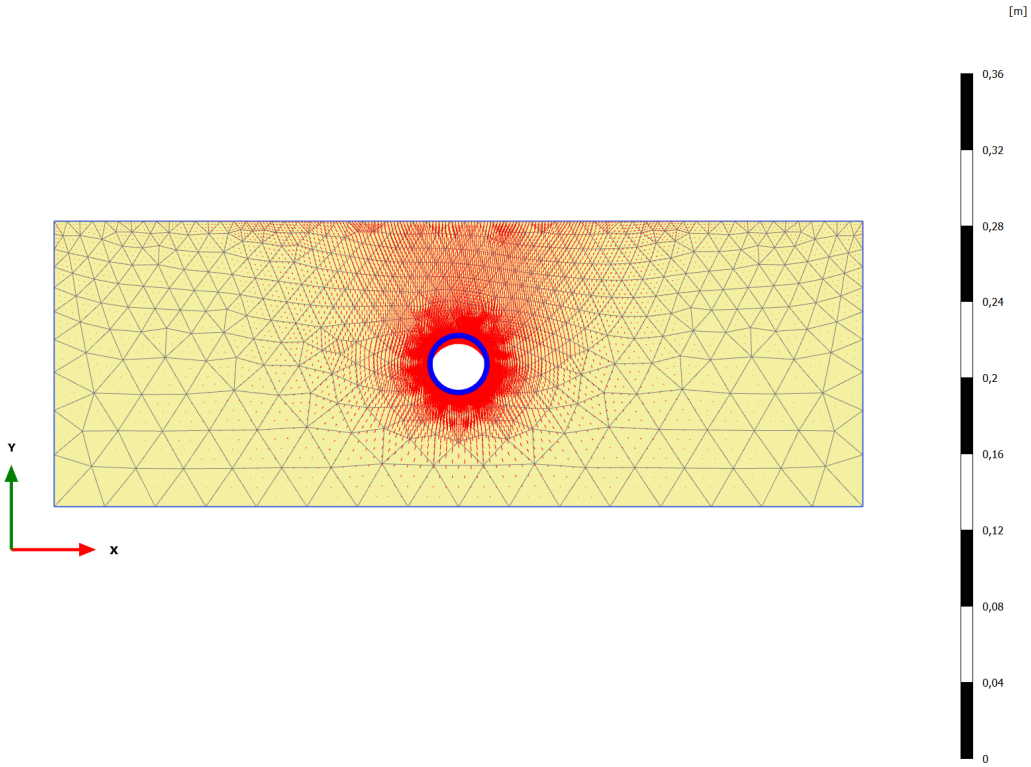

(a) Phase displacements (arrows) due to thawing of the frozen soil body (maximum displacement = 0.60 cm)

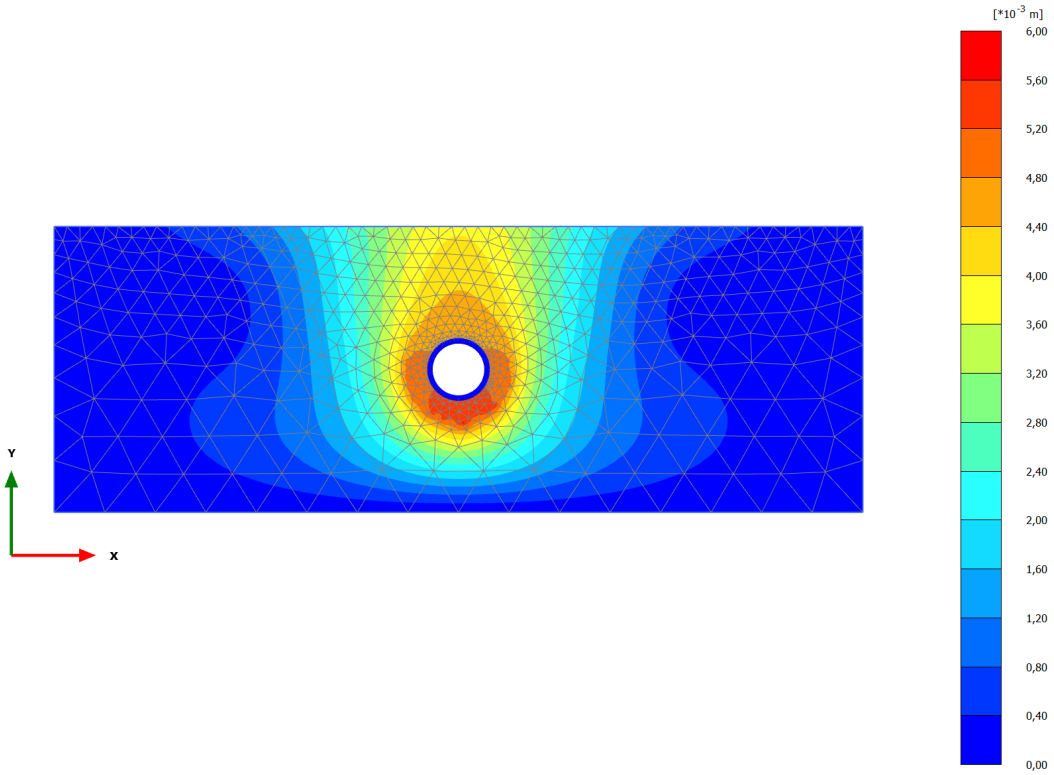

(b) Phase displacements (shading) due to thawing of the frozen soil body (maximum displacement = 0.60 cm)

Figure D.13: Phase displacements due to thawing of the frozen soil body

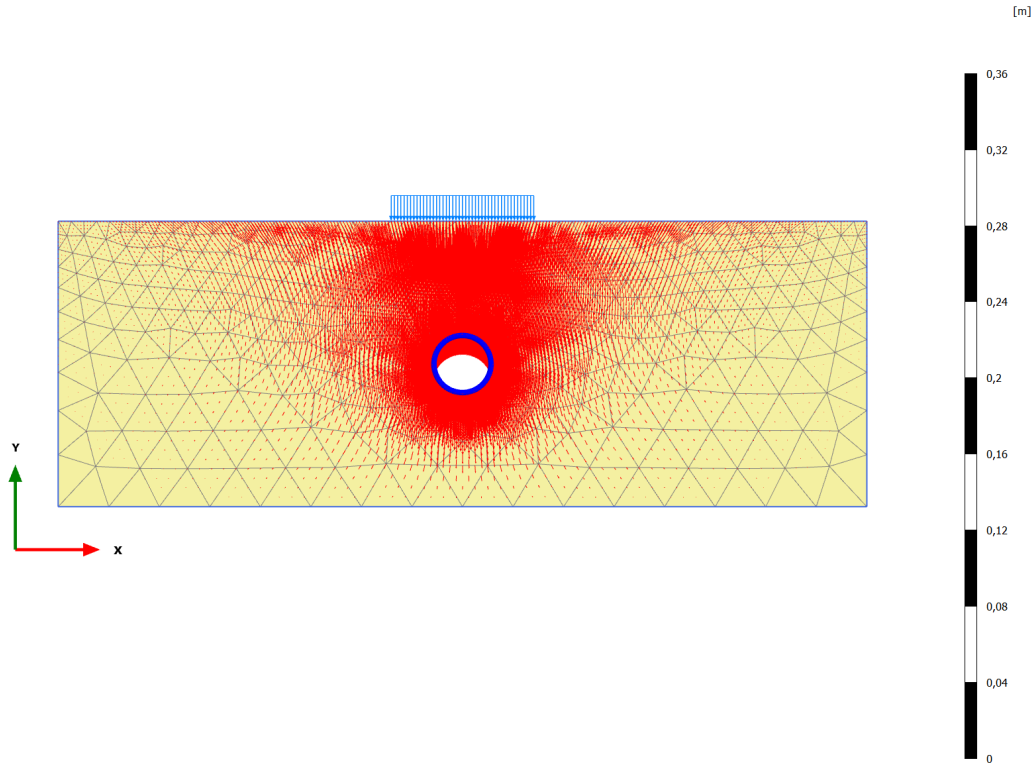

(a) Phase displacements (arrow) due to thawing of the frozen soil body and surcharge(maximum displacement = 1.80 cm)

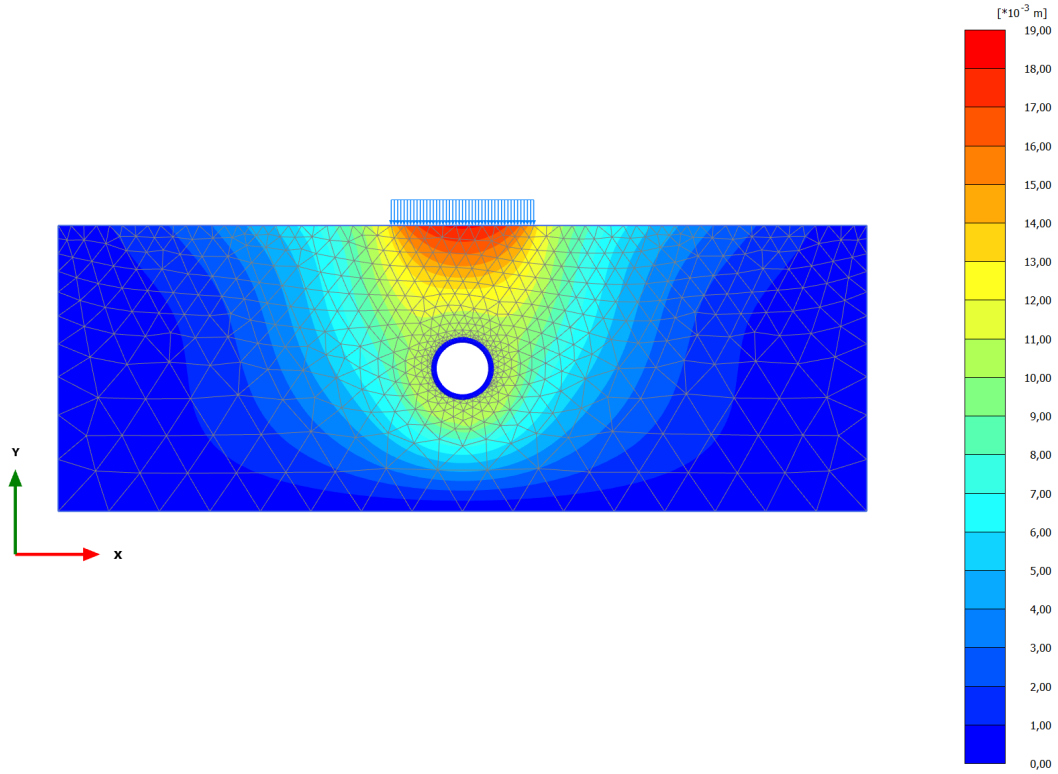

(b) Phase displacements (shading) due to thawing of the frozen soil body (maximum displacement = 1.80 cm)

Figure D.14: Phase displacements due to thawing of the frozen soil body and surcharge

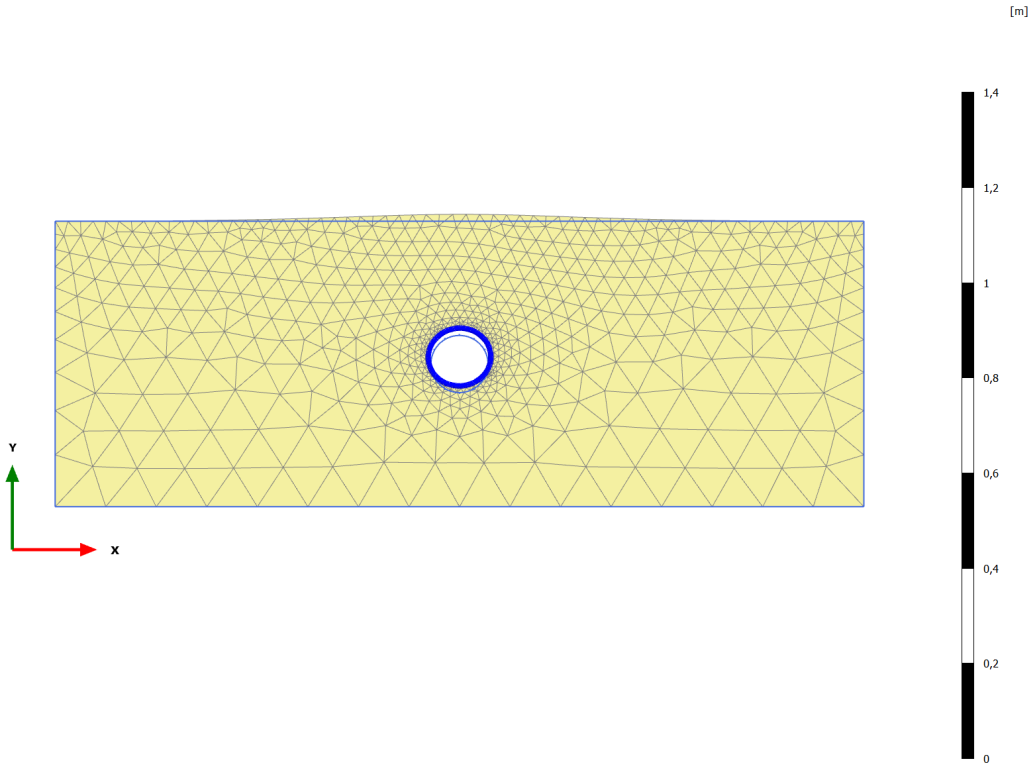

(a) Deformed mesh after freezing and thawing without surcharge loading (maximum value = 1.9 cm, scaled up 50 times)

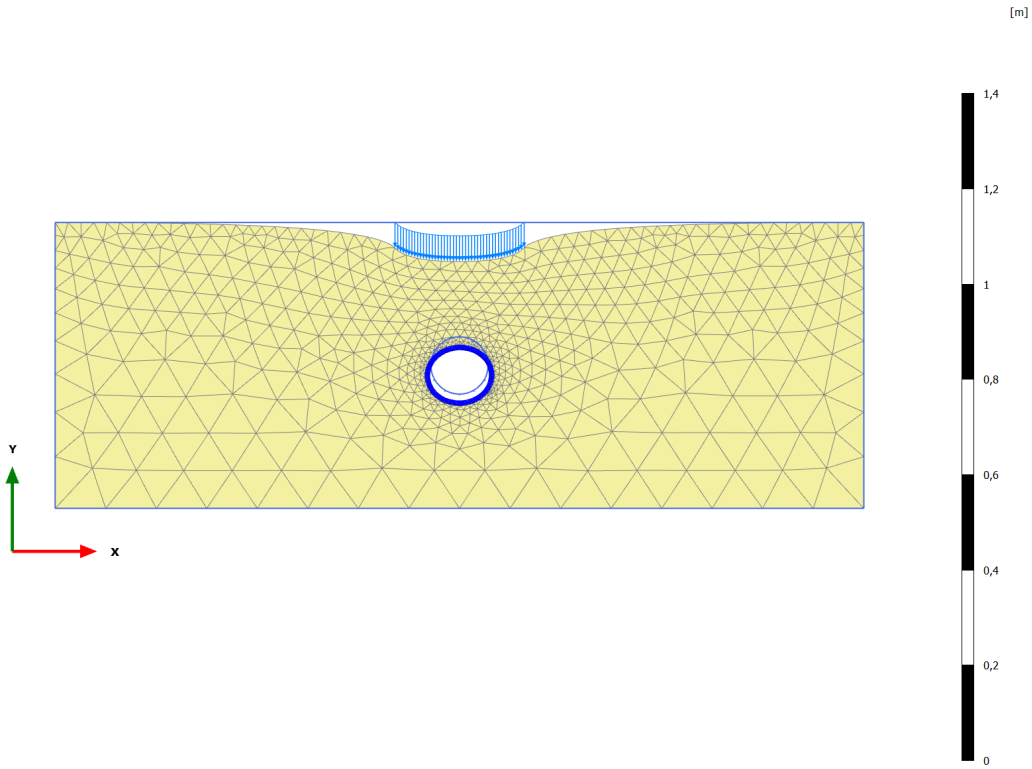

(b) Deformed mesh after freezing and thawing with surcharge (maximum value = 8.2 cm, scaled up 50 times)

Figure D.15: Final displacements after the artificial ground freezing and thawing period with and without surcharge loading